NOVEMBER 2018 M.Sc. in Aircraft and Aerospace Engineering YÜKSEL ERASLAN

UNIVERSITY OF GAZİANTEP

GRADUATE SCHOOL OF

NATURAL & APPLIED SCIENCES

A TRAINING SAILPLANE DESGIN

M.Sc. THESIS

IN

AIRCRAFT AND AEROSPACE ENGINEERING

BY

YÜKSEL ERASLAN

NOVEMBER 2018

A Training Sailplane Design

M.Sc. Thesis

in

Aircraft and Aerospace Engineering

University of Gaziantep

Supervisor

Prof. Dr. İbrahim Halil GÜZELBEY

Co-Supervisor

Assist. Prof. Dr. Mehmet Hanifi DOĞRU

by

YÜKSEL ERASLAN

November 2018

REPUBLIC OF TURKEY

UNIVERSITY OF GAZİANTEP

GRADUATE SCHOOL OF NATURAL & APPLIED SCIENCES

AIRCRAFT AND AEROSPACE ENGINEERING

Name of the thesis: A Training Sailplane Design

Name of the student: Yüksel ERASLAN

Exam date: 28.11.2018

Approval of the Graduate School of Natural and Applied Sciences

Prof. Dr. Ahmet Necmeddin YAZICI

Director

I certify that this thesis satisfies all the requirements as a thesis for the degree of Master of Science.

Assist. Prof. Dr. M. Orkun ÖĞÜCÜ

Head of Department

This is to certify that we have read this thesis and that in our consensus opinion it is fully adequate, in scope and quality, as a thesis for the degree of Master of Science.

Assist. Prof. Dr. Mehmet Hanifi DOĞRU	Prof. Dr. İbrahim Halil GÜZELBEY
Co-Supervisor	Supervisor

Examining Committee Members:	Signature
Prof. Dr. İbrahim Halil GÜZELBEY	……..
Prof. Dr. Naki TÜTÜNCÜ	……..
Prof. Dr. Abdülkadir ÇEVİK	……..

I hereby declare that all information in this document has been obtained and presented in accordance with academic rules and ethical conduct. I also declare that, as required by these rules and conduct, I have fully cited and referenced all material and results that are not original to this work.

Yüksel ERASLAN

ABSTRACT

A TRAINING SAILPLANE DESIGN

ERASLAN, Yüksel

M.Sc. in Aircraft and Aerospace Engineering

Supervisor: Prof. Dr. İbrahim Halil GÜZELBEY

Co-Supervisor: Assist. Prof. Dr. Mehmet Hanifi DOĞRU

November 2018

90 pages

In this study, the first general three phases of sailplane design, which are requirement defining, conceptual design and preliminary design have been studied and applied for a two-seater electric-powered self-sustaining training sailplane design. The critical performance specifications of two-seater sailplanes existing in the literature have been described and taken into consideration as a starting point. In requirement defining phase, critical objective parameters were tried to be realistically estimated depending on this collected data. General layout of the sailplane was determined at the conceptual design phase depending on advantages and disadvantages of wing, tail and fuselage configurations. In preliminary design phase, with the objective of designing aerodynamically efficient wing, tail and fuselage combination, each of the geometries were optimized to satisfy stability and especially level flight trim conditions by means of numerical analyzes. Trial-error optimization of the wing and tail designs were carried out especially depending on the criteria of having high lift to drag ratio and low induced drag. For this purpose, main wing was tried to be designed to have span-wise lift distribution similar to the elliptical lift distribution. Center of gravity calculations were carried out, its location was optimized and limitations were determined. In the end of the study, the aerodynamic performance parameters of the concluded design were obtained and revealed with numerical analyses. The obtained results were found to be in good agreement with the previous studies.

Key Words: Sailplane design, aerodynamic performance, flight mechanics.

ÖZET

BİR EĞİTİM PLANÖRÜ TASARIMI

ERASLAN, Yüksel

Yüksek Lisans Tezi, Uçak ve Uzay Mühendisliği

Tez Yöneticisi: Prof. Dr. İbrahim Halil GÜZELBEY

Yardımcı Tez Yöneticisi: Dr. Öğr. Üyesi M. Hanifi DOĞRU

Kasım 2018

90 sayfa

Bu çalışmada, planör tasarımının ilk üç aşaması olan tasarım girdi tespiti, kavramsal tasarım ve ön tasarım aşamaları çalışılmış ve çift kişilik elektrik motorlu kendisini idame ettirebilen bir eğitim planörü tasarımı için uygulanmıştır. Başlangıç noktası olarak literatürde yer alan çift kişilik planörlerin kritik performans değerleri derlenmiş ve göz önünde bulundurulmuştur. Tasarım girdi tespiti aşamasında kritik hedef parametreler, derlenen bu bilgilere dayanarak gerçekçi olarak tahmin edilmeye çalışılmıştır. Kavramsal tasarım aşamasında kanat, kuyruk ve gövde konfigürasyonlarının avantaj ve dezavantajlarına dayanarak planörün genel hatları belirlenmiştir. Ön tasarım aşamasında aerodinamik olarak verimli bir kanat, kuyruk ve gövde kombinasyonu tasarlamak hedefiyle, her bir geometri stabilite ve özellikle düz uçuş denge şartlarını sağlayacak şekilde nümerik analizler yardımı ile optimize edilmiştir. Kanat ve kuyruk tasarımlarının deneme-yanılma ile optimizasyonu özellikle yüksek süzülme oranı ve düşük indüklenmiş sürüklenmeye sahip olma kriterlerine dayanarak gerçekleştirilmiştir. Bu amaçla kanat, kanat boyunca kaldırma kuvveti dağılımı eliptik kaldırma kuvveti dağılımına benzeyecek şekilde tasarlanmaya çalışılmıştır. Ağırlık merkezi hesapları gerçekleştirilmiş, ağırlık merkezi konumu optimize edilmiş ve sınırları belirlenmiştir. Çalışmanın sonunda, nihai tasarımın aerodinamik performans parametreleri nümerik analizlerle elde edilmiş ve ortaya konulmuştur. Elde edilen sonuçların geçmiş çalışmalarla iyi bir uyum içerisinde olduğu görülmüştür.

Anahtar Kelimeler: Planör tasarımı, aerodinamik performans, uçuş mekaniği

To my family…

ACKNOWLEDGEMENTS

Firstly, I wish to express my grateful appreciation to my supervisor Prof. Dr. İbrahim Halil GÜZELBEY and my co-supervisor Assist. Prof. Dr. Mehmet Hanifi DOĞRU for their guidance, supports and encouragement from the beginning to the end of this study.

And my family, their support was the biggest source of my power. The deepest thankfulness is to my family and my wife for their love, patience, and prayers during this research.

TABLE OF CONTENTS

LIST OF FIGURES

Page

LIST OF TABLES

Page

CHAPTER 1

INTRODUCTION

Sailplane is defined as an aircraft heavier than air and supported with its fixed lifting surfaces by the dynamic reactions during its flight. In addition, a powered sailplane is defined as an aircraft equipped with one or more engines which has the characteristics of a sailplane even if engine(s) are inoperative [1].

Powered sailplanes are categorized into two groups in terms of purpose of their propulsion units. Self-launching category sailplanes are capable of taking-off with the help of its propulsion unit, but self-sustaining category sailplanes are only capable of using their propulsion unit to sustain their flights. Therefore, self-sustaining or unpowered sailplanes needs an external support to launch. In order to satisfy this need, there are three most common launching methods termed as launching by ground winch, launching by automobile tow and launching by airplane tow.

Gliding and soaring are two of the main flight phases of sailplanes. Gliding can be defined as flying with a sailplane or a glider, but soaring have a different meaning of gaining altitude and traveling without power. There are mainly two types of soaring, which are thermal and ridge/wave soaring. During the thermal soaring, pilots use the advantage of the vertical movement of air masses caused by the temperature differences. On the other hand, during the ridge soaring, they use the advantage of a vertical lifting component, which is provided by a horizontal air movement striking a mountain, hill or cliff [2,3].

The names “glider” and “sailplane” are both in use in the literature, but there are differences between sailplanes and gliders which comes from their aerodynamic performance characteristics. Even though, both terms are acceptable and synonyms, sailplane wings differ from gliders by providing relatively high lift and low drag and being suitable for sustained flight using atmospheric lifting forces [2,4].

A sailplane design needs to be compatible with corresponding local and international regulations to be able to certify, as all aircrafts. In European countries, regulations for sailplane certifications are regulated by European Aviation Safety Agency (EASA). The regulations are designated as CS-22 and named as "Certification Specifications for Sailplanes and Powered Sailplanes". As a European country, Turkish local authority of Directorate General of Civil Aviation (DGCA) is a member of European Aviation Safety Agency. Therefore, sailplane certification specifications of EASA are accepted and applied by DGCA.

Designing a sailplane is a multidisciplinary process requiring expertise on flight dynamics, aerodynamics, propulsion, structure, management and engineering design. As for all aircraft design processes, sailplane design has five major steps which are requirement defining, conceptual design, preliminary design, detail design and fabrication. The process starts with defining realistic requirements and continues with conceptual design phase consisting of defining the initial specifications and external geometry of the sailplane. After different configurations and specifications are taken into consideration, the preliminary design phase starts and completely answers whether the idea generated at the conceptual design phase is viable in terms of so many disciplines. Detailed design and drawings of each part of the sailplane is drawn in detail design phase which will be resulted in something that can be built and ultimately flown [5,6].

In this study, the first three phases of sailplane design, which are requirement defining, conceptual design and preliminary design will be studied and applied for a two-seater electric-powered self-sustaining training sailplane. The critical performance specifications of two-seater sailplanes existing in the literature will be taken into consideration as a starting point. In requirement defining phase, critical objective parameters will be estimated depending on this collected data. General layout the sailplane will be determined at the conceptual design phase depending on advantages and disadvantages of each of wing, tail and fuselage configurations. In preliminary design phase, with the objective of designing aerodynamically efficient wing, tail and fuselage combination, each of the geometries should be optimized to satisfy stability and especially level flight trim conditions by means of numerical analyzes. Trial-error optimization method of the wing and tail designs will be carried out especially

depending on the criteria of having high lift to drag ratio and low induced drag. For this purpose, main wing may also be tried to be designed to have span-wise distribution similar to the elliptical distribution. Center of gravity calculations should be done, its location must be optimized and limitations should also be determined with respect to stability considerations. In the end, the aerodynamic performance parameters of the concluded design will be obtained and revealed with numerical analyses.

CHAPTER 2

LITERATURE SURVEY

2.1 Introduction

A literature review related to aircraft design and additionally especially sailplane design is given in this chapter. First of all, historical review of sailplane design is presented. Studies about the static and dynamic aeroelasticity throughout the history is briefly given in the second part. It is continued with specially literature review of each part of sailplane which are categorized as wing, tail and fuselage sections. This review includes also studies about the experimental analyzes methods and the numerical solution methods used during aircraft design processes. Lastly, the general conclusion of the literature survey is revealed.

2.2 Historical Review

Throughout the history, flying has always attracted the attention of mankind. The first flying attempts of human had been carried out by Abbas Ibn Firnas in 9th century and Ismail Ibn Hammad al-Cevher at the beginning of the 11th century [7]. In the 15th century, Leonardo da Vinci improved and reinvented the attempts and sketched many designs of flying machines and mechanisms. It is not known whether da Vinci ever built or tested any of his designs [8]. In the early 17th century, Hezarfen Ahmet Çelebi made a successful gliding flight from Galata Tower to Üsküdar in Istanbul [9,10]. All these unpowered flight attempts were the gliding flights with the help of wind.

In 1799, George Cayley built the first fixed-wing flying machine in history. His flying machine separately had a mechanism for propulsion, a fixed-wing for lift, and cruciform tail for control. When it comes to the middle of the 19th century, Jean-Marie Le Bris designed successful two gliders as illustrated in Figure 2.2. At the end of the 19th century, Otto Lilienthal designed and flew the first successful controlled gliders in history. He made more than two thousand successful glider flights. In addition,

Samuel Pierpont Langley achieved the first sustained heavier-than-air, unmanned and powered flight in the history with his small-scale Aerodrome in 1896 [8,11].

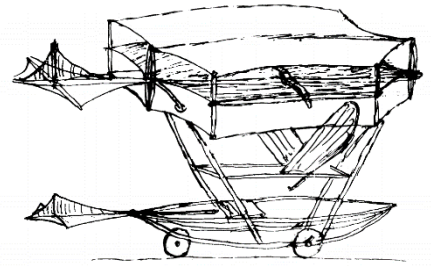

Figure 2.1 The glider designed by Sir George Cayley in 1852 [8]

At the beginning of the 20th century, Wright brothers made a flight with their glider which was a rudder controlled machine. Their attempts were continued with the first aircraft capable of performing the controlled and powered flight in history [8,11]. All these attempts and accumulation prepared a substructure for the accelerating development of aviation and gliding in the 20th century.

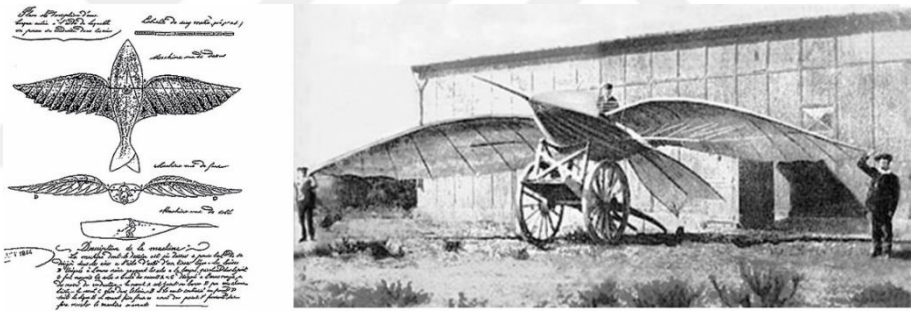

Figure 2.2 The glider designed by Jean-Marie Le Bris [12,13]

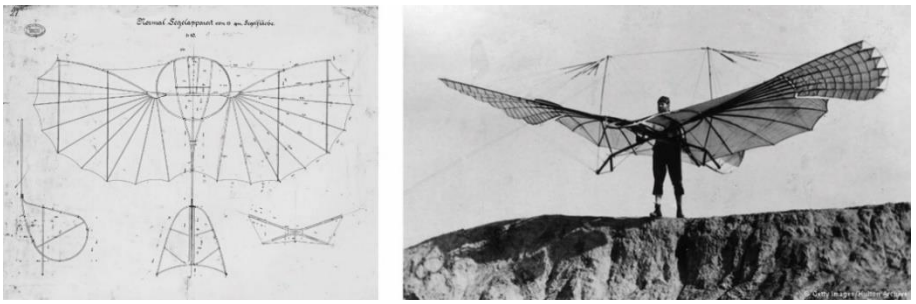

Figure 2.3 The flight machine designed by Otto Lilienthal [14,15]

2.3 Aeroelasticity

Since aeroelasticity considerations are not in the scope of this thesis, the literature review of this subject will not be in detail. Aeroelasticity is an important subject

especially during the structural designs of the aircrafts. The main concerns of aeroelasticity is the strength of the aircraft and its wing under aerodynamic and inertial forces. There are mainly two headings: static and dynamic aeroelasticity.

An aeroelastic high aspect ratio wing model produced and investigated the response in terms of the limit-cycle oscillations and flutter in wind tunnel test by Tang and Dowell. Theoretical verification was performed to validate experimental data. Combined aerodynamic stall model and beam theory were used for the theoretical calculations. Experimental and theoretical results were shown that the results are in good agreement for the measured parameters [16].

Aerobatic aircraft wing structure was investigated in terms of the aeroelastic tailoring and minimum weight concepts. Finite element and analytical model were created for the improved composite wing and original wing. Experimental studies were performed to validate these model results. Weight reductions were also examined for the composite materials by using different fiber orientations on the skin of the wing by Guo [17].

A study by Afonso et. al. have presented a review about the nonlinear aeroelasticity of high aspect ratio wings. Applications and methodologies employed to analyze high aspect ratio wings were given in the study. Important observations from the state-of-the art studies were obtained and the current challenges were specified [18].

2.4 Sailplane Design

The main parts of a sailplane can be divided into three parts as its fuselage, wing and tail assemblies. In the literature, there are so many studies including these parts' structural, aerodynamic and production considerations. As our study is about aerodynamic considerations of the sailplanes, the further parts of the literature survey will include general design and aerodynamic considerations of fuselage, tail and wing parts.

2.4.1 Fuselage Design

Contour line drawings for Torva sailplane fuselage were produced by W. B. Hart [19] with a computer program written to investigate an interactive design method using

Coon's surface patches. The study is included various steps for the fuselage design and there is a comparison between the method with the alternative hand lofting.

Investigation of the undergoing nose down impact was presented in terms of the crash dynamics and energy absorption of composite sailplane fuselage segments by Kampf et. al. [20]. Many structurally similar test articles, which are related to high performance sailplane designs, were investigated for this study. Fuselage segments were produced from composite materials. Dynamic and Quasistatic tests were performed. Substantial increases in crash-worthiness were indicated by structural improvements and combining material.

Tailless Standard sailplane was introduced as a conceptual design by Otani and Maughmer [21]. The center of gravity concept was examined in terms of the aerodynamic and geometric center. It was presented that a fuselage design helps to support the stabilizing function. The cross-country performance of the tailless aircraft was predicted and compared with conventional sailplane.

2.4.2 Tail Design

It is well known that laminar separation bubbles play detrimental role on the horizontal tail-plane of a sailplane operating at low Reynolds number. Wortmann applied extensive instability regions on the airfoils FX71-L-150/20/25/30 to avoid these bubbles. In order to make longer laminar flow regions possible, horizontal tail-plane design of the standard class sailplane ASW-24 was produced by Alexander Schleicher Segelnugzeugbau, Germany [22].

Flutter physics of T tail with detailed explanation was presented by describing potential flow modeling alternative in this study. Also, detailed experimental and numerical results were investigated to compensate the shortage of reproducible data. Three approaches, which are the direct incorporation of supplementary T tail effects as additional terms in the flutter equations, a generalization of the boundary conditions and air loads calculation on the double lattice and linearization of the unsteady vortex lattice method with arbitrary kinematics, were used to compare the results. The validated models were tested in easy-to-duplicate canonical test cases [23].

A study was performed by using Vortex Lattice Method and combination of semi-empirical techniques by Carmono and Rejado [24]. The obtained results of method and techniques were applied to the reference aero-plane substituting its conventional tail by a parametrized Vee-tail configuration. Four parameters were investigated, which are root chord, span, dihedral angle and taper ratio. At the end of the study, according to the Vee-tail geometry, minimum size must be between 60% and 80% of the half-span of the tail.

2.4.3 Wing Design

Wing design has a critical importance for sailplanes as well as for all the aircrafts in terms of aerodynamic performance. There are mainly two important phases of wing design, which are airfoil selection (or design) and planform geometry design. An airfoil is the two-dimensional section geometry of a wing and has very critical aerodynamic performance effects on the wing. On the other hand, planform geometry has many variable geometric parameters which should be taken into consideration and optimized.

2.4.3.1 Airfoil Selection

Airfoil selection of a wing design firstly requires performing aerodynamic performance analysis of different airfoils to compare according to determined requirements. In conceptual design stage of aircrafts, generally it is not preferred to perform expensive and time-consuming wind-tunnel experiments for airfoil analysis. There are many different computer programs and codes, which can perform these analyses quickly and easily. XFOIL [25], XFLR5 [26], Eppler Code [27] and ANSYS Fluent are some of the well-known programs. For two-dimensional airfoil aerodynamic performance analysis, user-friendly interfaced XFLR5 program uses a fully coupled viscous/inviscid interaction method with a high-order panel method to evaluate drag, boundary layer transition and separation. In the literature, there are many studies about aerodynamic performance analysis and comparison of airfoils.

Hansman and Craig investigated different airfoils with wind-tunnel experiment conductions. The study includes comparison of three different airfoils in terms of aerodynamic performance degradations under a rain rate [28].

Smith et al. performed two-dimensional CFD (Computational Fluid Dynamics) analysis for a Wortmann airfoil in ground effect at different angles of attacks. They compared results with data from previous experimental studies and validated that use of this airfoil is useful for a ground effect aircraft in terms of aerodynamic performance [29].

Lasauskas and Naujokaitis analyzed aerodynamic performances of different airfoils with Eppler Program System, RFOIL and XFOIL. The study includes comparison of codes in terms of accuracy with respect to existing wind-tunnel experimental results at different Reynolds numbers [30].

Wahidi and Bridges investigated laminar separation bubble behaviors not only at different Reynolds numbers but also at different angle of attacks on NACA 0012 and LA2573 by experimental wind-tunnel analyses. At the end of the study, experimental data of surface pressure distributions compared and found in agreement with the results obtained from XFLR5 program [31].

Xin et al. performed aerodynamic performance analysis on ANSYS Fluent for a NACA and seagull airfoils at different Reynolds numbers. They found that seagull airfoil is aerodynamically more efficient than the NACA airfoil and proper to use on small-power wind driven generators [32].

Sudhakar et al. computed aerodynamic characteristics of a modified version of an existing airfoil geometry, which was obtained using inverse design method of XFLR5 program. With the aim of providing better longitudinal stability for a MAV configuration, they compared aerodynamic performance of the modified airfoil with its original geometry according to XFLR5 analysis results [33].

Vuruşkan et al. (2014) performed aerodynamic performance analysis of VTOL (vertical take-off and landing) aircraft having blended wing body with VLM (vortex-lattice method), NLL (Non-linear numeric lifting line) and CFD (computational fluid dynamics) methods. They used XFLR5 program to obtain airfoil characteristics of airfoils used. They obtained that VLM and CFD methods results in agreement with experimental data existing in literature more than NLL method [34].

Hasan et al. investigated aerodynamic performances of three airfoils with the help of analysis on Qblade program. With the results of the analysis, mixed airfoil wind turbine blade designed, and its aerodynamic performance investigated with CFD analysis on ANSYS Fluent [35].

2.4.3.2 Planform Design and Numerical Analysis

Selection of the optimum sailplane aspect ratio concept was presented for the lowest sinking speed and flattest gliding angle with simplifying assumptions by Castles [36].This study was performed for the given drag of fuselage, span, tail, and wing section. Also, variation of the optimum aspect ratio concept was examined according to sailplane parameters.

Numerical optimization for the wing design was performed by Hicks and Henne [37]. Full potential, inviscid aerodynamics code was combined with a conjugate gradient. This technique was applied to three different design problems. This problem was defined as geometric and aerodynamic problems by the authors. The authors obtained from the study that the technique is sufficiently accurate to permit substantial improvement in the design objectives.

Basic results of the wing planform optimization were presented for the maximum lift and minimum drag with constraints on structural weight by Wakayama and Kroo [38]. Analyses were developed and integrated to yield optimization. Importance of weight constraints, maximum lift, compressibility drags, and static aeroelasticity on wing shape were demonstrated.

Flight weight concept was investigated in terms of the range capability and efficiency goal by Takahashi [39]. Analytical model was used to indicate the influence of design parameters and key constraints. The model was created according to optimum wing loading and aspect ratio to develop efficiency and range. Different flight weights were examined for example over 200000 lb and under the 100000 lb. The statistical design approach to improve these configurations was revealed with an intuitive design approach by the author.

The influence of dihedral layout on the lateral directional dynamic stability of the tailless flying wing aircraft was presented by Lei et. al. [40]. A tailless flying wing

aircraft which has a large aspect ratio was used to perform the study. The dihedral angle along the spanwise sections was investigated as three parts. Vortex lattice method code was utilized to calculate stability derivatives. Also, linearized small-disturbance equations of the lateral modes were used to determine the mode dynamic characteristics. It was found that the flight quality close to Level 2 requirements were achieved according to the optimized concepts.

Torsion deformations of highly flexible aircraft and optimum wing bending concepts were investigated to obtain optimum wing geometry in terms of the distributed control loads through the wing-span by Hammerton et. al. [41]. Shape optimization was performed to achieve the aim of the study. Also, optimization, which is multi objective, is created and realized for both reducing the gust induced wing bending moment and minimizing the drag. At the end of the study, desired wing planform geometry and insights of the required control effort were presented with efficient way to search.

Della Vecchia et al. [42] investigated effects of propellers on wing aerodynamics by means of a computational fluid dynamics program. The study includes effects of propellers mounted at both tip and middle of the wing. Firstly, mesh accuracy of the program was done and it was shown that the program results are in good agreement with experimental results. Later on, by means of using the validated method on numerical analyses, they obtained that the tip-mounted propeller can decrease the induced drag from up to 10% and middle-mounted propellers can increase the maximum lift coefficient of the wing up to 30%.

Bravo-Mosquera et al. [43] presented conceptual design and prototype of an agricultural aircraft. Following the traditional design methods applied, six different winglet designs, which have different cant angles were analyzed by means of a computational fluid dynamics program using Reynolds–Averaged–Navier–Stokes (RANS) equations. The aim of the analyses was determining the winglet design providing the best aerodynamic characteristics. Later on, these analyses were expanded to complete aircraft and obtained lift, drag and pitching moment coefficients were investigated together with wingtip vortex structures. At the end of the study, they obtained that multi winglet devices were contributing on improving performance of

the aircraft, providing control on the sprayed product, reducing the induced drag and bending moment of the wing.

Qin et al. [44] performed computational fluid dynamics analyses using Reynolds-averaged Navier–Stokes (RANS) equations on a baseline blended wing body configuration with the aim of obtaining the effects of span-wise lift distribution. After the grid sensitivity study on total drag, they obtained the main factor decreasing the aerodynamic performance of the baseline body is wing loading together with shock wave. They revised the body to three models having different span-wise lift distributions and investigated the change in aerodynamic performances.

Lee et al. [45] investigated the effect of winglet dihedral on a tapered and swept wing at a low Reynolds number. Experimental analyses of the winglets having different dihedral angles were performed at a wind tunnel in McGill University at 35 m/s freestream velocity. According to results of the analyses, it was obtained that the induced-drag of a wing always reduces with the use of a winglet and the winglet, which have negative dihedral, decreases lift-induced drag more than positive dihedral. Moreover, it was revealed that, the inner region of the tip vortex behaviors is similar for the wing with or without winglets.

2.5 Conclusions of Literature Survey

The literature survey demonstrated that, although not as many for other types of aircrafts, there are so many publications about sailplanes. Few studies have focused on the general design phases of the sailplanes, but most of the researchers have focused on only wing, tail or fuselage designs. In this study, a conceptual and preliminary study of a sailplane design will be started for the further work. In this sense a number of tasks have been designed.

In this thesis, a two-seater electric-powered training sailplane design will be carried out. After defining the requirements of the design, conceptual design and preliminary issues will be taken into consideration. Aerodynamic performance analysis of the final design will be performed.

CHAPTER 3

DESIGN REQUIREMENTS AND CONCEPTUAL DESIGN

3.1 Introduction

Designing a sailplane is a multidisciplinary process requiring expertise on flight dynamics, aerodynamics, propulsion, structure, management and engineering design. Sailplane design has five major steps: defining design requirements, conceptual design, preliminary design, detail design and fabrication as shown in Figure 3.1. In this chapter, the design requirements and conceptual design (configuration design) phases were defined in detail and carried out for an experimental, electric-powered self-sustaining two-seater sailplane design.

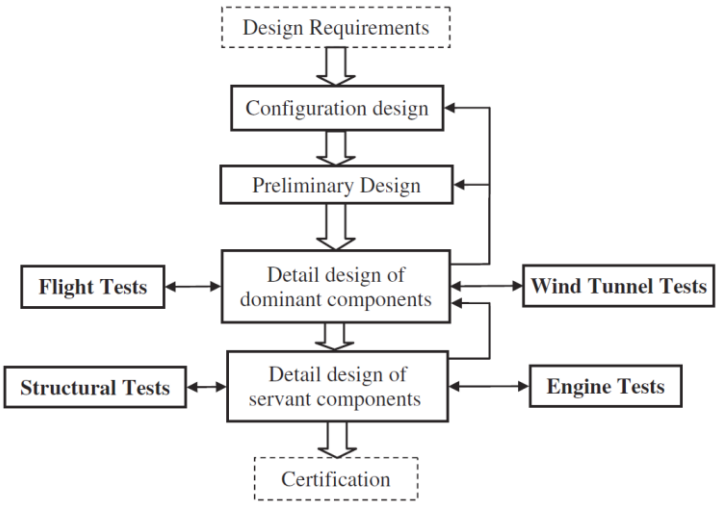

Figure 3.1 General flow chart for aircraft design [5]

3.2 Design Requirements

Design requirements can be defined as a list of expectations that a new design should meet. Therefore, defining realistic requirements is the first step of an aircraft design process, which depends on customer demands for a commercial product. In the case of an experimental study, these can be determined more flexible and far from commercial concerns. Thus, as an experimental sailplane design study, the design

requirements of the sailplane design that is the scope of this thesis can be determined more flexibly according to our preferences.

In this part, firstly, mission profile of our target design will be specified and drawn. Later on, the general certification requirements of European Aviation Safety Agency will be revealed. Lastly, the primary target design values, which are speed limitations, maximum takeoff weight (MTOW), wing span and glide ratio will be determined according to the certification requirements and collected data of some similar sailplanes.

3.2.1 Mission Profile

Mission profile is the complete and detailed description of the activities that an aircraft needs to successfully carry out during all its flight phases. Sailplane flight phases and correspondingly mission profile is a bit different than general aviation aircrafts. For example, cruising flight of general aviation aircrafts is named as gliding for sailplanes. Sailplanes also have a different flight phase named soaring. For our new design of powered sailplane, a mission profile was determined and drawn as shown in Figure 3.2. This mission profile includes the phases of takeoff-run, towing climb and climbing with propeller engine, gliding, soaring, descending and landing. All of these flight phases are limited with service ceiling of 3000 meters from the sea level due to the need for pressurized cockpit at higher altitudes [46]. In the further parts of the thesis, all of the considerations and calculations will be carried out according to limits of this mission profile.

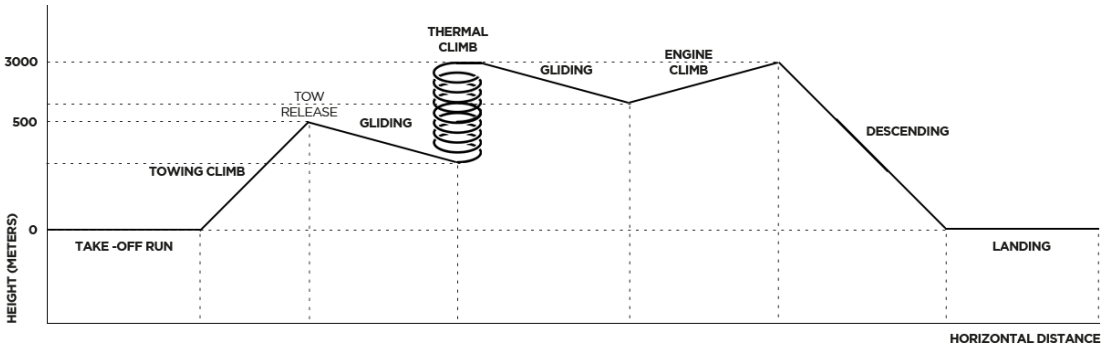

Figure 3.2 Target mission profile

3.2.2 General Certification Requirements

Certification rules are the primary limitations to consider before the preferences of customer or designer while defining the design requirements. The designer or customer is free to change the parameters as desired if only certification requirements are provided. In European countries, regulations for sailplane certifications are regulated by European Aviation Safety Agency (EASA). These regulations are designated as CS-22 and named as "Certification Specifications for Sailplanes and Powered Sailplanes".

EASA categorizes sailplanes in two groups as Utility and Aerobatic in terms of certification. The Utility Category is limited to sailplanes intended for normal soaring flight. Aerobatic Category is for sailplanes intending aerobatic maneuvers like spins, lazy eights, chandelles, stall and steep turns and positive loops. For both of the categories, allowed maximum takeoff weight is 750 kg for sailplanes and 850 kg for single engine powered sailplanes. Moreover, the number of the occupants cannot exceed two. Powered sailplanes need to have a weight (kg) to span (m^2) ratio (W/b^2) design value not greater than 3 [47]. In this thesis, except for these general rules, the specific certification requirements will presented and will be taken into consideration in each related design step separately.

3.2.3 Target Design Requirements

Aircraft designers usually rely on years of past experience and statistical or empirical methods that developed from previous projects as a starting point for their designs. In this study, while defining requirements, it has been inspired by the existing data about sailplanes. Critical geometric and performance values of the sailplanes existing in the recent past were collected and presented in Table 3.1. This information has given an idea to use as a starting point for our new design sailplane. In this part, the primary target design values, which are wing span, speed limitations (stall, cruise and never exceed speeds), maximum takeoff weight and glide ratio will be determined.

Table 3.1 Collected sailplane specifications data

Sailplane Model	Wing Span (m)	MTOW (kg)	Stall Speed (km/h)	W/b^2	AR	Propulsion
SF 25 D	14.7	580		2.68	12.6	Self-launching
Taurus Electro G2	15	550	71	2.44	18.6	Self-launching
SF 25 B	15.25	555		2.39		Self-launching
SF 25 K	15.25	630		2.71		Self-launching
Schweizer SGS 2-33	15.5	472		1.96	11.85	Pure
Diamond HK36 S. Dimona	16	710		2.77	16.8	Self-launching
F 28 A “Tandem-Falke”	16.3	590		2.22		Self-launching
SF 36 A	16.38	715		2.66	17.2	Self-launching
SF 25 A	16.6	485		1.76		Self-sustaining
SZD-50-3 Puchacz	16.7	570	60	2.04	15.3	Pure
ASK 21	17	600	65	2.08		Pure
ASK 21 Mi	17	705	80	2.44	16.1	Self-launching
TST 14 Bonus	17	580	65	2.01	23.9	Self-launching
AMT-200 S. Ximango	17.47	805		2.64	16	Self-launching
fs31 - Ferdinand Porsche	17.5	560		1.83	17.2	Pure
Grob G103c Twin III SL	18	710	63	2.19	18.5	Self-launching
SF 25 E	18	650		2.01	17.8	Self-launching
HPH Twin Shark	20	850	68	2.13	26.5	Self-launching
ASG 32 Mi	20	850	86	2.13	25.5	Self-launching
DG1001M	20	790		1.98	22.8	Self-launching
Arcus M	20	800	87	2.00	25.7	Self-launching
DG 500-MB	20	825		2.06	22.7	Self-launching
Arcus E	20	810		2.03	25.7	Self-launching
Arcus T	20	800		2.00	25.7	Self-sustaining
Duo Discus xL T	20	750	72	1.88	24.4	Self-sustaining
DG 1001T	20	750	80	1.88	22.8	Self-sustaining
ASG 32 EL	20	850		2.13	25.5	Self-sustaining
fs33 - Gavilàn	20	640		1.60	27.8	Pure
D-41	20	760		1.90	28.6	Pure
SB 15	20	640		1.60	32.4	Pure
Average	18.0	686.1	72.5	2.14	21.5	

3.2.3.1 Maximum Takeoff Weight (MTOW)

Maximum takeoff weight or maximum gross takeoff weight is the maximum weight of an aircraft that it is allowed to takeoff. Two-seater sailplanes generally has MTOW of approximately larger than 500 kg and lower than 850 kg from the collected data in

Table 3.1. The maximum takeoff weights of the sailplanes in the table should be evaluated with taking into consideration whether they have propulsion unit and water ballast. In this study, our design will not have any water ballast but have a propulsion unit. Therefore, by evaluating the statistics in the table, it was decided for our design to have a target MTOW value of 700 kg, which is proper for the EASA weight limitations. The distribution of this determined weight of our design will be detailed in next parts of the study.

3.2.3.2 Wing Span

Wing span is the horizontal distance between tips of the wing of an aircraft. Wing span determination needs to be considered together with maximum takeoff weight due to the EASA's certification rule about the ratio between weight and wing span. Powered sailplanes need to have a weight (kg) to span^2 (m^2) ratio (W/b^2) design value of which is not greater than 3. On this basis, with determined MTOW of 700 kg, our new sailplane design is not allowed to have wing span value lower than 15.2 meters.

Gliding Commission of World Air Sports Federation (FAI), which is the sporting body overseeing air sports at the international level, categorizes sailplanes in seven different classes for their competitions. The classifications are mainly based on the sailplanes' wing span and configurations. The classes are named as 13.5-meter Class, 15-meter Class, 18-meter Class, 20-meter Class, Club Class, Open Class and Standard Class. Also, powered sailplanes are divided into two classes as self-launching and self-sustaining.

Each class has different restrictions about configurations and wing spans of the sailplanes. 13.5-meter Class sailplanes allowed to have maximum wing span of 13.5 meters and maximum wing loading of 35 kg/m2. On the other hand, 15-meter Class sailplanes allowed to have maximum wing span of 15 meters and maximum takeoff weight of 525 kg. Also, lift-enhancing devices are allowed for this class sailplanes. 18-meter Class sailplanes are allowed to have maximum wing span of 18 meters and maximum takeoff weight of 800 kg. Two-seater Class sailplanes are restricted to have maximum wingspan of 20 meters and maximum takeoff weight of 850 kg. Open Class sailplanes has no restrictions except for maximum takeoff weight limit of 850 kg. In addition, this class sailplanes can be one or two seater. Standard Class sailplanes

restricted to have a maximum wing span of 15 meters and maximum takeoff weight of 525 kg. In this class, flaps and lift enhancing devices are not allowed. Lastly, Club Class sailplanes allows a wide range of older small gliders with the scores being adjusted by handicapping. Water ballast is not allowed in this class [48].

In this thesis, it was decided to have 18 meter wing-span for our design rather than a higher wing-span with more complex structural issues and dominant aeroelastic considerations. Hence it will be also possible to participate in FAI competitions at open class or 18-meter classes thanks to this defined wing-span and MTOW. Consequently, W/b^2 ratio of our design was determined as 2.16 with the Equation (3.1), which is very close to the average of the sailplanes stated in the Table 3.1.

$$\frac{W}{b^2} = 2.16 \tag{3.1}$$

3.2.3.3 Speed Limitations

Speed limitations is an important topic need to be considered at the beginning of a new design aircraft. Stall speed (V_s), which means the minimum speed to maintain level flight for an aircraft, is a critical value, which need to be defined firstly. Stall speeds of various sailplanes have a wide range of values between 63 to 87 km/h, as seen in Table 3.1. It was decided our design to have a stall speed lower than 75 km/h with the aim of having a moderate and acceptable value.

Cruise speed can be defined as the average speed value of gliding flight between thermal regions for sailplanes, although it means for aircrafts as comfortable level flight operation speed. It is a speed value for aircrafts between their stall and never-exceed speed values. It is decided for our design to have a cruise speed of 120 km/h.

Never-exceed speed (V_{NE}) is the maximum permitted speed to operate for aircrafts. It is not safe to fly higher than this speed. Actually, this limitation depends on the aircraft structure and can be accurately defined after structural design and analyzes. On this basis, at the beginning of the design process, it was decided for our design to have a never-exceed speed value of 230 km/h. This value should be revised and re-calculated after structural design and investigations are done.

3.2.3.4 Glide Ratio

Glide ratio, which is given in Equation (3.2), is the ratio between lift and drag forces or coefficients for an aircraft. It is also the ratio of the horizontal travelled distance and loss of altitude in a given time. Therefore, it is also mentioned as aerodynamic performance of aircrafts. Sailplanes usually have glide ratios higher than other air vehicles as gliding aircrafts, and this value is generally higher than 10 and can achieve 40 or above for modern sailplanes [6, 49].

$$E = \frac{L}{D} = \frac{C_L}{C_D} \tag{3.2}$$

At the beginning of the design, as a moderate and acceptable value among the existing sailplanes, it is decided to have our design a maximum glide ratio target value higher than 25. During the design process, it will be tried to achieve or enhance this value for our design.

3.3 Conceptual Design

Conceptual design is one of the important tasks during a sailplane design process which means defining the conceptual layout. Defining wing configuration and its vertical location, tail configuration, seating configuration, propulsion system configuration and landing gear configuration are some of the tasks during this design phase. Each different configuration of each section of an aircraft both has advantages and disadvantages. Therefore, for each part of a new design, it is important for a designer to select the most suitable configurations according to determined requirements at design requirement phase.

3.3.1 Wing Configuration

Aircraft wing configurations are categorized in terms of number of wings they have. Monoplane, biplane, sesquiplane and triplane are some of the most popular configurations, which are illustrated in Figure 3.3.

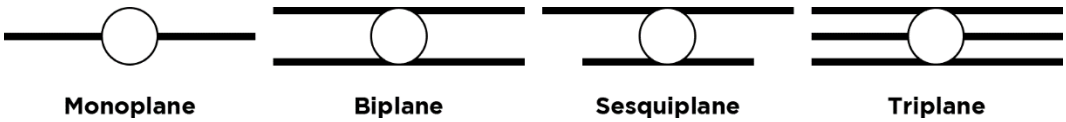

Figure 3.3 Wing configurations

In history, with old manufacturing technologies, single and long wing was not practical to stay level and rigid. Therefore, biplane and triplane wing configurations were developed to have more wing area with short wing spans. These configurations use the advantage of having larger wing area although having smaller wing span. High maneuverability and low stalling speeds without flaps are another advantages of them. The biggest disadvantage of these configurations is aerodynamic inefficiency because of having higher induced drag. Wings affect each other with their pressure regions and the aircraft needs higher angle of attacks to generate the same lift [6, 50].

Sesquiplane configuration has two wings as a similar configuration to biplane. The only difference of sesquiplane than biplane is having shorter lower wing. This configuration is common among the agricultural aircrafts.

The aircrafts with tandem and canard wing configurations have secondary wings on their fuselages. These additional wings also provides lift like main wings. The only difference between these two configurations is the size of their secondary wings.

Monoplane wing configuration is very common among not only sailplanes but also almost all of today's modern aircrafts. Therefore, in this study, monoplane configuration is selected as wing configuration for our design due to its being the easiest configuration for aerodynamic efficiency.

3.3.2 Wing Vertical Location and Structural Configuration

Wing vertical location has an important influence on other component designs of an aircraft including landing gear design, tail design and center of gravity [6]. There are mainly four types of wing vertical location relative to the fuselage center line, which are named as high, mid, low and parasol configurations, as shown in Figure 3.4. Each of them has different advantages and disadvantages. For our design, parasol and low wing configurations are out of the options because of their rarely usage on sailplanes.

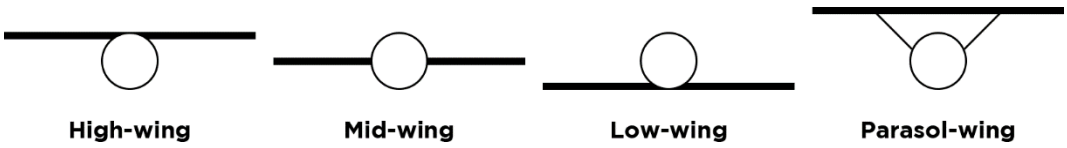

Figure 3.4 Wing vertical location according to fuselage

3.3.2.1 High-wing

High-wing configuration aircrafts have their main wings vertically higher than their fuselage center lines. The pilots of aircrafts having this configuration has a better lower-than-horizon view and more empty space inside the fuselage. This configuration is heavier than low-wing configuration [51]. For instance, horizontal tail areas are larger than low-wing configuration aircrafts because of the higher downwash.

High-wing configuration aircrafts tends to have more frontal area that increases drag. Drag force on the wing causes a nose-up pitching moment, which causes an adverse effect on longitudinal stability. This configuration makes sailplane to have more laterally dynamic stability and by means of increasing effect of dihedral, sailplane is laterally more stable. Therefore, lateral control is weaker than the other configurations [5].

The configuration makes the aerodynamic lower section of the fuselage possible to be also smoother than mid-wing. In addition, this configuration provides more lift than mid-wing configuration. Therefore, the design concludes in higher induced drag, higher maximum lift coefficient and correspondingly lower stall speed. During take-off and landing phases, when compared with low-wing configuration, the lower ground-effect of high-wing configuration causes lowering lift and results in long take-off run for an aircraft.

3.3.2.2 Low-wing

Low-wing configuration aircrafts have their main wings vertically lower than their fuselage center lines. Thus, the pilots are seated above the wing and has better higher-than-horizon view. The aircrafts having this configuration wings has lighter structure and lighter tail than high-wing configuration [5].

Low-wing configuration provides less lift because of having its wing as separate two parts and lowers maximum lift coefficient which causes lower stall speeds. This results in also lower landing performance, which means an increased need for more landing run. On the other hand, by means of the ground-effect, takeoff performance is better than high-wing configuration. Moreover, tail is more effective due to having less downwash on the tail.

Low-wing configuration has less frontal-area than other configurations and correspondingly drag is lower and the wing has less induced drag. Wing drag causes a nose-down pitching moment which is longitudinally stabilizing. Sailplanes having this configuration has higher lateral control than high-wing configuration, so they have less lateral static stability. In addition, the wings makes a lower contribution to the aircraft dihedral effect, thus the aircraft is laterally dynamically less stable. In conclusion, they are laterally more controllable, and thus more maneuverable.

3.3.2.3 Mid-wing

Mid-wing configuration aircrafts have their main wings almost intersecting with their fuselage center lines. In general, the advantages and disadvantages of mid-wing configuration is between high-wing and low-wing configurations. The most used vertical location for wings is mid-wing configuration among the sailplanes [2].

The main difference of mid-wing configuration from others is cutting wing spar into two separate parts. Therefore, the sailplane structure is heavier because of the necessity of reinforcing the wing root at the intersection with the fuselage. On the other hand, the volume inside the fuselage decreases.

The most important advantages of this configuration are having less interference drag and having aerodynamically more streamlined shape than the other configurations. It has neutral roll stability and also its maneuverability is higher than others. The pilots have both better higher-than-horizon and lower-than-horizon views.

Aerodynamic efficiency and the pilot visibility is the most important considerations because of the because of the objective of this study, which is aiming to design an experimental training sailplane. Therefore, mid-wing configuration is the most suitable wing vertical location configuration for our project owing to having the highest aerodynamic efficiency, the highest pilot visibility and other moderate characteristics.

3.3.2.4 Wing Structural Configuration

Wing structural configurations are divided into two groups named as strut-braced and cantilevered configurations, which are illustrated in Figure 3.5. Each configuration has advantages and disadvantages similar to other conceptual design parameters.

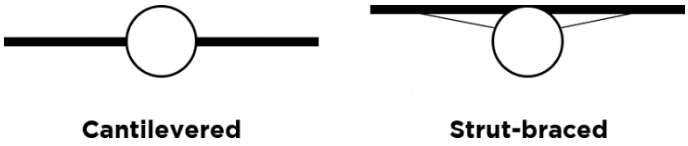

Figure 3.5 Wing structural configuration

Strut-braced wing structure have a supporting external structural member between wing and fuselage, which is named as strut. This member provides aircraft to have strength in terms of both compression and tension in flight. It increases drag of the aircraft by means of enhancing frontal area even though this type structure is lighter than cantilevered configuration.

Cantilevered configuration has main wing buried in the fuselage. This type of structure gives clean view and provides low drag for aircrafts. The disadvantage of this configuration is having higher maximum shear and bending loads than strut-braced which results in heavier wing structure so as to provide strength. The maximum shear is 2.3 times and moment is 4 times greater for the cantilevered structure than that of the strut-braced as stated in Figure 3.6.

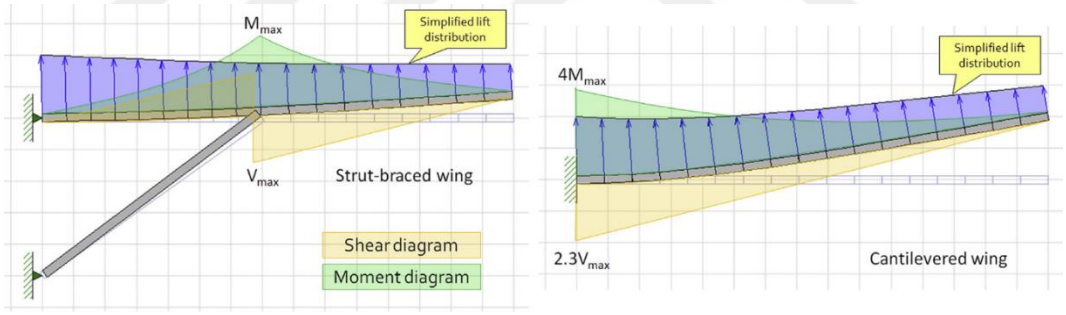

Figure 3.6 Wing shear and moment diagrams with simplified lift distributions for strut-braced and cantilever wings [6]

The objective of this thesis makes aerodynamic efficiency to be the more important consideration for our design. Therefore, cantilevered configuration is selected as the most suitable wing structural configuration for our design by means of having lower drag and being aerodynamically more streamlined.

3.3.3 Landing Gear Configuration

Landing gear configuration is the other configuration that is needed to be decided during conceptual design phase. There are ten most common type of landing gear configurations existing for aircrafts. These are: single main, bicycle, tail-gear, tricycle

or nose-gear, quadricycle, multi-bogey, releasable rail, skid, human leg and seaplane landing devices [1].

Figure 3.7 Single main landing gear configuration sailplane DG-1001T [52]

Most of the modern sailplanes uses mainly two of these landing gear configurations, which are named as single main and bicycle [6]. Single main landing gear configuration has one large main gear which is near the center of gravity of the sailplane and carries the main portion of the weight and load, as shown in Figure 3.7. There is other small gear at the aft portion of the sailplane. In the case of the main landing gear is located at the aft of the sailplane center of gravity, a skid can be located under the nose of the fuselage. On the other hand, bicycle configuration is extended version of single main configuration. Bicycle configuration differently has same sized two gears and each of these gears has the same distance from aircraft center of gravity. Therefore, each gear carries similar loads.

Due to being the simplest, cheapest and lightest one; single main landing gear configuration is selected as most suitable landing gear configuration for our design. It is decided to use retractable landing gear to make the sailplane aerodynamically more efficient.

3.3.4 Tail Configuration

In history, aircraft designers have used so many different aft tail configurations on their designs. Conventional, cruciform, T-tail, H-tail, V-tail, Y-tail, twin vertical tail, boom mounted are some of the existing popular configurations. Some of them are illustrated in Figure 3.8. The most popular tail configuration among the modern

sailplanes is the T-tail configuration, although the most common one among the general aviation aircrafts is the conventional configuration [51].

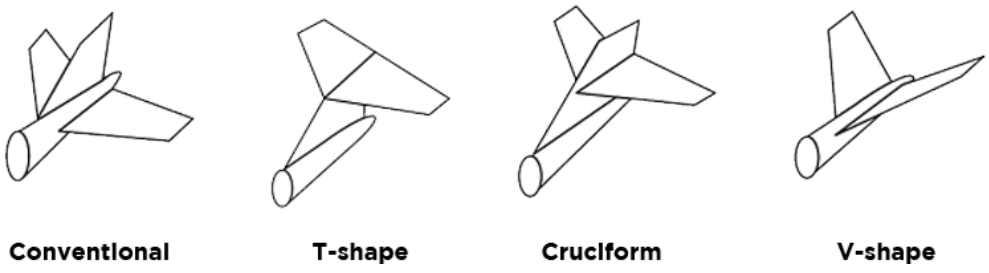

Figure 3.8 Tail configurations [5]

T-tail configuration has horizontal tail located on top of vertical tail. The most important advantage of this configuration is that the disturbed flow coming from the main wing does not affect the horizontal tail. This configuration provides higher efficiency than other configurations by means of being out of the wing wake, wing downwash and wing vortices regions. In addition, it makes possible to have smaller horizontal tail area and safer structure.

The disadvantage of T-tail is its heavier structure and the case of deep stall. The need for transferring bending moment, which is developed by the horizontal tail, to the fuselage makes structure of this configuration heavier. The reason of this weight increase is that vertical tail requires to have a strong main spar to overcome this bending moment.

The case of the deep stall is mentioned as a dangerous condition for T-tail configuration aircrafts. It is the stall condition of aircraft, when it has very high angle of attack than its normal stall angle. In this case, horizontal tail of the aircraft is exposed to the disturbed airflow coming from the main wing as stated in Figure 3.9. Moreover, the pitching up tendency of an aircraft can lead itself not to be recovered from the stall. [51].

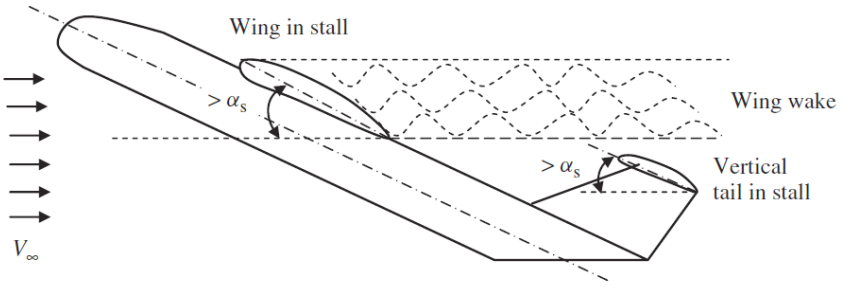

Figure 3.9 Deep-stall condition [5]

In this study, as the T-tail configuration is the most efficient and most common tail configuration among the sailplanes, it is decided to use on our design. Deep stall condition will be taken into consideration during preliminary design phase.

3.3.5 Seating Configuration

There are mainly two types of seating configurations for two-seater sailplanes, which are tandem and side-by-side configurations. Side-by-side configuration have both of the pilots sitting side to side. The sailplanes having this seating configuration has more drag because of their higher frontal area of fuselage.

Figure 3.10 Two-seater sailplane seating configurations [53,54]

Tandem seating configuration has student pilot sitting in front of the instructor pilot. Most of the training sailplanes have this configuration as pilot seating arrangement. In this study, with the aim of designing a training sailplane, tandem seating configuration is determined as the seating configuration.

3.3.6 Propulsion System Configuration

Propulsion system configurations are divided into two groups in terms of their engine locations. Pusher configuration has its engine located behind the center of gravity of

the aircraft and tractor configuration has its engine ahead of the aircraft center of gravity.

The sailplanes with the pusher propulsion system configuration generally has a foldable propeller at the nose of their fuselage. The main idea of this configuration is to reduce drag force of the sailplane while gliding and soaring operations. The system is started only during the climb or level flight operations and propeller is opened. Otherwise, propeller blades are folded to the fuselage. The main disadvantage of this configuration is the ground clearance limitation for the propeller diameter.

The sailplanes which have tractor propulsion system configuration has the same idea of reducing the drag force. They have a retractable mechanism different than the pusher configuration. The location of the propulsion system is generally at the top of the fuselage and also behind the pilots. The propeller diameter can be increased more flexible than other configuration. The need for extra volume inside the fuselage for the retracting mechanism is the main disadvantage of this configuration.

Figure 3.11 Sailplane propulsion system configurations [55,56]

In this study, which is aimed to design a self-sustaining sailplane, it is decided to use tractor propulsion system configuration. This selection will provide a possibility to improve the design to a self-launching sailplane in the future by means of more flexible propeller diameter limitations.

3.4 Conclusion

In this chapter, requirement defining and conceptual design phases of a new design two seater sailplane were carried out and presented. At requirement defining phase, mission profile was drawn as stated in Figure 3.2 and some critical target values were determined as stated in Table 3.2. At conceptual design phase, some critical

configurations were defined and conceptual layout of our target design was determined as stated in Table 3.3.

Table 3.2 Determined design requirements

Variable	Target Design Values
Maximum Takeoff Weight	700 kg
Wing Span	18 m
Cruise Speed	120 km/h
Never Exceed Speed	230 km/h
Stall Speed	Lower than 75 km/h
Maximum Glide Ratio	Higher than 25

Table 3.3 Determined conceptual layout

Configuration Type	Determined for Conceptual Design
Seating Configuration	Tandem Seating
Landing Gear Configuration	Retractable Single-main Landing Gear
Wing Configuration	Monoplane Configuration
Wing Vertical Location	Mid-wing Location
Tail Configuration	T-tail Configuration
Propulsion System Configuration	Retractable Propulsion Mechanism (Tractor)

CHAPTER 4

PRELIMINARY DESIGN

4.1 Introduction

The preliminary design phase of an aircraft design process starts after the conceptual design phase is completed. The aim of this stage is answering whether the generated conceptual design idea is viable in terms of so many disciplines. Wing, fuselage and tail design considerations are the main assignments that should be handled in this phase. Since structural assessments are out of the scope of this study, all of the parts will be considered externally and especially aerodynamic issues will be taken into consideration. Therefore, the main considerations of this phase will be based upon flight performance and mechanics.

4.2 Flight Performance and Mechanics

4.2.1 Flight Mechanics

There are mainly four forces acting on an aircraft during its flight as shown in Figure 4.1. These are thrust, drag, lift and weight forces. Weight force is the force generated due to gravity, and thrust force is the propulsive force generated by a propulsion unit such as propeller engines used on some powered sailplanes.

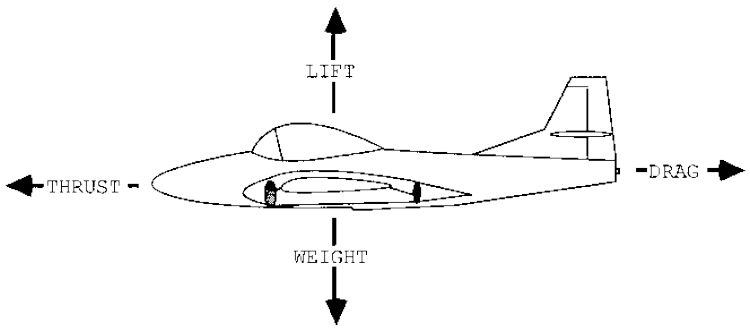

Figure 4.1 Forces on an aircraft during flight [57]

On the other hand, drag and lift forces are the aerodynamic forces given in Equation (4.1) and Equation (4.2), which are generated by the aircraft geometry. In these equations, ρ is the air density (kg/m^3), A is the corresponding area (m^2), V_∞ is the freestream velocity (m/s) and C_L and C_D are the dimensionless lift and drag coefficients, respectively.

$$L = \frac{1}{2}\rho A V_\infty^2 (C_L) \tag{4.1}$$

$$D = \frac{1}{2}\rho A V_\infty^2 (C_D) \tag{4.2}$$

Drag coefficient can be defined as sum of the parasitic (D_P) and form drags (D_F) as shown in Equation (4.3). Parasitic drag also can be divided into components named as zero-lift drag coefficient (C_{D_0}) and induced drag coefficient (C_{D_i}) as shown in Equation (4.4). In the Equation (4.5), AR is the wing aspect ratio and e is the Oswald efficiency factor (or wing planform efficiency factor). This formulation can be written also in the form of Equation (4.6) with a constant of K (drag due to lift factor).

$$D_{TOTAL} = D_\mathrm{P} + D_\mathrm{F} \tag{4.3}$$

$$C_D = C_{D_0} + C_{D_i} \tag{4.4}$$

$$C_{D_i} = \frac{C_L^2}{\pi * AR * e} \tag{4.5}$$

$$C_{D_i} = K C_L^2 \tag{4.6}$$

4.2.2 Steady Flight Performance

In steady flight of a sailplane along a straight line, whether it is level flight, climb or dive, summation of vertical and horizontal forces, stated in Figure 4.3, are zero. Thus, as given in Equation (4.7), thrust force is equal to drag force and as given in Equation (4.8) weight force is equal to lift force.

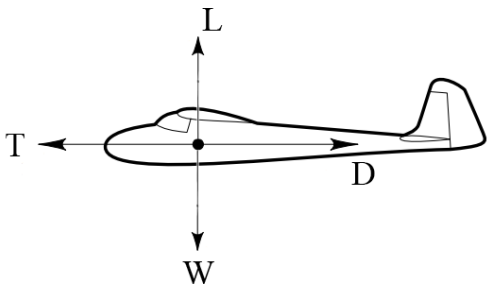

Figure 4.3 Forces acting on an aircraft during a steady flight [4]

$$D = T = \frac{1}{2}\rho A V^2 (C_D) \tag{4.7}$$

$$L = W = \frac{1}{2}\rho A V^2 (C_L) \tag{4.8}$$

The wing loading of an aircraft is an important parameter during design phases. It means the ratio of weight of the aircraft (W) and its wing area (S). Wing loading critically effects so many flight performance parameters such as takeoff and landing distances, stall speeds, sink speeds, maneuverability and stability. In order to have a function of wing loading (W/S), Equation (4.8) can be written as stated in Equation (4.9), where φ is glide angle.

$$V = \sqrt{\frac{W}{S}\frac{2cos\varphi}{\rho C_L}} \tag{4.9}$$

Thus, the horizontal (V_x) and vertical (V_y) components of the velocity will be as stated in Equations (4.10) and (4.11).

$$V_x = V cos\varphi = cos\varphi \sqrt{\frac{W}{S}\frac{2cos\varphi}{\rho C_L}} \tag{4.10}$$

$$V_y = \frac{V_x}{E} = \frac{1}{E} cos\varphi \sqrt{\frac{W}{S}\frac{2cos\alpha\varphi}{\rho C_L}} \tag{4.11}$$

At normal flight conditions of a sailplane, φ is a very small angle that makes the value of $cos\varphi$ very close to 1. Therefore, without too much error, $cos\varphi$ can be said to have the value 1. Hence, the equations will be as stated in Equations (4.12) and (4.13).

$$V_x = \sqrt{\frac{W}{S}\frac{2}{\rho C_L}} \tag{4.12}$$

$$V_y = \frac{1}{E}\sqrt{\frac{W}{S}\frac{2}{\rho C_L}} \tag{4.13}$$

As for all aircrafts, sailplanes has a minimum horizontal speed to maintain their flights, which is called as stall speed. The minimum horizontal speed has a relation with wing loading, air density and maximum lift coefficient as stated in Equation (4.14).

$$V_{x_{min}} = V_S = \sqrt{\frac{W}{S}\frac{2}{\rho C_{L_{max}}}} \tag{4.14}$$

The other critical velocity for sailplanes is the sink speed (rate of descent), which is the vertical speed of the aircraft. It is desired for sailplanes to have minimum sink speed as possible. From the Equation (4.13), the minimum value of the vertical speed can be written as Equation (4.15).

$$V_{y_{min}} = V_s = \sqrt{\frac{2W}{\rho S}} \cdot \frac{1}{E\sqrt{C_L}} \tag{4.15}$$

It can be clearly seen from the equation that the value of $E\sqrt{C_L}$, which is called as climbing index, has critical importance on a sailplane's sink speed. This expression can be also written as Equation (4.16), which represents the importance of lift and drag coefficients on the sink speed. In order to increase endurance of a sailplane, climbing index need to be maximized during design phases.

$$E\sqrt{C_L} = \frac{C_L^{3/2}}{C_D} \tag{4.16}$$

4.2.3 Gliding Flight Performance

Cross country flight of a sailplane includes a number of gliding flights and thermal circling flights. Therefore, gliding flight is an important flight phase for a sailplane to take into consideration. A gliding sailplane's flight path follows a linear slope with an angle called as glide angle (φ) shown in Figure 4.2. During this flight, a sailplane is subjected to total aerodynamic forces (F), which is the summation of the drag force (D) and the lift force (F). Moreover, weight of the sailplane (W) has vertical component (W') and horizontal thrust force components (T). For the simplicity, the

point, where the forces are applied, is assumed to be at center of gravity of the sailplane.

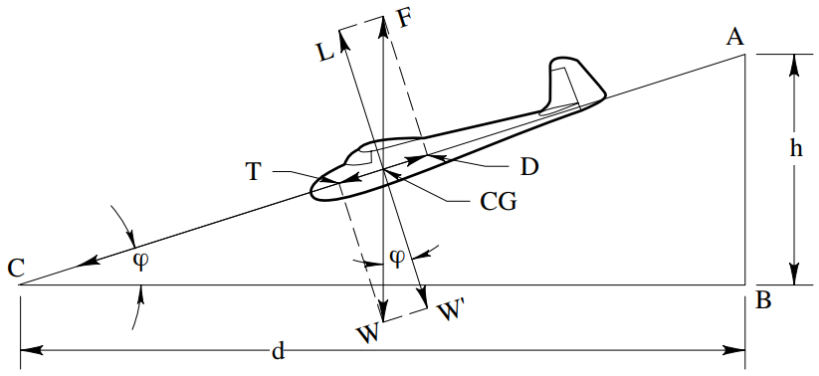

Figure 4.2 Forces acting on an aircraft during gliding flight [4]

When the forces divided into their components, from the similarity of the triangles and knowing that the glide ratio formula in Equation (3.2); an equilibrium can be written as given in Equation (4.17) and Equation (4.18).

$$E = \frac{L}{D} = \frac{C_L}{C_D} = \frac{d}{h} \tag{4.17}$$

$$tan\varphi = \frac{D}{L} = \frac{h}{d} = \frac{1}{E} \tag{4.18}$$

This formulas represents that when the aerodynamic efficiency of a sailplane is increased, the trajectory slope will decrease. Moreover, for a given altitude loss (h), higher aerodynamic efficiency means that the horizontal distance travelled (d) is increased. In other words, range is increased. Therefore, in this study, as desired for all the sailplanes, an effort will be made to increase the glide ratio during the design. The initial target of this study to have a glide ratio of our design higher than 25 as it was stated before in Table 3.2.

4.2.4 Turning Flight Performance in Thermals

In thermals, the achieved climb rate of a sailplane strongly depends on its turning flight performance. Therefore, the mechanics of turning flight should be investigated. The forces acting on sailplane during turning flight was given in Figure 4.4 where CF is the centrifugal force, W is the weight, L is the lift force, Ω is the turn rate and φ is the bank angle.

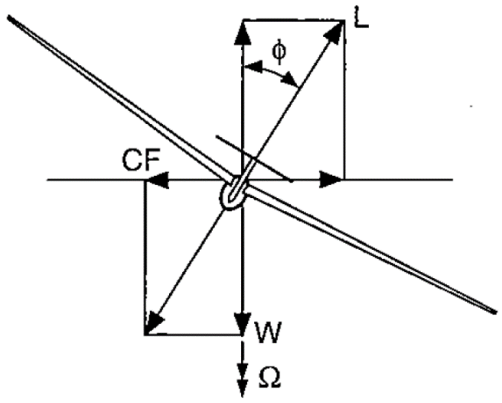

Figure 4.4 Forces acting on an aircraft during turning flight [3]

From the figure, Equations (4.19) and (4.20) gives the relationships according to force balance between lift force, centrifugal force and weight. Here m is the mass of the sailplane, g is the acceleration of gravity (9.61 m/s^2), V_K is the circling airspeed and r is the turn radius of the sailplane.

$$CF = Lsin\phi = \frac{mV_K{}^2}{r} \tag{4.19}$$

$$W = Lcos\phi = mg \tag{4.20}$$

In turning flight, as they were written for the steady flight condition in the Equation (4.9) and (4.15), airspeed and sink rate can be written as given in Equation (4.21) and (4.22), respectively.

$$V_K = \sqrt{\frac{W}{S}\frac{2cos\phi}{\rho C_L}} \tag{4.21}$$

$$V_{S_C} = \frac{C_D}{C_L^{3/2}cos^{3/2}\phi}\sqrt{\frac{W}{S}\frac{2}{\rho}} \tag{4.22}$$

These equations lead to Equations (4.23), (4.24) and (4.25). The third variable among the variables ϕ, V_K and r can be easily determined from the Equations (4.21) and (4.23).

$$tan\phi = \frac{CF}{W} = \frac{\frac{mV_K^2}{r}}{mg} \tag{4.23}$$

$$V_K = \sqrt{rgtan\phi} \tag{4.24}$$

$$r = \frac{V_K^2}{gtan\phi} \tag{4.25}$$

There is a strong relationship between the turn radius, sink rate, airspeed and bank angle of a sailplane during turning flight as it can be clearly seen in Figure 4.5. At a constant circling airspeed and turn radius, increasing the bank angle decreases the sink rate of the sailplane. Likewise, at constant airspeed and bank angle, the increase in turn radius decreases the sink rate. These relationships can be very useful to increase the desired performance of a sailplane during turning flight inside the thermals.

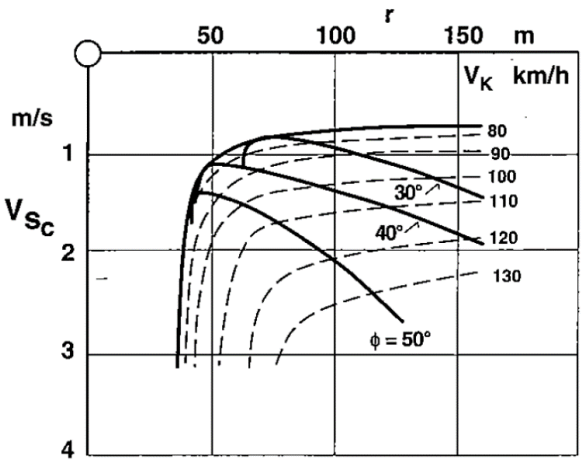

Figure 4.5 Turn diagram relating the turn radius and bank angle to the sink rate [3]

The rate of climb (V_C) during the circling thermal flight is also a function of thermal strength and the sink rate as stated in Equation (4.26). In order to have a high climb rate, a high strength thermal and low sink rate is desirable for a sailplane.

$$V_C = V_T - V_{S_c} \tag{4.26}$$

Therefore, the strength of a thermal is an important parameter for a sailplane, which changes depending on the profile of the thermal. The change of thermal strength versus distance from center of thermal, according to Horstmann model [58], is given in Figure 4.6.

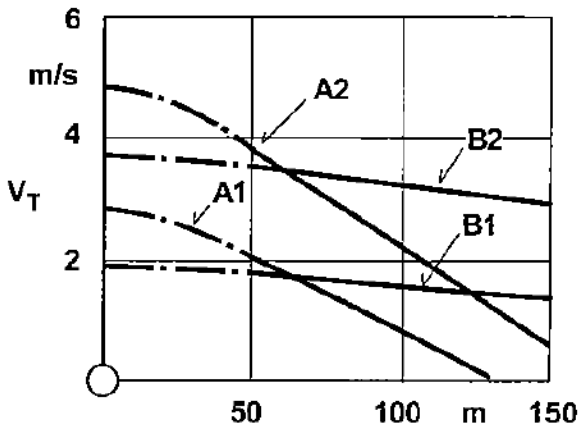

Figure 4.6 Thermal strength versus distance from center of thermal according to standard thermal profiles in Horstmann model [3]

4.3 Wing Design

Wing design is one of the most important tasks for a designer to overcome during an aircraft design process. In three-dimension, as for all aircrafts, wing can be defined as the body, which is the lifting surface of a sailplane. In two-dimension, cross section shape of a wing is named as airfoil and the top-view shape of a wing is named as planform geometry. An aerodynamically efficient wing can be designed when the suitable airfoil(s) and planform geometry coupled. A designer need to optimize these geometrical parameters with the aim of obtaining an efficient wing geometry complying with requirements of the design. Therefore, this part of the study includes the airfoil selection together with the design of suitable planform geometry and numerical analyses of the final wing design.

4.3.1 Airfoil Selection

An airfoil is usually identified with geometrical terms as defined in Figure 4.7. The line drawn horizontally from leading to trailing edge of the airfoil is named as chord-line. The mean-camber is the line that determines amount of the curvature of the airfoil with respect to its upper and lower surfaces. The airfoil is called as symmetrical if the mean-camber and chord-line of an airfoil are intersected. Additionally, maximum thickness is another important parameter that describes the airfoil geometry. Its value and its distance from the leading edge is generally described as a percentage of the airfoil chord-line length.

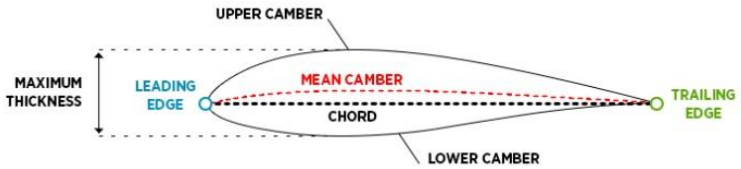

Figure 4.7 An airfoil geometry

In this study, two different airfoils will be selected for root and tip sections of our sailplane wing from historical usage data existing in University of Illinois at Urbana-Champaign's database [59] rather than designing new airfoils. With the aim of our study, the airfoils which have the most frequent usage on two-seater sailplanes were selected to compare their aerodynamic performances. The airfoil geometries of selected airfoils Eppler E603, NACA 23012, Wortmann FX S-02-196, Wortmann FX 73-K170, Wortmann FX 60-126, Wortmann FX 61-184, Wortmann FX 62-K-153, Goettingen 533 and Goettingen 549 were given in Figure 4.8. The data shows not only frequent usage of the selected airfoils but also their application trends at root or tip sections of sailplane wing designs. The selected airfoils were divided into two groups as stated in Table 4.1 by means of this data.

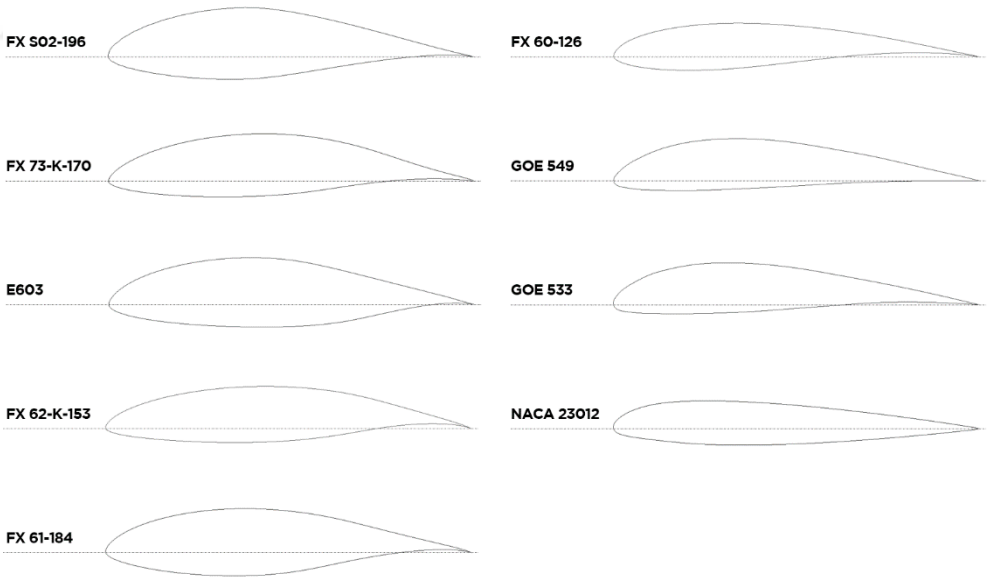

Figure 4.8 Selected airfoil geometries

Table 4.1 Groups of Selected Airfoils

Root Section Airfoils	Max. Thickness	Tip Section Airfoils	Max. Thickness
Eppler E603	19%	Goettingen 533	13,82%
Wortmann FX S-02-196	19,6%	Goettingen 549	13,85%
Wortmann FX 73-K170	17%	NACA 23012	12%
Wortmann FX 61-184	18,4%	Wortmann FX 60-126	12,6%
Wortmann FX 62-168	16,8%		

On the purpose of obtaining and comparing aerodynamic performances of the airfoils, numerical analyses should be performed. There are so many programs able to perform these analyses, such as XFLR5, AeroFoil, VisualFoil, Ansys FLUENT and Solidworks Flow Simulation. In this study, XFLR5 program will be used to perform the analyses.

4.3.1.1 XFLR5 Program Background

XFLR5 is a user-friendly design and analysis program for airfoils and bodies. The program uses XFOIL codes for two-dimensional airfoil aerodynamic performance analysis. The program is capable of calculating lift, drag, pitching moment and pressure coefficients of airfoils in two-dimension by using fully coupled viscous/inviscid interaction method with high-order panel method.

XFLR5 inviscid analysis in two-dimension has a linear-vorticity stream function formulation. For the analysis, the program constructs an inviscid airfoil flow field in two-dimension. This flow field consists of not only a freestream flow but also a vortex sheet on the airfoil together with a source sheet on the wake and airfoil surface. Thus, stream function can be expressed as

$$\Psi(x,y) = u_\infty - v_\infty + \frac{1}{2\pi}\int \gamma(s) lnr(s;x,y) + \frac{1}{2\pi}\int \sigma(s)\theta(s;x,y)ds \qquad (4.27)$$

where σ is source sheet strength, γ is vortex sheet strength, s is the coordinate through the vortex and source sheets, $v_\infty = q_\infty sin\alpha$ and $u_\infty = q_\infty cos\alpha$ are freestream velocity components, r is the magnitude of the vector between the field point x, y and the point s and θ is the angle of the vector.

The airfoil surface and wake trajectory are both divided into a number of flat panels. As shown in Figure 4.9, the number of panel nodes on the airfoil is N and the number of panel nodes on the wake is N_w. There are linear vorticity distributions (γ_i) at each airfoil panel. Additionally, there is a constant source strength (σ_i) for each airfoil and wake panel associated with them.

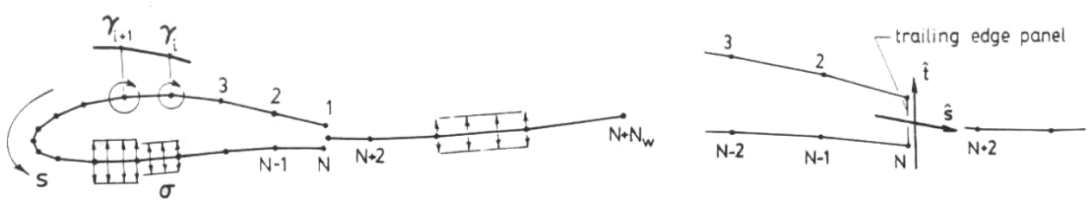

Figure 4.9 Vorticity and source distributions and panels of airfoil and wake

Defining the unit stream functions with local panel coordinates and equating the stream function Ψ_0, which has some constant value, at each node on the airfoil gives Equation (4.28)

$$\sum_{j=1}^{N}\left(a_{i,j}\gamma_j\right) - \Psi_0 = -u_\infty y_i + v_\infty x_i - \sum_{j=1}^{N+N_w-1}\left(b_{i,j}\sigma_{0,j}\right) \;;\; 1 \le i \le N \quad (4.28)$$

where $a_{i,j}$ and $b_{i,j}$ are the coefficient matrices and x_i and y_i are airfoil panel nodes. Combining linear system with Kutta condition, which means equating sum of the strengths of vortex panels at trailing edge nodes to zero, gives Equation (4.29)

$$\gamma_1 + \gamma_N = 0 \quad (4.29)$$

which is a linear system with N+1 equations and N+1 unknown values of γ_i. Inside the airfoil, the flow is stagnant. Hence, the surface velocity is equal to surface vorticity and expressed as

$$\gamma_i = q_i \quad (4.30)$$

where q_i is surface velocity. Hence, pressure coefficient can be expressed with respect to surface vorticity by applying Bernoulli's equation

$$C_p = 1 - \left(\frac{\gamma}{q_\infty}\right)^2 \quad (4.31)$$

where freestream velocity is $q_\infty = \sqrt{{v_\infty}^2 + {u_\infty}^2}$.

For a viscous analysis with a known airfoil geometry, XFLR5 program gives solution for airfoil surface vorticity by solving matrix equation and Kutta condition by means of Gaussian elimination as

$$\gamma_i = \gamma_{0i} cos\alpha + \gamma_{90i} sin\alpha + \sum_{j=1}^{N+N_w-1} \left({b'}_{i,j} \sigma_{0,j} \right) \quad ; \quad 1 \leq i \leq N \quad (4.32)$$

where γ_0 and γ_{90} are the vorticity distributions, which is a freestream α of 0 and 90 degrees. ${b'}_{i,j} = -{a^{-1}}_{i,j} b_{i,j}$ is the source influence matrix. For viscous flows, the boundary layer equations should be added to the Equation (4.30) to obtain solvable closed system because of the source strengths are unknown [25].

4.3.1.2 Numerical Analysis Validity Verification

For the reliability verification of XFLR5 two-dimensional viscous analysis results, an analysis was performed on Eppler E387 airfoil at the same conditions with wind tunnel experiment results at Langley Low-turbulence Pressure Tunnel [60]. XFLR5 analyses were performed at $2x10^5$ Reynolds number and 0.06 Mach number, which was same as the reference experimental study. As it is observed by [61], to define an airfoil in XFLR5, using more than 150 number of panels does not show an important difference in the results. Although it is enough to use 150 number of panels, it is selected to use 250 panels as performing analyses takes very little time for XFLR5.

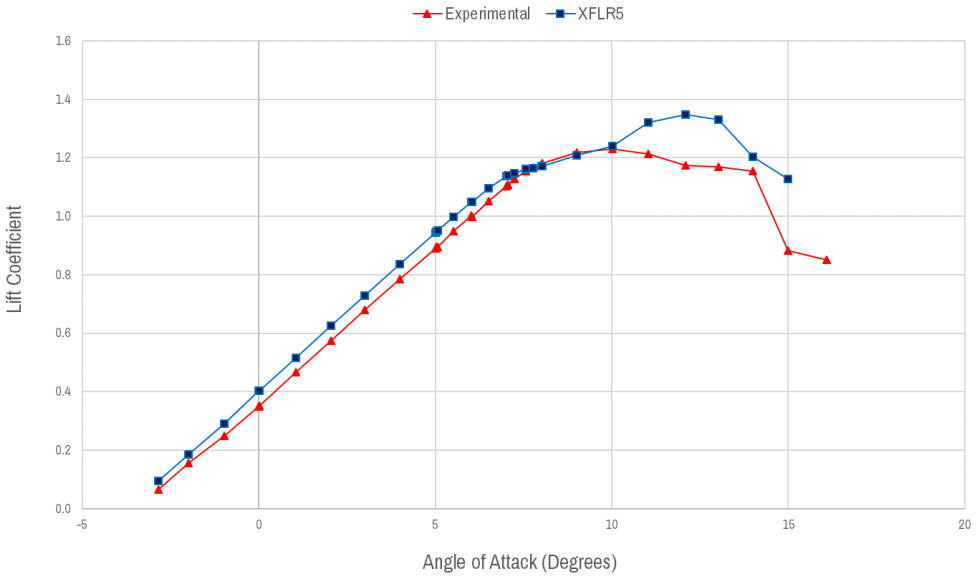

Figure 4.10 Comparison of experimental results with XFLR5 analysis results in terms of lift coefficient changing with angle of attack

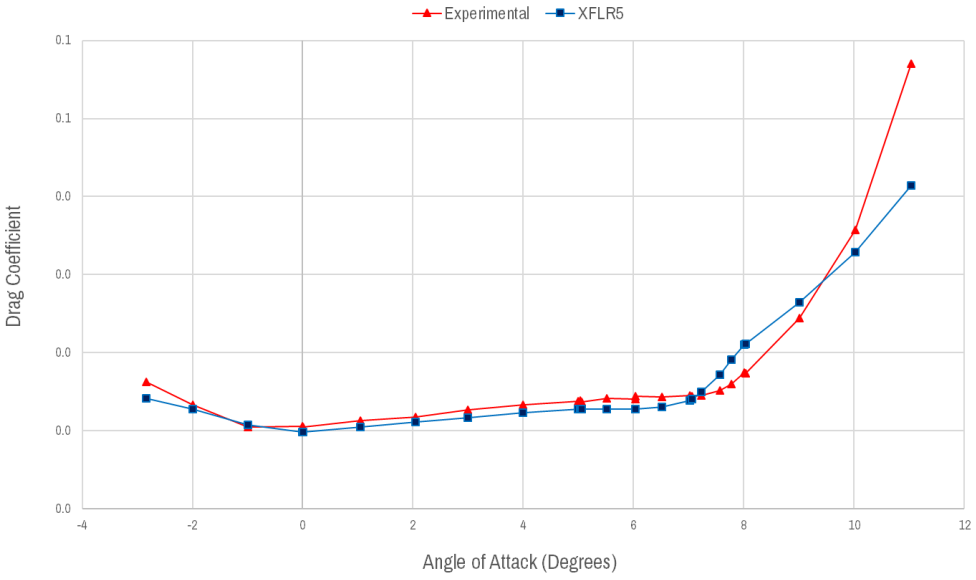

Figure 4.11 Comparison of experimental results with XFLR5 analysis results in terms of drag coefficient changing with angle of attack

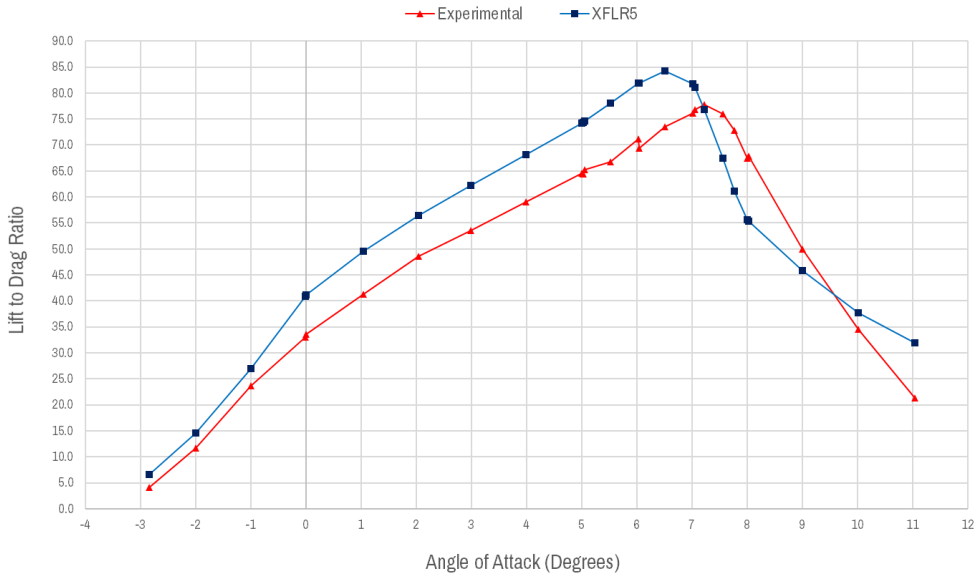

Figure 4.12 Comparison of experimental results with XFLR5 analysis results in terms of lift to drag ratio changing with angle of attack

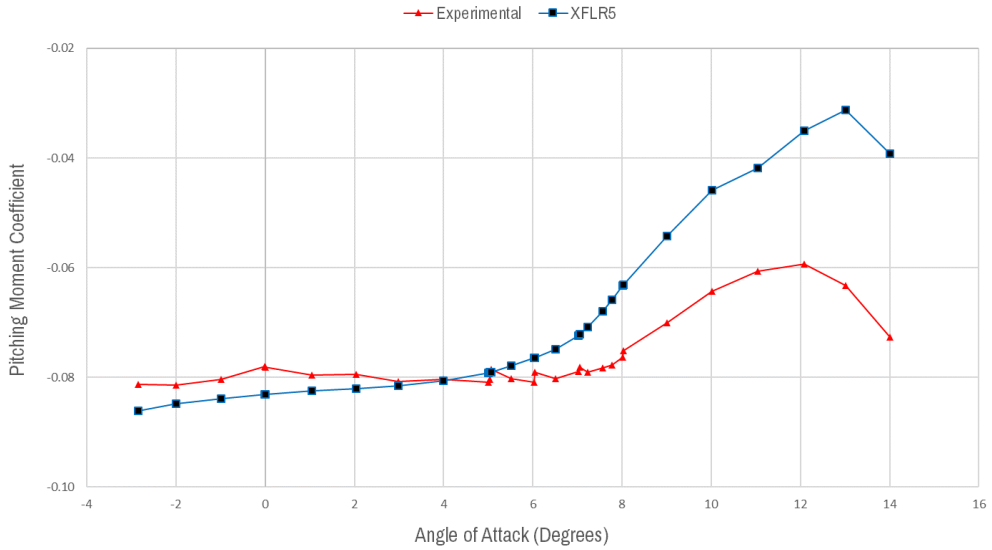

Figure 4.13 Comparison of experimental results with XFLR5 analysis results in terms of pitching moment coefficient changing with angle of attack

As a result of the analyses, Figure 4.10 and Figure 4.11 shows that XFLR5 gives very close lift coefficient and drag coefficient results to experimental data up to stall angle of attack, which is 10 degrees. Lift and drag coefficients results of XFLR5 and experimental data have difference lower than 10 percent in average. As it can be clearly

seen in Figure 4.12, lift to drag ratio results of XFLR5 and experimental data have difference lower than 15 percent in average. Additionally, maximum lift to drag ratio is 8.3 percent more than the experimental data. Figure 4.13 indicates that, pitching moment coefficient results of XFLR5 are compatible with experimental data. In average, their difference is lower than 15 percent in terms of their values. At low angle of attacks, XFLR5 gives very close results to experimental data with difference lower than 6 percent.

Consequently, it was obtained that, XFLR5 gives results with difference, which is lower than 10 percent in average from experimental data in terms of drag, lift and pitching moment coefficients.

4.3.1.3 Numerical Analysis Results, Discussion and Airfoil Selection

The analyses were performed on XFLR5 at $2x10^5$ Reynolds number and from -5 to 20 degrees with 0.5 degree intervals. For selected tip section airfoils, depending on changing angle of attack; lift coefficient, drag coefficient, lift to drag ratio, pitching moment coefficient and climb index diagrams were shown in Figure 4.14, 4.15, 4.16, 4.17 and 4.18, respectively. The diagrams including same parameters were given for the root section airfoils in Figure 4.19, 4.20, 4.21, 4.22 and 4.23.

In Figure 4.14 and 4.19, it is observed that, lift coefficient of each airfoil increased up to different angle of attacks and decreased after their peak values. For the selected airfoils, it can be clearly seen in Table 4.2, FX 73-K170 and FX 60-126 airfoils have the maximum $C_{L_{max}}$ value among their groups, which were root and tip section airfoils. Regarding the flight mechanics, higher $C_{L_{max}}$ refers lower stall speed for a wing. Hence, these two airfoils were found to provide lower stall speeds among the other selected airfoils. Moreover, angle of attack of maximum lift condition ($\alpha_{C_{L_{max}}}$) is another important parameter that determines stall angle of attack. The higher the $\alpha_{C_{L_{max}}}$, the higher the stall angle of attack of a wing. In Table 4.2, it was obtained that E603 and FX 60-126 airfoils have the maximum values of $\alpha_{C_{L_{max}}}$. Hence, these two airfoils were found to provide maximum stall angle of attack among the other selected airfoils.

In Figure 4.15 and 4.20, as expected, drag coefficient of each airfoil varied a little up to different angle of attacks and later on increased suddenly in a short angle of attack interval. At maximum lift condition, drag coefficients of the selected airfoils were given in Table 4.2. Having smaller drag coefficient at maximum lift condition is important in terms of thermaling performance of sailplanes. As it was stated in Table 4.2, FX 62-K-153 has the minimum value of drag coefficient at maximum lift condition among the root section airfoils. Additionally, at the maximum lift condition, GOE 549 has the minimum drag coefficient value among the tip section airfoils. Thus, these two airfoils were found the most efficient airfoils among the selected airfoils in terms of thermaling performance.

In Figure 4.18 and Figure 4.23, diagrams of the climb indexes of the airfoils were given changing with angle of attack. Higher climb index means lower power required to maintain flight and lower sink rate. From the results, it was obtained that, FX 62-K-153 and GOE 533 airfoils has the maximum climb index values among the others. So, these two airfoils were found the most efficient airfoils among the other selected airfoils in terms of climb index.

Figure 4.16 and 4.21 shows that, each airfoil has increasing lift to drag ratio up to different angle of attacks. Later on, it was seen that, after the peak value, glide ratio decreased with the increasing angle of attack for all the selected airfoils. For sailplanes, lift to drag ratio is a parameter, which determines the aerodynamic efficiency. The higher the glide ratio, the higher the horizontal distance travelled in a time interval, which has a crucial importance for sailplanes. It can be clearly seen in Table 4.3, FX 62-K-153 and FX 61-184 airfoils have the maximum glide ratios among the other root and tip section airfoils, respectively. Hence, these two airfoils were found the most efficient airfoils among the selected airfoils in terms of lift to drag ratio.

As it is observed in Figure 4.17 and 4.22, except for NACA 23012, each of the airfoils has negative values for entire of the angle of attack interval. Zero lift pitching moment coefficient has an important role on sailplane stability. If C_{M_0}has a negative value, sailplane is said to be stable. Also, stability increases if C_{M_0} has closer value to zero. It was observed from Table 4.2, E603 and NACA 23012 airfoils has not only negative,

but also the closest C_{M_0} values to zero. Hence, these two airfoils were found to be most suitable in terms of stability.

As it is stated before, for tip section airfoils, it is desirable to have smaller maximum thickness value because thin airfoils produces lower induced drag. Oppositely, the root section airfoils desired to be as thick as possible because of needed structural strength and volume for water ballast tanks.

Taking results of the analyses into consideration, all of the selected root and tip section airfoils were scored from 1 to 5 according to the determined criteria, as stated in Table 4.4 and Table 4.5.

Table 4.2 Analysis Results for Each Airfoil in terms of Maximum Lift Coefficient and Its Angle of Attack, Pitching Moment Coefficient at Zero Lift Condition and Drag Coefficient at Maximum Lift Condition

Airfoil Name	$C_{L_{max}}$	$\alpha_{C_{L_{max}}}$**(degree)**	C_D **at** $C_{L_{max}}$	C_{M_0}
E603	1.34	12	0.2920	-0.0712
FX S02-196	1.38	10	0.0226	-0.098
FX 61-184	1.40	10.5	0.0253	-0.1018
FX 73-K-170	1.44	11	0.0284	-0.1045
FX 62-K-153	1.36	8.5	0.02	-0.1315
NACA 23012	1.31	13.5	0.037	-0.0079
GOE 533	1.62	13	0.033	-0.0112
GOE 549	1.53	12.5	0.028	-0.1034
FX 60-126	1.55	14	0.052	-0.1177

Table 4.3 Analysis Results for Each Airfoil in terms of Maximum Glide Ratio and Its Angle of Attack

Airfoil Name	$(L/D)_{max}$	$\alpha_{(L/D)_{max}}$**(degree)**	$(C_L^{3/2}/C_D)_{max}$
E603	58.1	10.5	66.8
FX S02-196	68.6	8.5	79.6
FX 61-184	69.9	8.5	81.5
FX 62-K-153	76.7	7.5	88.5
FX 73-K-170	62.4	8.5	76.2
NACA 23012	51.1	9.5	55.4
GOE 533	74.1	8	88.6
GOE 549	74.3	7.5	86.7
FX 60-126	79.6	5.5	85.2

Table 4.4 Root Section Airfoils Comparison Scores

Airfoil Name	$(L/D)_{max}$	$C_{L_{max}}$	$\alpha_{C_{L_{max}}}$	$C_D\ at\ C_{L_{max}}$	$(C_L^{3/2}/C_D)_{max}$	C_{M_0}	**Thickness**	**AVE.**
E603	1	1	5	1	1	5	4	2.57
FX S02-196	3	3	2	4	3	4	5	3.43
FX 61-184	4	4	3	3	4	3	3	3.43
FX 73-K-170	2	5	4	2	2	2	2	2.71
FX 62-K-153	5	2	1	5	5	1	1	2.86

Table 4.5 Tip Section Airfoils Comparison Scores

Airfoil Name	$(L/D)_{max}$	$C_{L_{max}}$	$\alpha_{C_{L_{max}}}$	$C_D\ at\ C_{L_{max}}$	$(C_L^{3/2}/C_D)_{max}$	C_{M_0}	**Thickness**	**AVE.**
NACA 23012	1	1	3	2	1	4	4	2.29
GOE 533	2	4	2	3	4	3	2	2.86
GOE 549	3	2	1	4	3	2	1	2.29
FX 60-126	4	3	4	1	2	1	3	2.57

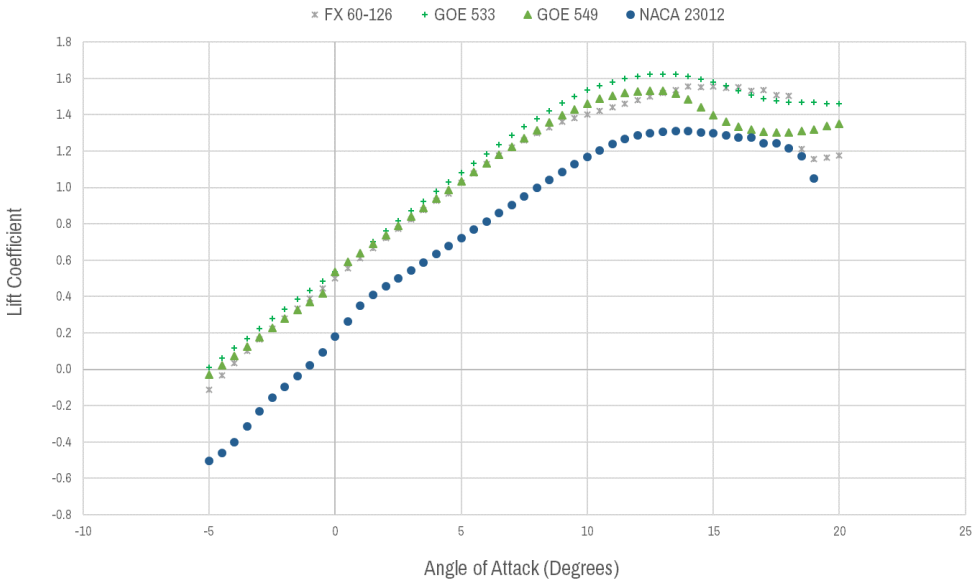

Figure 4.14 Lift coefficients of tip section airfoils changing with angle of attack

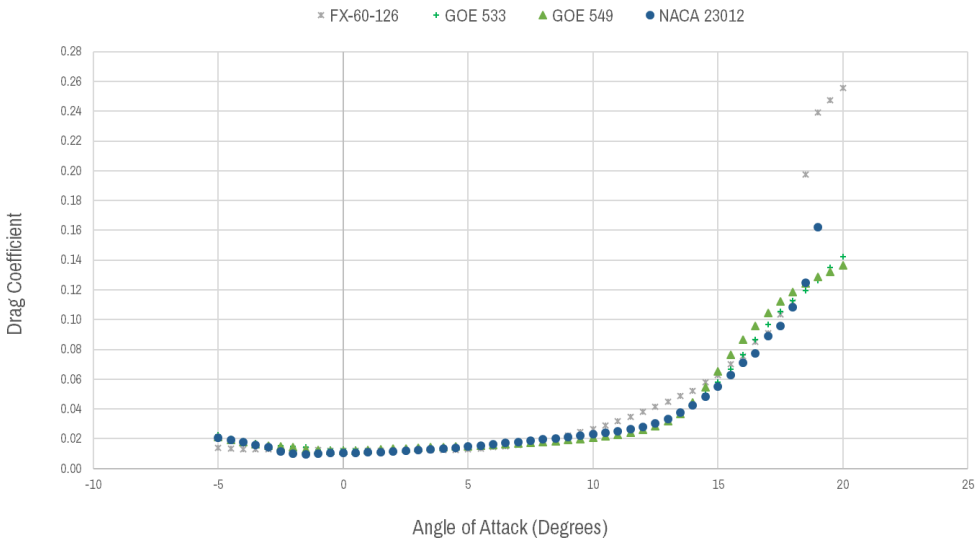

Figure 4.15 Drag coefficients of tip section airfoils changing with angle of attack

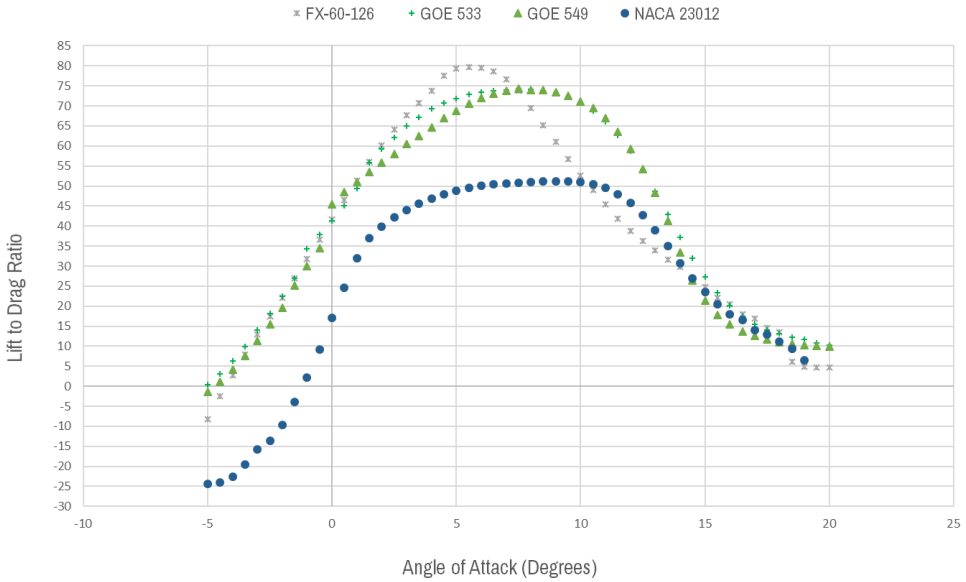

Figure 4.16 Lift to drag ratios of tip section airfoils changing with angle of attack

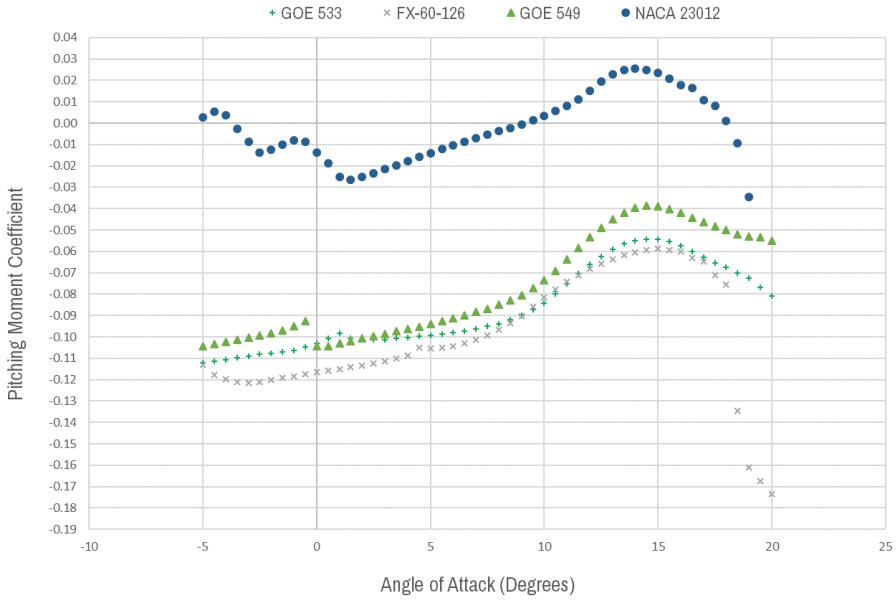

Figure 4.17 Pitching moment coefficients of tip section airfoils changing with angle of attack

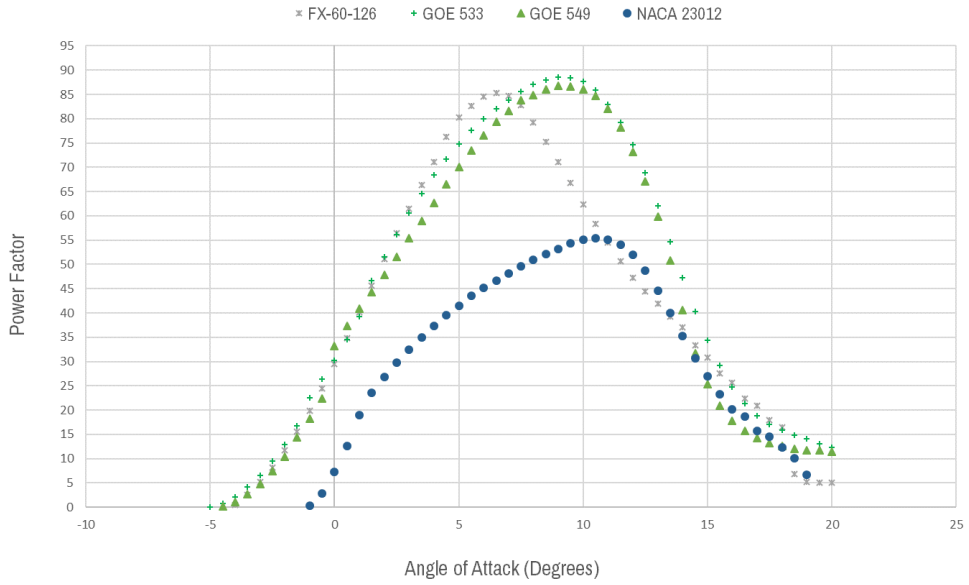

Figure 4.18 Climb indexes of tip section airfoils changing with angle of attack

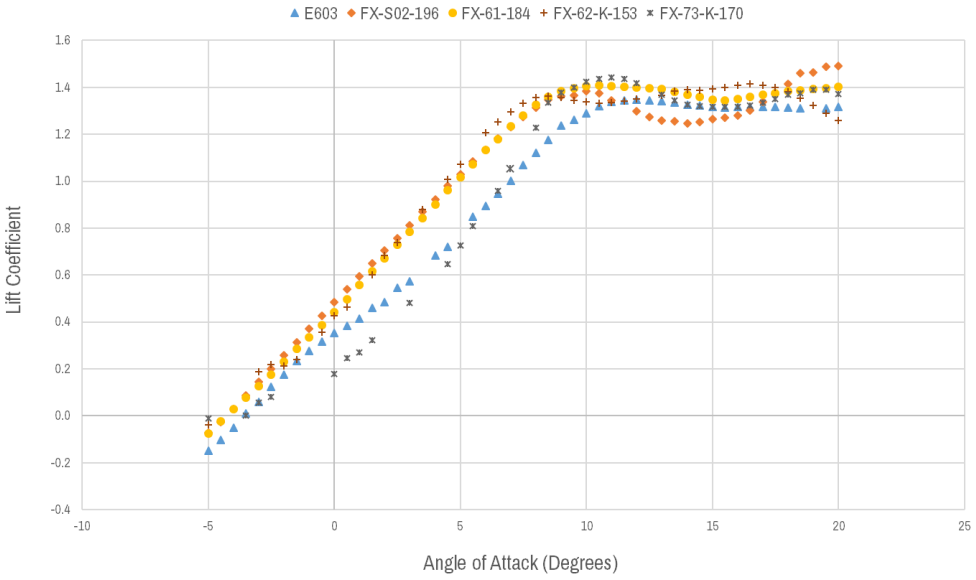

Figure 4.19 Lift coefficients of root section airfoils changing with angle of attack

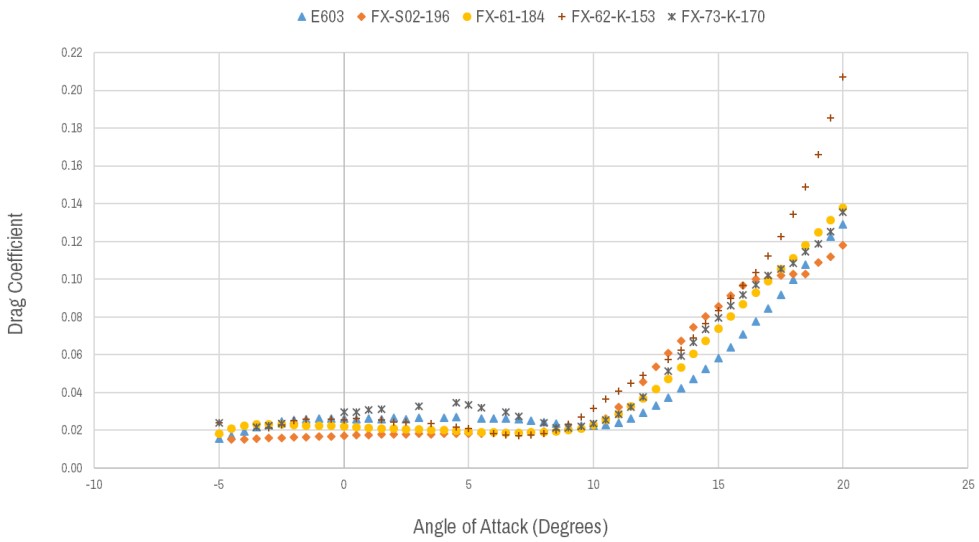

Figure 4.20 Drag coefficients of tip section airfoils changing with angle of attack

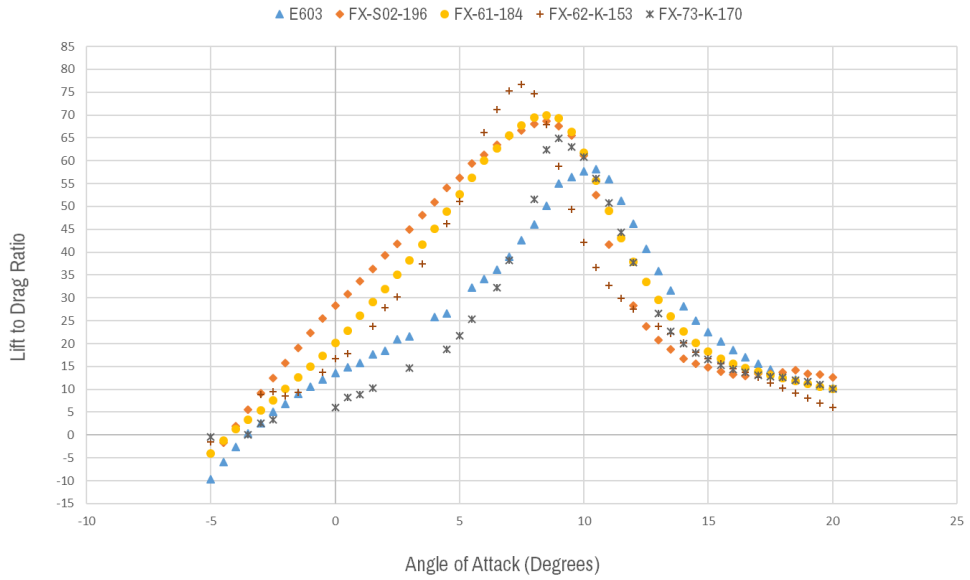

Figure 4.21 Lift to drag ratios of tip section airfoils changing with angle of attack

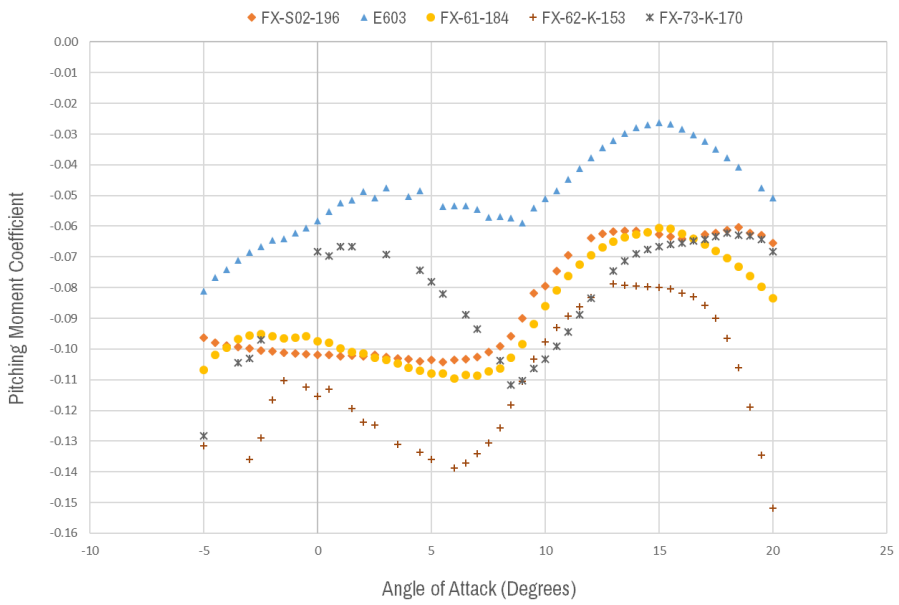

Figure 4.22 Pitching moment coefficients of root section airfoils changing with angle of attack

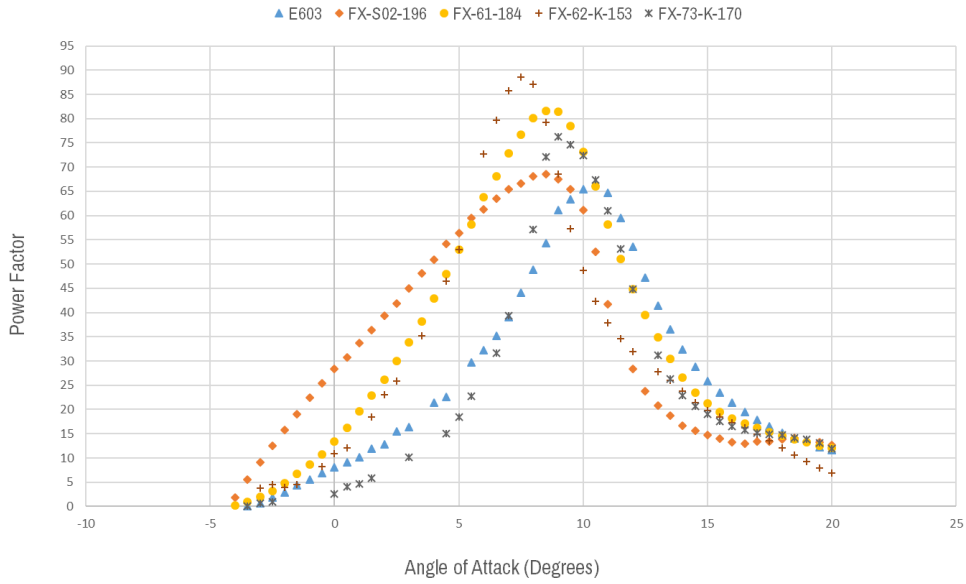

Figure 4.23 Climb indexes of root section airfoils changing with angle of attack

With the results of the analyses, airfoils were scored from 1 to 5 with respect to determined criteria as stated in Table 4.4 and Table 4.5. Consequently, in terms of determined seven criteria, Wortmann FX S02-196 and FX Wortmann FX61-184 airfoils were equally found to be the most efficient airfoils for root section of a sailplane wing design among the selected five root section airfoils. Similarly, in terms

of determined seven criteria, GOE 533 and FX 60-126 airfoils were found to be the most efficient airfoils for tip section of a sailplane wing design among the selected four tip section airfoils.

In this study, Wortmann series airfoils of FX 61-184 and 60-126 were selected as the airfoils to use on our wing design, since the historical usage data verifies that, generally wing airfoils were selected from the same airfoil family. After the selection of the airfoils, numerical analysis of the airfoils at Reynolds Numbers depending on requirements at flight conditions of the sailplane.

Reynolds number is a dimensionless parameter, which is equal to division of inertial and viscous forces as stated in Equation (4.33). It can be defined as;

$$Re = \frac{inertial\ force}{viscous\ force} = \frac{\rho V L}{\mu} \tag{4.33}$$

where ρ is the fluid density, V is the flow velocity, L is the characteristic length, and μ is dynamic viscosity of the fluid. In order to calculate our Reynolds Numbers' maximum and minimum values, dynamic viscosity and air density was taken from [62] depending on our altitude limits represented in our mission profile. Mean chord was initially approximated as 1 meter. Speed limits were taken as stall speed and never exceed speeds. In conclusion, our maximum and minimum Reynolds numbers were 10^6 and 4.3×10^6, respectively and approximately cruise Reynolds Number is 2×10^6.

4.3.2 Planform Design

Planform geometry is the top-view shape of a wing and effective on wing aerodynamic performance [9,10]. Therefore, the geometrical parameters of a wing planform geometry are also important for a wing design. Changing these geometrical parameters properly with respect to their effects on the wing aerodynamic parameters can provide an improved aerodynamic performance to wing. In two-dimensions, taper ratio, aspect ratio and sweep angle are the main planform geometry variables. But in three-dimensions, the geometrical parameters are twist angle, dihedral/anhedral angle and incidence angle.

4.3.2.1 Wing Area, Wing Loading and Aspect Ratio

At the beginning of a wing design process, some initial values should be determined depending on requirements determined at the requirements phase of the design. As it was stated in Table 3.2, the desired stall speed is lower than 75 km/h. Therefore, the parameters affecting the value of stall speed should be taken into consideration. In other words, wing loading (W/S) and maximum lift coefficient ($C_{L_{max}}$) should be determined to calculate stall speed as it was stated in the Equation (4.14).

The change in wing area, depending on maximum lift coefficient for 70 km/h and 75 km/h stall speeds, were represented in Figure 4.24. As it can be seen from the figure, with the increase in V_s, maximum lift coefficient is increasing for all of the wing loading values.

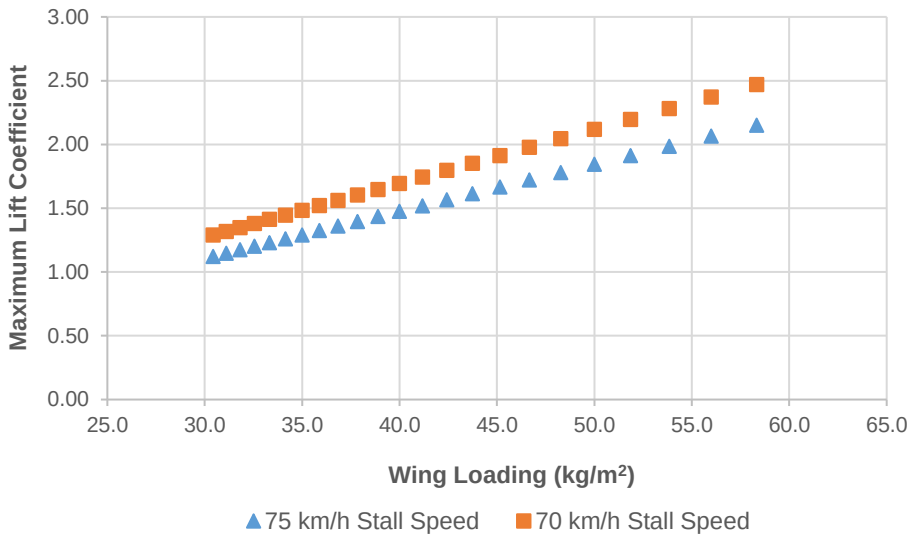

Figure 4.24 Maximum lift-coefficient changing with wing loading

On the other hand, estimating maximum lift-coefficient of the wing can give an idea about suitable wing loading for the design. Therefore, at the beginning of the preliminary design phase, the method of rapid estimation for maximum lift coefficient [6] can be used. It is given in Equation (4.34), where $C_{l_{max}}$ is the estimated maximum lift coefficient in two-dimension from the root and tip section airfoils. Moreover, the geometric parameters y_{MGC} and b are mean geometric chord and span for the wing, respectively.

$$C_{l_{max}} = (C_{l_{max}})_{root} + \frac{2y_{MGC}}{b}((C_{l_{max}})_{tip} - (C_{l_{max}})_{root}) \quad (4.34)$$

In other words, to make the initial wing loading determination of the design, primarily maximum lift coefficient calculations of root and tip airfoils should be performed. The performed analysis results of the airfoils at cruise Reynolds Number of 2 x10^6 were given in Figure 4.25.

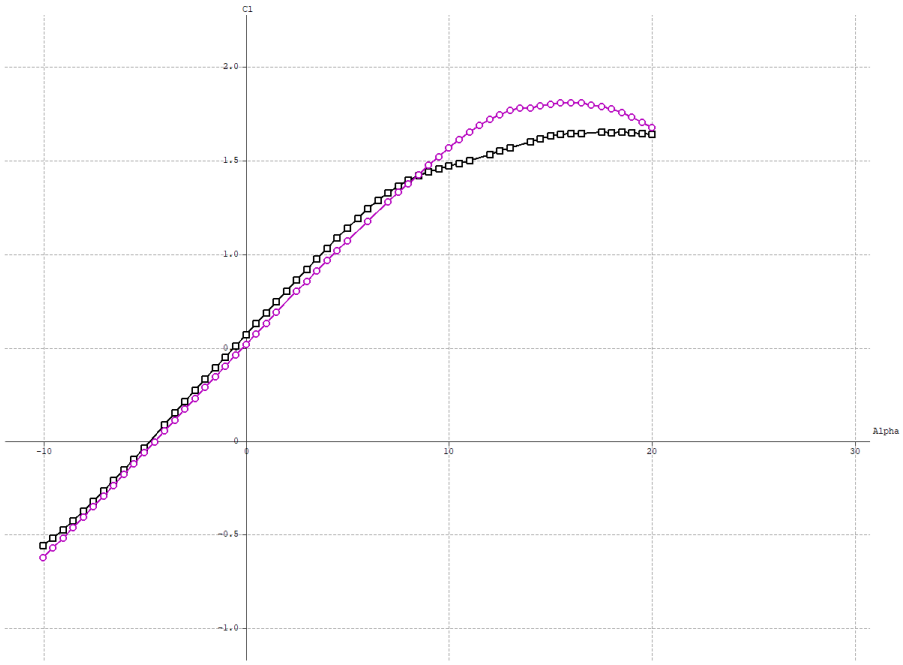

Figure 4.25 Lift coefficients versus angle of attacks of the airfoils at 2 x10^6 Reynolds Number

Figure shows that, root airfoil reaches maximum lift coefficient of 1.8 and tip airfoil reaches the value of 1.64. As it was before validated, XFLR5 program gives approximately 10% higher results than experimental results for two dimensional airfoil analysis. Therefore, the values will be taken into consideration 10% lower to have more reliable design values. Correspondingly, tip airfoil will have a maximum lift coefficient value of 1.62 and root airfoil will have a value of 1.47.

In conclusion, using the obtained analysis results, our $C_{l_{max}}$ value can be calculated as 1.63 for our design from the Equation (4.34). This means, it is suitable for our design to have a wing loading (W/S) value of 38.5 kg/m^2 according to Figure 4.24. Wing area of our sailplane will be 18.5 m^2 depending on determined wing loading.

4.3.2.2 Aspect Ratio (AR) and Taper Ratio (λ)

The main geometrical variables of a wing are shown in Figure 4.26. In the figure, b is the wing span, s is the semi-span, S is the wing area, $c_r$and c_t are root and tip chord lengths, Λ_{LE} is the leading-edge sweep angle, $\Lambda_{.25}$ is the quarter-chord sweep angle, α_{g1} (root section) and α_{g2} (tip section) are the wing twist angles, y_k is the span-wise location of taper change and c_k is the chord length at taper change point.

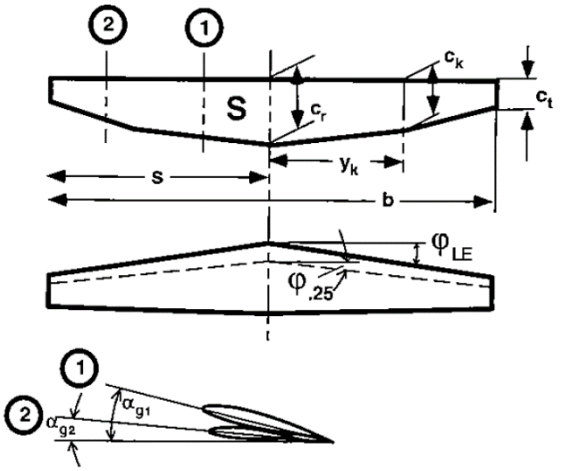

Figure 4.26 Geometrical parameters of a wing [3]

Taper ratio (λ), as a part of the wing planform geometry, is one of the most important parameters to take into consideration during an aircraft wing design process. It is the ratio as stated in Equation (4.35), which is the ratio of the root (c_r) and tip (c_t) chord lengths as shown in Figure 4.26.

$$\lambda = \frac{c_t}{c_r} \tag{4.35}$$

There are different types of taper ratios applied on today's sailplanes and it is a geometrical planform parameter that needs to be optimized during a wing design process [6] because of its important role on span-wise lift distribution of a wing design. As it was stated in Equation (4.5), taper ratio affects the variable named as the Oswald efficiency factor (e), which defines the similarity of a wing span-wise lift distribution to elliptical wing lift-distribution.

In the Figure 4.27, there are three different tapered wing designs existing that were compared with elliptical wing design in terms of their span-wise lift distributions. It is

clear that, the design which have the most similar distribution is double-tapered. Therefore, in this study, our wing design will have a double-tapered planform.

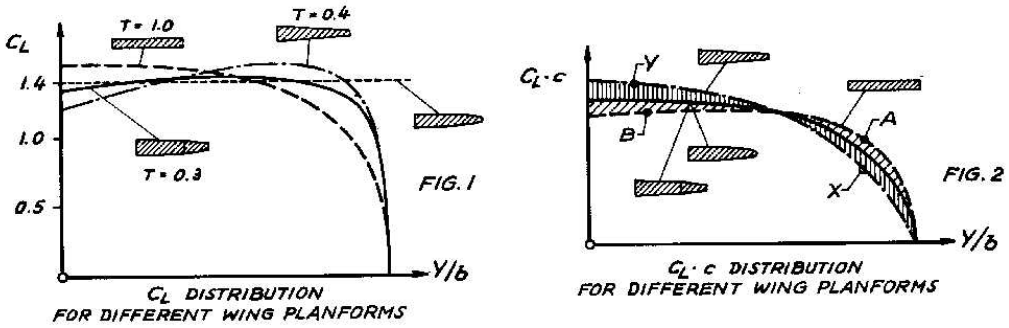

Figure 4.27 Span-wise lift distributions of different tapered wing designs [63]

Aspect ratio (AR) is the other important geometrical parameter, which is defined as the ratio between square of the wing span and wing area, as shown in Equation (4.36).

$$\mathrm{AR} = \frac{b^2}{S} \tag{4.36}$$

As shown in Figure 4.28, aspect ratio has an optimum value with respect to drag coefficient and lift coefficients. It is clear that, there is an aspect ratio value for a wing design that has both lower parasitic and induced drag coefficients.

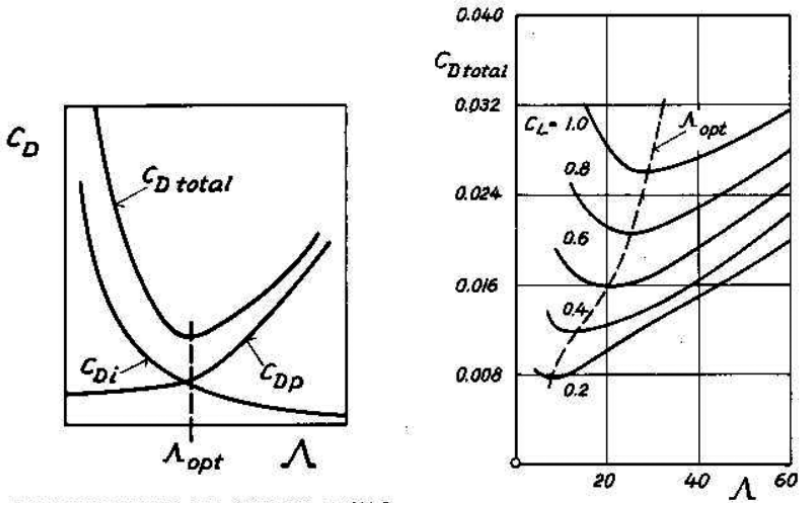

Figure 4.28 Aspect ratio versus drag and lift coefficients [64]

Also, Figure 4.29 represents the change in aspect ratio with the wing loading for our design. During wing design process, aspect ratio also should be optimized to minimize drag coefficients of the wing.

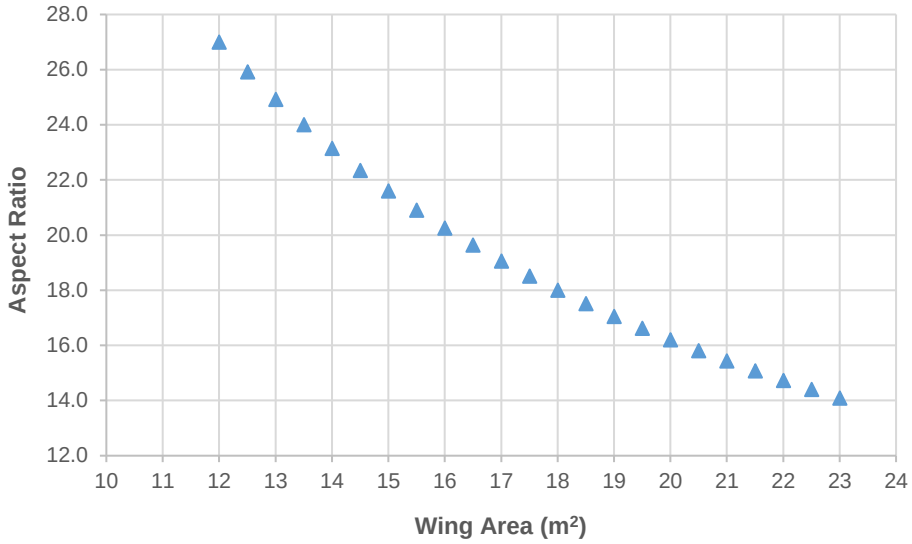

Figure 4.29 Aspect ratio changing with wing area

In this study, since the wing loading of our design was calculated before as 38.5 kg/m^2 and wing area as 18.5 m^2, our design will have an aspect ratio of 17.5. This value was found to be acceptable when it was compared to sailplanes having similar wing-spans in Table 3.1.

Suitability of our selected aspect ratio can be validated with the empirical method from [6] which is used to estimate the aspect ratio of powered sailplanes depending on their target maximum glide ratios. When our target glide ratio of 30 applied to this formulation, it can be found that our determined aspect ratio of 17.5 is suitable.

$$AR = \frac{L/D_{max}+0.443}{1.7405} \tag{4.37}$$

4.3.2.3 Sweep Angle (Λ)

Wing sweep is used primarily on the purpose of reducing the adverse effects of transonic and supersonic flows. The angle between the wing leading edge and the y-axis of the aircraft is called the leading edge sweep (Λ_{LE}) as shown in Figure 4.6, which is generally concerned with supersonic flight. If it is referenced to quarter chord line, it is called quarter-chord line sweep angle ($\Lambda_{.25}$), which is generally related to subsonic flight [51]. There is an estimation method for Oswald span-efficiency factor of straight wing designs as stated in Equation (4.38) [5].

$$e = 1.78(1 - 0.045AR^{0.68}) - 0.64 \tag{4.38}$$

For low subsonic aircrafts, generally swept wings are not recommended due to eliminating advantages with its disadvantages. On sailplanes, swept wings generally used with the aim of moving center of gravity to desired range if it is necessary [5].

In this study, for the initial wing design, sweep angle was not applied and it was aimed to design simpler wing structure. In the next steps of the design, if it was needed to move center of gravity, sweep angle can be applied and optimized.

4.3.2.4 Dihedral/Anhedral Angle (Γ)

Dihedral/anhedral angle of the wing is the angle with respect to the horizontal axis when it is seen from the front. The name of the angle changes with its orientation and if the angle is positive it is named as dihedral, if it is negative it is named as anhedral, as shown in Figure 4.30.

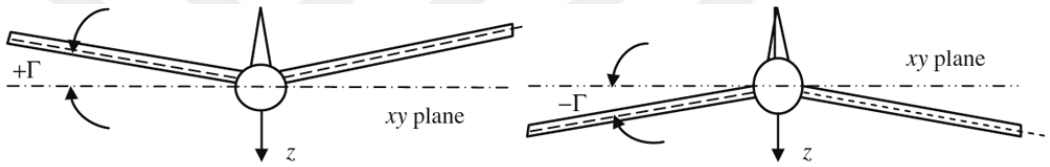

Figure 4.30 Dihedral and anhedral angles [5]

Wing dihedral applications has the primary aim of improving lateral stability of the aircraft. The tendency of an aircraft to return to its original trim level-wing flight condition when it is disturbed by a gust and rolling around the x-axis, is called as the lateral stability. Then, a wing dihedral angle provides the needed restoring rolling moment as shown in Figure 4.31.

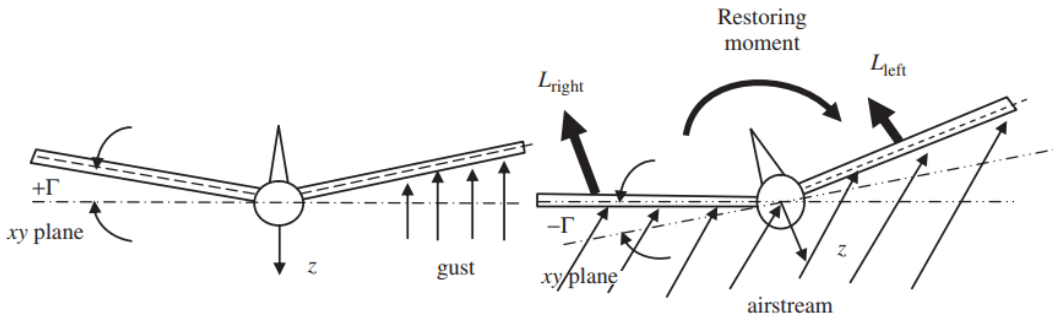

Figure 4.31 Dihedral effect on lateral stability [5]

In this study, taking the existing sailplanes' data [6] into consideration, it was decided to use 4 degrees dihedral angle for the initial wing design.

4.3.2.5 Twist Angle and Angle of Incidence

The angle of incidence of a wing (i_w) can be defined as the angle between the fuselage center line and the wing's root chord line as shown in Figure 4.32. The wing of an aircraft must be able to generate desired lift coefficient and minimum drag coefficient during cruising flight. Therefore, this angle should be selected taking into consideration of these conditions.

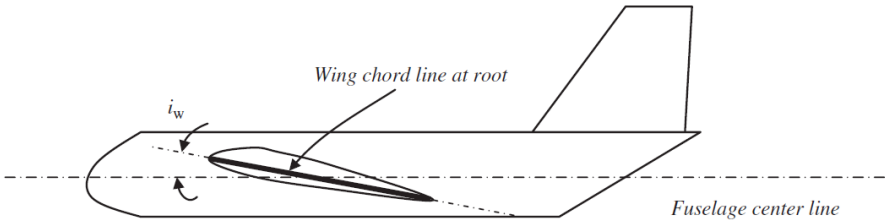

Figure 4.32 Wing incidence angle (i_w) [5]

Historical data of sailplanes shows us that there is common usage of angle of incidences of 0-1.5 degrees [6]. Thus, in this study, angle of incidence was tried to be in this interval and was optimized together with the twist angle of the airfoils and the geometry of the fuselage.

Twist means for a wing that the change in angle of incidence along its span-wise as shown in Figure 4.26. Twist angle is generally used with the aim of preventing tip stall and adjusting the lift-distribution. The typical wing twist angles are changing between zero and five degrees [51]. There are two types of twist called as geometric twist and aerodynamic twist. Geometric twist is the actual difference of the airfoil incidence angle and usually measured with respect to the root airfoil. If the wing tip airfoil is at the negative angle and nose-down, it is called as wash-out. On the other hand, aerodynamic twist is the angle between zero-lift angles of an airfoil and the root airfoil.

In this study, twist angle will be optimized with the aim of have a lift-distribution similar to elliptical distribution together with providing steady flight conditions.

4.3.3 Final Wing Design

Sailplanes spend their times in gliding flight mostly. Although, our sailplane also have the cruising flight ability by its propulsion unit, our wing design will have the target of satisfying steady gliding flight conditions. In a steady gliding flight, the lift force

need to be equal to weight since gliding angles are commonly between 1 and 3 degrees [3]. Accordingly, when MTOW of 700 kg, cruise altitude of 1000 meters (ρ=1.112 kg/m^3), wing area of 18.5 m^2 and cruise speed of 33.5 m/s applied to the Equation (4.8), the needed lift coefficient to make steady gliding flight for our wing design was found to be 0.60.

In this study, the wing was designed to have the target value of minimum lift coefficient of 0.60 during its gliding flight. In addition, lift distribution of the design was tried to make familiar to elliptical distribution with the trial-error optimization of the wing geometrical parameters. Also our design will not have any high-lifting device as it is common among sailplanes.

4.3.3.1 Design Geometry

The planform geometry was optimized in terms of its two and three dimensional geometrical parameters by trial-error to have increased aerodynamic performance. The obtained geometry and dimensions are given in Figure 4.33. Twist angles of the sections are α_1=2.25°, α_2=1.5° and α_3=0°. Angle of incidence of the wing was designed to be 1.25°. Taper ratio of the sections were determined as $\lambda_{1\text{-}2}$=0.65 and $\lambda_{2\text{-}3}$=0.26. Dihedral angle of the wing was applied as 4° which can be seen at Figure 4.34.

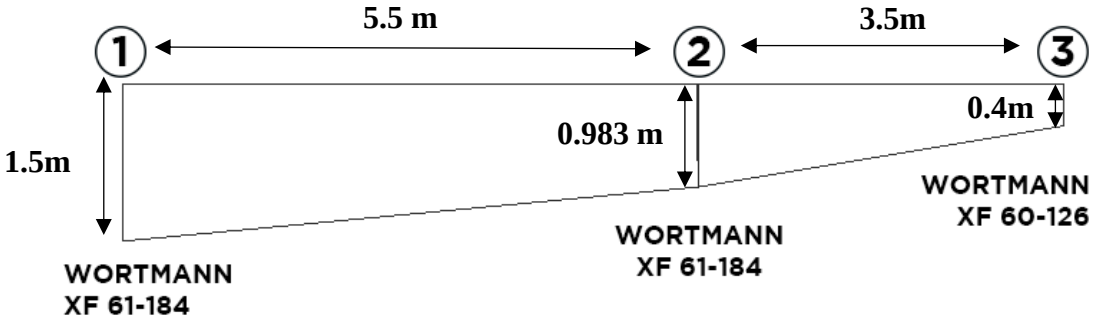

Figure 4.33 The final wing design dimensions and airfoil locations

Chord length of the sections were c_1=1.5m, c_2=0.983m and c_3=0.4m. So, mean aerodynamic chord (MAC) can be calculated from Equation (4.39) as 1.122m. Final wing design geometrical parameters were given in the Table 4.6.

$$MAC = \frac{MAC_{1-2}S_{1-2}+MAC_{2-3}S_{2-3}}{S_1+S_2} \quad (4.39)$$

Table 4.6 Final wing design geometrical properties

Mean Aerodynamic Chord	1.122 m
Aspect Ratio	17.5
Wing Span	18 m
Wing Area	18.5 m^2
Taper Ratio (Root to tip)	0.266
Sweep Angle	0^o
Dihedral Angle	4^o

Figure 4.34 The final wing design front view

4.3.3.2 Numerical Analysis

Numerical analysis of the final design was performed at XFLR5 program. XFLR5 have options for wing analysis, which are vortex lattice method (VLM), lifting line theory (LLT) and 3D panel method [26]. In vortex lattice method there are two options as VLM1 and VLM2 implemented in the general VLM. These have differences in the treatment of the horse-shoe vortices. On the other hand, 3D panel method is implemented in the code for thick wings and analysis of complete aircraft together with its fuselage. The method uses uniform source and doublet distributions [64].

Our wing aerodynamic performance analyses were performed with VLM1 method on XFLR5 program at 33.5 m/s airspeed, 1.112 kg/m^3 density and dynamic viscosity (μ) of $1.758x10^{-5}$ Ns/m^2. The obtained streamlines and wing design is as shown in Figure 4.35.

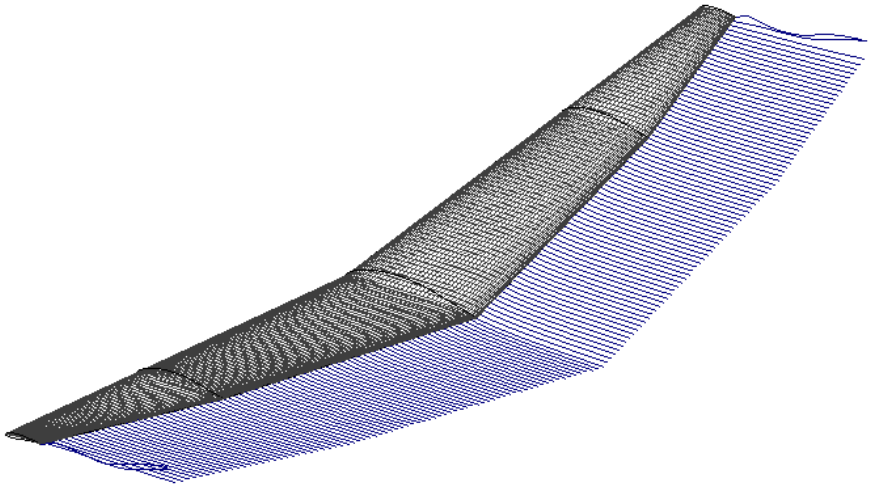

Figure 4.35 The final wing design and streamlines

The results of the analyses given in the Figure 4.36 shown that the lift coefficient of the wing design reaches the desired value of 0.6 when the angle of attack is higher than -2 degrees. Moreover, the wing has its maximum lift to drag ratio at the -3 degree angle of attack approximately, as stated in Figure 4.37. In addition the stall angle of attack is seen as higher than 8 degrees as given in Figure 4.38.

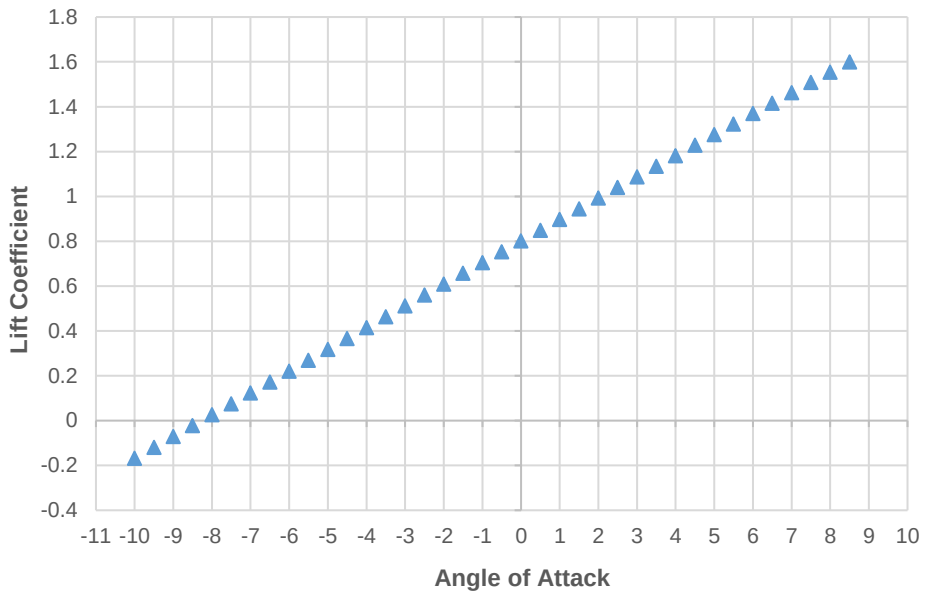

Figure 4.36 The final wing design lift coefficient versus angle of attack

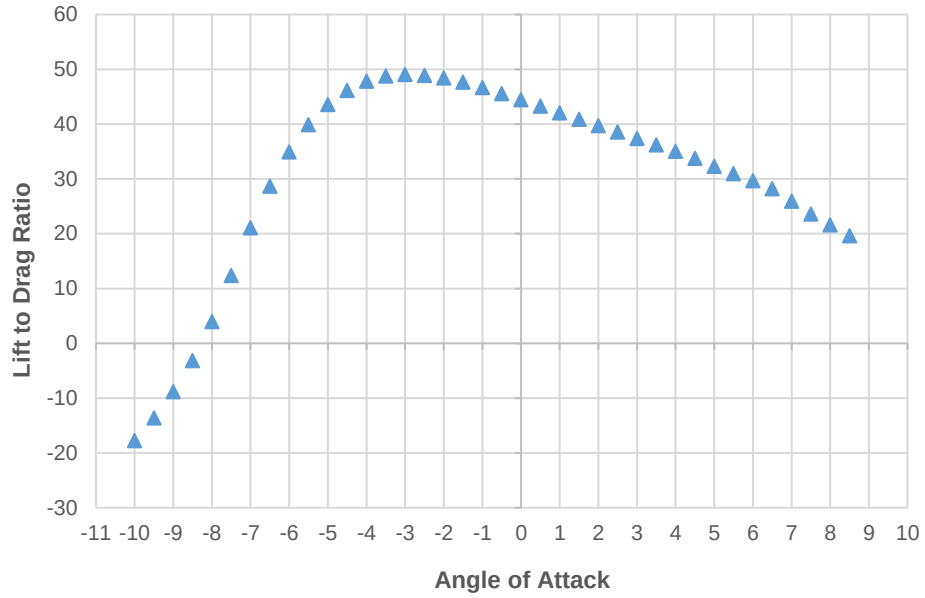

Figure 4.37 The final wing design lift to drag ratio versus angle of attack

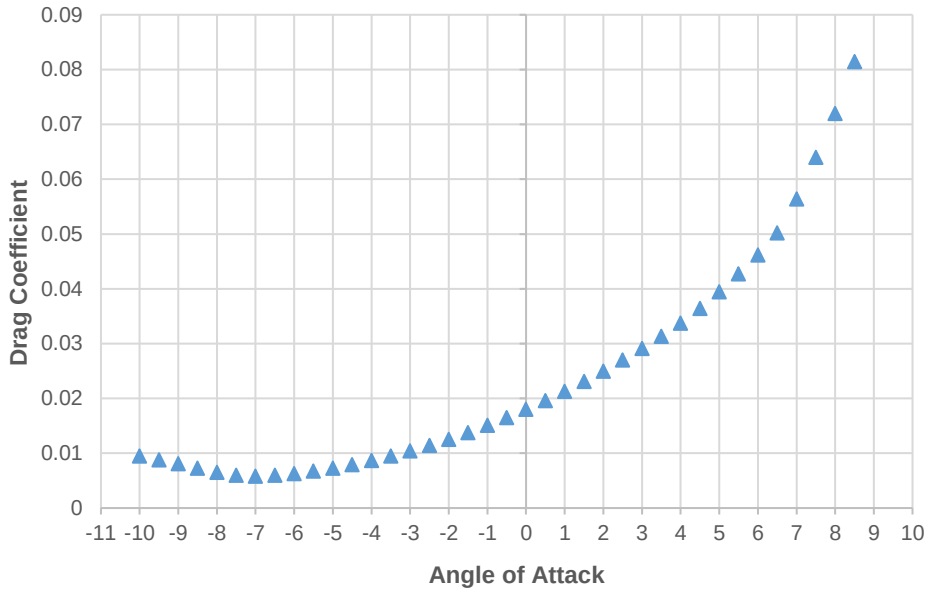

Figure 4.38 The final wing design drag coefficient versus angle of attack

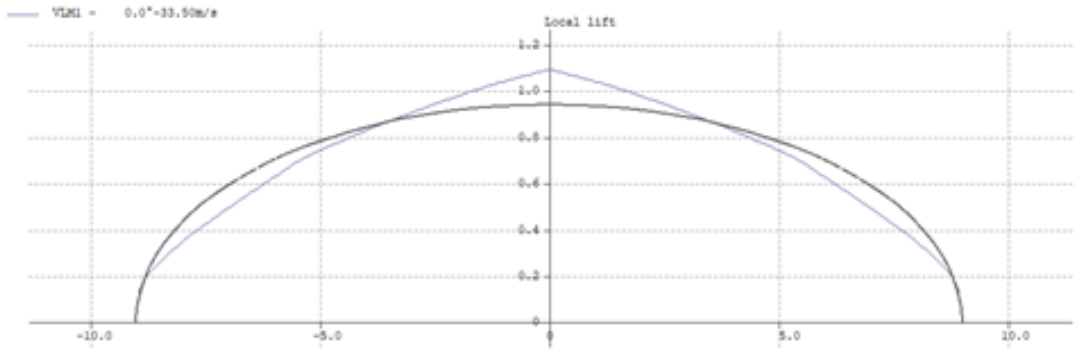

Figure 4.39 The final wing design lift distribution and elliptical distribution

Figure 4.39 represents that our wing design has acceptable span-wise lift distribution. Oswald efficiency factor of the wing was obtained as 0.97. According to the results of the analyses, wing design found to be acceptable for the steady gliding flight conditions at the angle of attacks higher than -2 degrees.

4.4 Tail Design

An aircraft tail has two fundamental lifting surfaces named as vertical tail and horizontal tail. The geometrical parameters of these tail parts are very similar to wing geometrical parameters. The main difference between tail and wing is their purposes on an aircraft. A wing is responsible for the required lift generation, but tail is responsible mainly trim, stability and control considerations in terms of longitudinal and directional (lateral). Vertical tail is responsible for providing desired directional trim conditions and horizontal tail is responsible for providing longitudinal trim conditions.

An aircraft design process requires satisfying trim conditions in three dimensions, which are lateral, longitudinal and vertical axes as shown in Figure 4.40. In this study, under the steady gliding flight conditions, as the wing and fuselage designs are symmetrical, the main consideration will be the longitudinal trim conditions rather than lateral and vertical trim conditions.

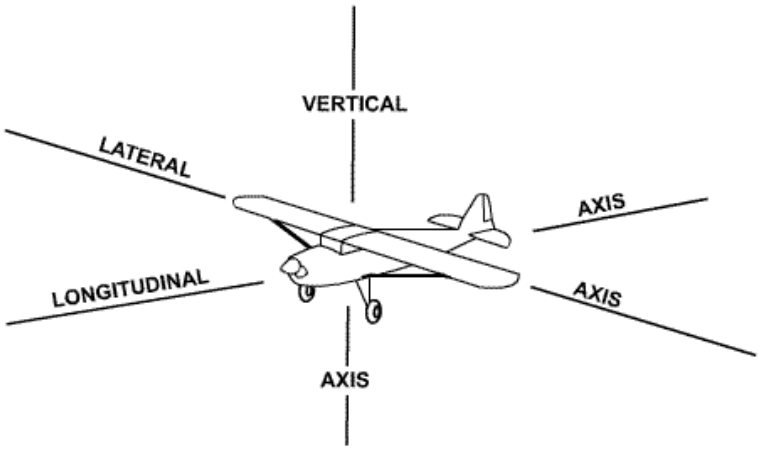

Figure 4.40 The axes of the aircraft [65]

Longitudinal trim conditions requires the sum of the forces and moments (with respect to center of gravity) acting on the vertical axis to be zero as stated in Equations (4.40) and (4.41). The responsibility of providing longitudinal trim conditions and make the sum of these forces and moments zero is on the horizontal tail.

$$\sum F_x = 0 \tag{4.40}$$

$$\sum M_{cg} = 0 \tag{4.41}$$

The steps of the tail design process is very similar to wing design steps. Airfoil selection is one of the most important phases of a tail design, as it is for wing design. In this study, as the use of symmetrical airfoils are very common on tail designs, symmetrical airfoils of NACA 0009 and NACA 0011 were selected for our horizontal and vertical tails, respectively.

The initial estimation of the tail planform areas can be possible with a dimensionless parameter named as volume coefficient. This coefficient is called for each part of the tail as horizontal tail volume coefficient (V_H) and vertical tail volume coefficient (V_V), as given in Equation (4.42) and (4.43). MAC is the wing mean aerodynamic chord (m), l is the tail moment arm (m), S_H is the horizontal tail planform area (m^2), S_V is the vertical tail planform area (m^2) and S is the wing reference area (m^2). As it can be seen from the equations, this coefficient is not a function of aircraft size or weight. The increase in volume coefficient means that the aircraft is more stable but less controllable.

$$V_H = \frac{l}{MAC}\frac{S_H}{S} \tag{4.42}$$

$$V_V = \frac{l}{MAC}\frac{S_V}{S} \tag{4.43}$$

The exact planform designs of the tail is not very critical during this stage of the design [51]. They can be revised during the further phases of design process. Therefore, at this stage, it is important to determine tail planform areas by means of volume coefficients. In general, for the initial design, historical approach is used for the estimation of tail size.

The typical sailplane horizontal and vertical tail volume coefficients are between 0.5-0.6 and 0.02-0.03, respectively [5,51]. Optimum horizontal tail arm initial estimation is possible with the Equation (4.44), where D_f is the maximum width of the fuselage and K_c is the correction factor depending on aircraft configuration.

$$l_{opt} = K_c\sqrt{\frac{4MACV_HS}{\pi D_f}} \tag{4.44}$$

Knowing that the maximum width of our fuselage is 0.7 m and estimating the correction factor as 1.2 and horizontal tail volume coefficient as 0.6, optimum tail arm can be calculated as 5.71 m for horizontal tail. Applying this calculated horizontal tail arm value to Equation (4.42) gives the planform area estimation of 2.18 m^2.

The same procedure was applied to find the vertical tail planform area, taking vertical tail volume coefficient as 0.02 and vertical tail arm as 5.71 m. The result of the process gave planform area estimation as 1.17 m^2 for the vertical tail.

The vertical and horizontal tail drawings and dimension are given in the Figure 4.41 and 4.42. These tail arm estimations can be optimized together with center of gravity calculations of our design. The trial-error optimization can be performed with the aim of having longitudinal stability and trim conditions.

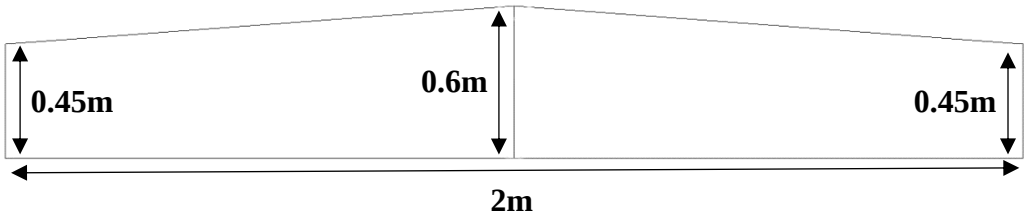

Figure 4.41 Dimensions of the horizontal tail design

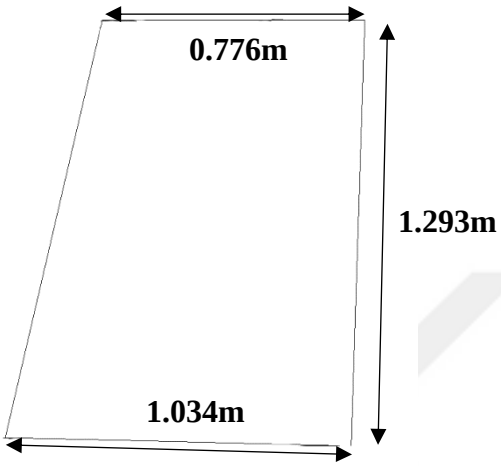

Figure 4.42 Dimensions of the vertical tail design

4.5 Fuselage Design

The fuselage is the part of the aircraft which aims to accommodate the payload. Longitudinal and directional stability and control directly affected by fuselage design since it provides a moment arm to the horizontal and vertical tails.

Cockpit type configuration is the most common configuration of the fuselage for sailplanes and it should have a canopy, which provides enough horizon view for the pilots. On the other hand, the fuselage design should be designed to have enough volume for the retractable propeller mechanism and landing gear, battery and pilots.

In this study, a fuselage design was drawn, which have an acceptable aerodynamics shape, have a length providing stability and have enough volume for the requirements by taking the similar sailplane dimensions as an example. Figure 4.43 and 4.44 represents the drawings together with its dimensions.

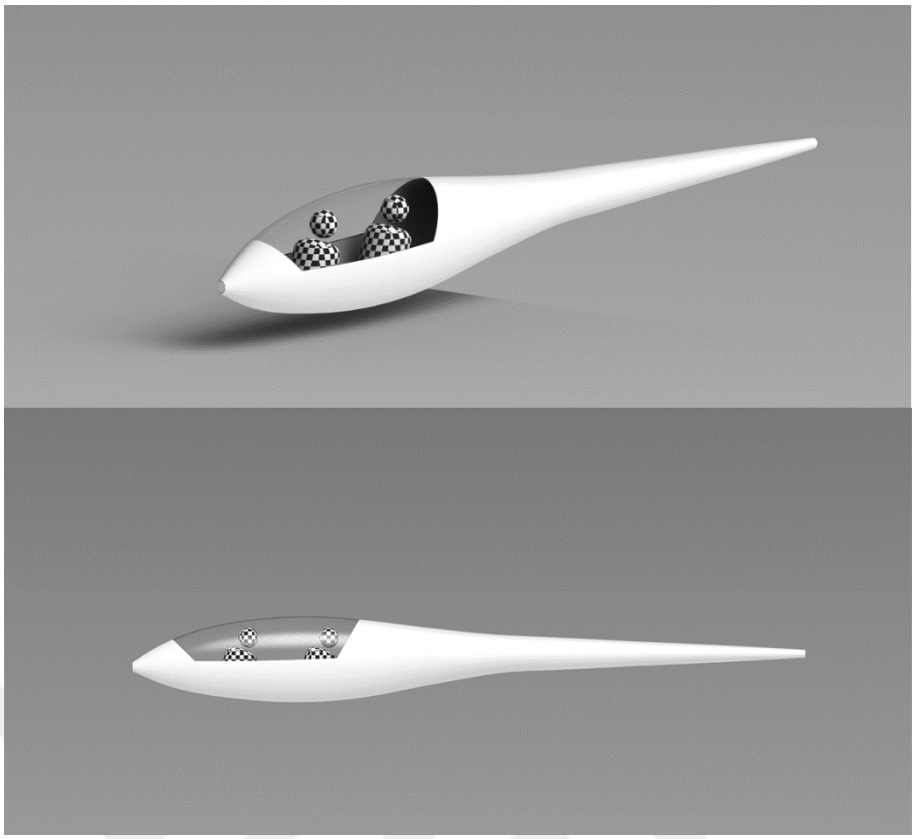

Figure 4.43 Top and side view drawings of the fuselage design

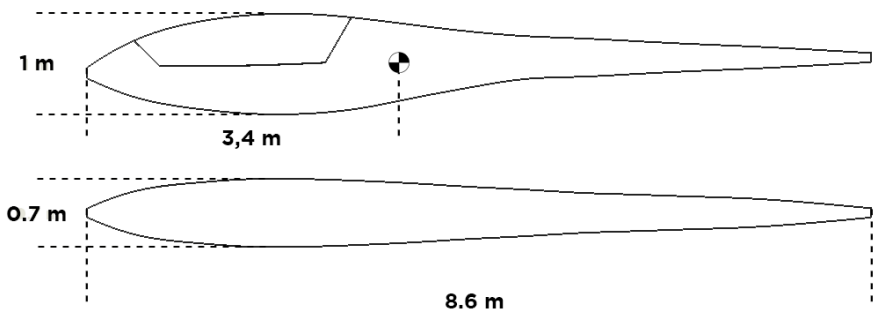

Figure 4.44 Dimension of the fuselage design together with the location of the fuselage center of gravity

4.6 Propulsion Unit Design

Powered sailplanes are categorized into two groups in terms of purpose of their propulsion units. Self-launching category sailplanes are capable of taking-off with the help of its propulsion unit, but self-sustaining category sailplanes are only capable of using their propulsion unit to sustain their flights.

The ratio of the thrust generated by the propeller and maximum takeoff weight of the aircraft is a critical parameter that affects the aircraft performance. This term, which is called as thrust-to-weight ratio, is generally associated with jet-engine aircrafts. There is a similar parameter for propeller aircrafts that is power-to-weight ratio (P/W). It is the ratio between the motor power and maximum takeoff weight of the aircraft [51].

Although self-launching sailplanes has higher values, the collected data shown in Table 4.7 demonstrates that self-sustaining sailplanes generally have power-to-weight ratio value between 0.028 and 0.031, approximately. Even so, by predicting some unexpected losses, it was decided to have power-to-weight ratio of 0.035 for our sailplane design. With respect to this selected value, as our design has a maximum takeoff weight of 700kg, it is needed to use an electric-motor having 25kW power.

Thrust generation is responsibility of engine together with a propeller. Therefore, selection of suitable propeller for a design is very critical. Raymer gives a method to estimate propeller diameter independent from the material, which is very useful at the beginning of the design steps [6]. Raymer's formula is given in Equation (4.45), where D is the propeller diameter (m), P is power in (BHP) and K_p is a coefficient changing with the number of propeller blades. Two blades, three blades and four or more blades requires to have K_p value of 0.56, 0.52 and 0.49, respectively.

$$D = K_p \sqrt[4]{P} \tag{4.45}$$

Smaller and lighter retracting mechanism is possible by means of using a propeller which have smaller diameter but have high number of blades. Therefore, K_p is applied as 0.49 together with 25 kW power and it was found suitable to use 1.1 meter diameter propeller with more than four blades with respect to the Equation (4.45).

Retracting mechanism beam length can be approximately 0.85 meters together with the clearance value of 0.2 meters between fuselage and propeller. The expanded and retracted view representations are given in Figure 4.45.

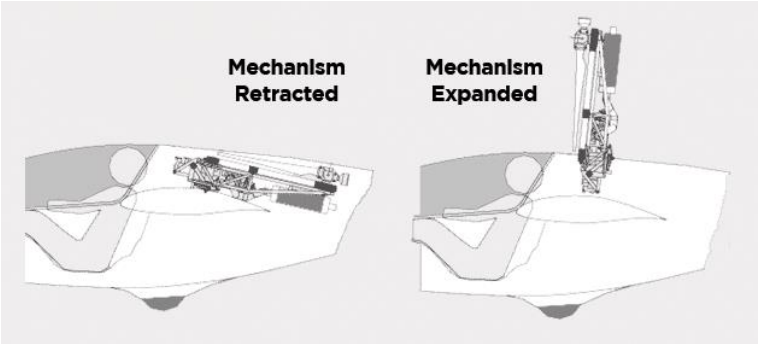

Figure 4.45 Retractable propulsion unit retracted and expanded views [66]

Maximum static thrust (T_{STATIC}) is the maximum amount of thrust that propeller capable of generate at sea-level with zero airspeed. The value of maximum static thrust can be calculated from Equation (4.46), where, T_{STATIC} is the maximum static thrust (lbf), P is the engine power (BHP), ρ is the sea-level air density (slugs/ft^3) and A_D is the propeller disc area (ft^2).

$$T_{STATIC} = P^{\frac{2}{3}}(2\rho A_D)^{1/3} \tag{4.46}$$

Table 4.7 represents some calculated maximum static thrust values of existing sailplanes of both self-launching and self-sustaining. It can be clearly seen that the self-sustaining sailplanes generally have T_{STATIC} values approximately between 105 kg and 145 kg. In this study, as our propeller diameter is 1.1 m and engine power is 25 kW, maximum static thrust value can be found as 115 kg, which is acceptable value with respect to existing data.

Table 4.7 Collected sailplane specifications data for propulsion unit design

Sailplane Model	**MTOW (kg)**	**P/W**	**Propulsion**	**Engine Power (kW)**	**Max. Static Thrust (kg)**
SF 25 D	580	0.062	Self-launching	36	180
Taurus Electro G2	550	0.073	Self-launching	40	205.8
SF 25 B	555	0.050	Self-launching	28	152.3
SF 25 K	630	0.057	Self-launching	36	180
Schweizer SGS 2-33	472		Pure		
Diamond HK36 S. Dimona	710	0.085	Self-launching	60	
F 28 A “Tandem-Falke”	590	0.066	Self-launching	39	189.9
SF 36 A	715	0.071	Self-launching	51	237
SF 25 A	485	0.031	Self-sustaining	15	104.9
SZD-50-3 Puchacz	570		Pure		
ASK 21	600		Pure		
ASK 21 Mi	705	0.058	Self-launching	41	198.9
TST 14 Bonus	580	0.059	Self-launching	34	
AMT-200 S. Ximango	805		Self-launching		
fs31 - Ferdinand Porsche	560		Pure		
Grob G103c Twin III SL	710	0.045	Self-launching	31.6	170.9
SF 25 E	650	0.060	Self-launching	39	189.9
HPH Twin Shark	850		Self-launching		
ASG 32 Mi	850	0.048	Self-launching	41	198.9
DG1001M	790	0.059	Self-launching	47	224.4
Arcus M	800	0.063	Self-launching	50	233.9
DG 500-MB	825	0.061	Self-launching	50	233.9
Arcus E	810	0.052	Self-launching	42	
Arcus T	800	0.028	Self-sustaining	22	105.5
Duo Discus xL T	750	0.029	Self-sustaining	22	105.5
DG 1001T	750	0.029	Self-sustaining	22	
ASG 32 EL	850	0.029	Self-sustaining	25	144.3
fs33 - Gavilàn	640		Pure		
D-41	760		Pure		
SB 15	640		Pure		
Average	686.1	0.062			

There is another method to estimate potential thrust force depending on airspeed. The method named as quadratic interpolation is based on the assumption that the propeller thrust varies from the static thrust at zero airspeed to the thrust at the maximum level airspeed [6]. This method makes it possible to write an equation for thrust force by using a quadratic polynomial form as stated in Equation (4.47).

$$T = AV^2 + BV + C \tag{4.47}$$

This can be written as in Equation (4.48), where T_{STATIC} is the maximum static thrust, V_{MAX} is the maximum airspeed and T_{MAX} is the thrust force at maximum airspeed.

$$T(V) = \left(\frac{T_{STATIC}-2T_{MAX}}{V_{MAX}^2}\right)V^2 + \left(\frac{3T_{MAX}-2T_{STATIC}}{V_{MAX}}\right)V + T_{STATIC} \tag{4.48}$$

In this study, as the maximum airspeed (never-exceed speed) was determined as 230 km/h at the requirements phase, by assuming propeller efficiency as 0.6, the change of thrust force with airspeed of our design was obtained as stated in Figure 4.46.

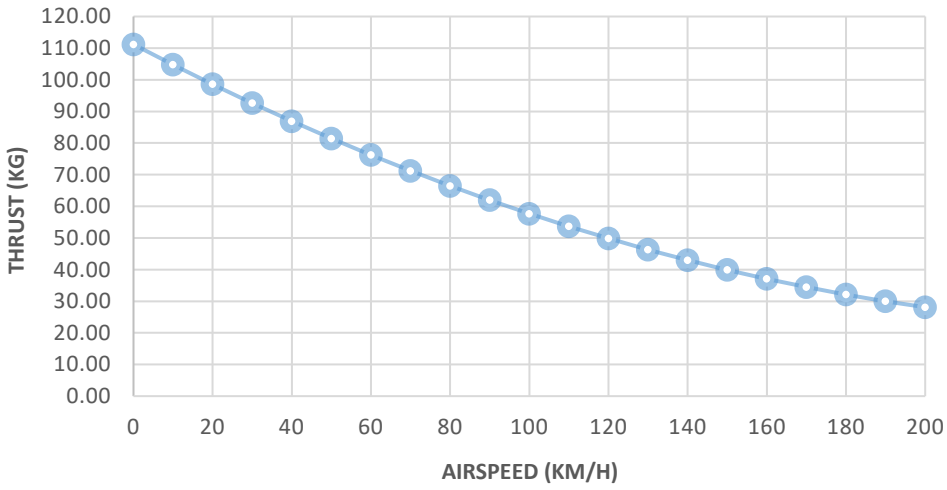

Figure 4.46 The change in thrust force with respect to airspeed

4.7 Weight Distribution and Center of Gravity Calculations

Maximum takeoff weight of determined 700 kg can be divided into some groups as flight instruments, occupants, parachutes and structural weights such as wing, tail, fuselage propulsion unit and landing gear. At this stage of the design, it is not possible to determine sensitive values of weights for each component and especially for

structure. Therefore, it is needed to estimate approximate values of weights to overcome this issue. In general, for sailplanes, structural weight takes 58% of the maximum takeoff weight. This value is roughly the sum of the wing weight of 30 percent, fuselage weight of 23 percent, tail weight of 3 percent and landing gear weight of 2 percent [5]. By means of this weight distribution percentages, the structural weights were approximately determined and shown in Table 4.8. Due to EASA weight limitations, weight of occupants including parachutes cannot have a weight higher than 180 kg for a two seater sailplane [47].

Table 4.8 Breakdown of the weights of the design

Structural Weights	
Wing	210 kg
Fuselage	160 kg
Tail	20 kg
Landing Gear	15 kg
Other Weights	
Batteries	45 kg
Flight Instruments	10 kg
Occupants and Parachutes	180 kg
Propulsion Unit	15 kg
Payload	45 kg
MTOW	**700 kg**

Center of gravity of an aircraft is important for its stability and trim conditions. Center of gravity along longitudinal axis can be calculated from Equation (4.49), where m is the mass of each part and x is the distance from the datum plane.

$$X_{cg} = \frac{\sum_{i=1}^{n} m_i x_{cg_i}}{\sum_{i=1}^{n} m_i} \tag{4.49}$$

In this study, datum plane was selected as the nose of the sailplane. As the sailplane design were almost symmetrical along the other axes, the main consideration of this study was to calculate the longitudinal center of gravity. The masses and distances of the parts were given in Table 4.9.

Table 4.9 Masses and distances of parts

Part	Distance from datum (m)	Mass (kg)	mx_{cg}
Pilot (Front Seat)	1.4	90	126
Pilot (Back Seat)	2.43	90	218.7
Batteries	3.6	45	162
Propulsion Unit (Retracted)	4.7	15	70.5
Propulsion Unit (Expanded)	3.85	15	57.75
Flight Instruments (Front Seat)	0.886	5	4.43
Flight Instruments (Back Seat)	1.917	5	9.585
Landing Gear (Retracted)	3.169	15	46.015
Landing Gear (Expanded)	2.969	15	47.535
Fuselage	3.509	160	561.44
Wing	3.291	210	691.11
Horizontal Tail	8.142	9	73.278
Vertical Tail	8.122	11	89.342
Payload	3.08	45	139.5

Applying the values at the Table 4.9 to Equation (4.49), gives us a center of gravity of at the distance 3,132 meters from the nose of our sailplane (datum), which means 29,6% MAC.

Center of gravity calculations requires to calculate all of the possibilities about the change in mass. The limitations of these changes can be drawn on a graphic named as center of gravity envelope. Our possibilities will have the absence of the pilot at the front seat and back seats. Also the possibilities will be extended together with the retracted or expanded positions of propulsion unit and landing gear. When these possibilities were calculated, it was found the center of gravity of the design moves between 51.2% MAC for the aft and 28.6% MAC forward positions.

There is a criteria for the longitudinal stability, which corresponds with a term called as neutral point. If center of gravity located at the neutral point, the aircraft stability can said to be neutral. The criteria between center of gravity and neutral point is that, an aircraft is longitudinally stable when the center of gravity location (X_{cg}) is behind the neutral point location (x_{NP}). Our sailplane's neutral point is calculated as 3.468 m from the nose of the sailplane and it was found that our sailplane is longitudinally stable.

CHAPTER 5

RESULTS AND DISCUSSION

On the purpose of obtaining accurate results independent from number of mesh elements, before the numerical analyses of the final design, the mesh accuracy of the program was done for drag, lift and pitching moment coefficients. Number of mesh elements were modified from 750 to 20000 and results were given in the Figure 5.1, 5.2 and 5.3. According to the results, final design model was prepared with the number of mesh elements higher than 20000.

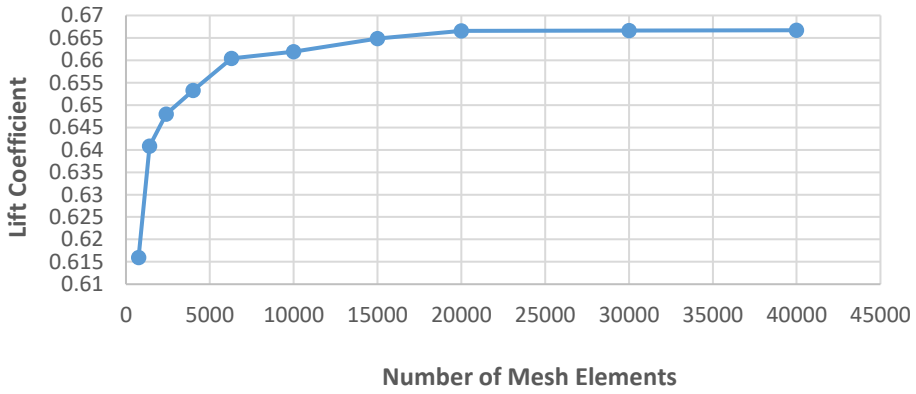

Figure 5.1 Lift coefficient mesh accuracy results

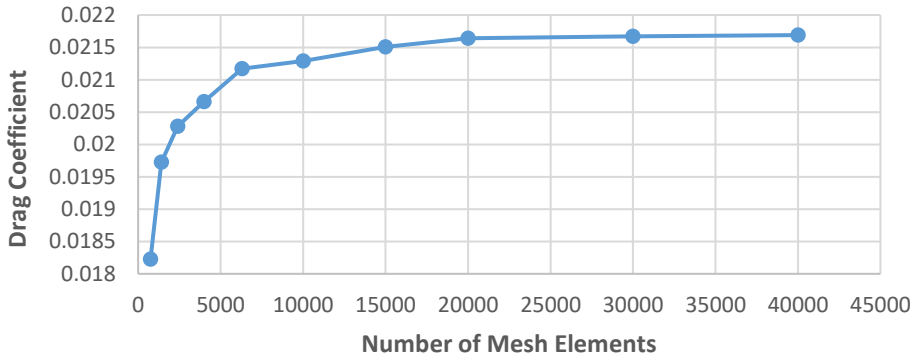

Figure 5.2 Drag coefficient mesh accuracy results

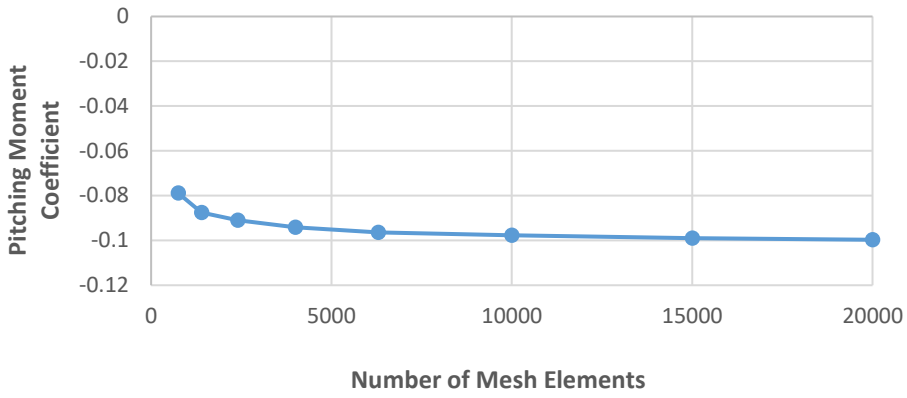

Figure 5.3 Pitching moment coefficient mesh accuracy results

The final design together with its mesh elements of our sailplane was illustrated in Figure 5.4 and Figure 5.5. The number of mesh elements on our design was found to be approximately $2x10^4$.

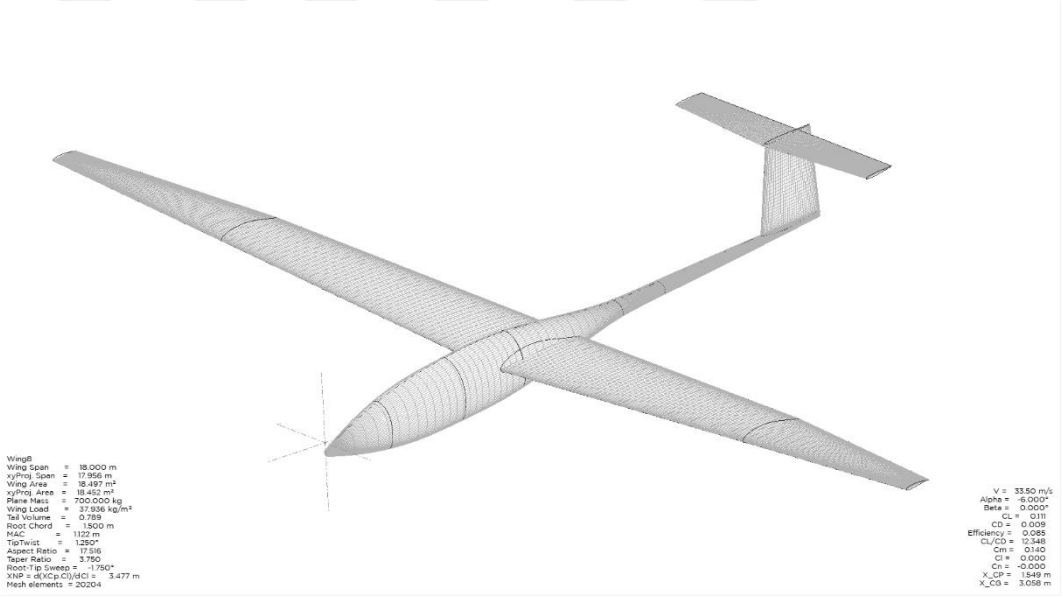

Figure 5.4 Final design mesh elements

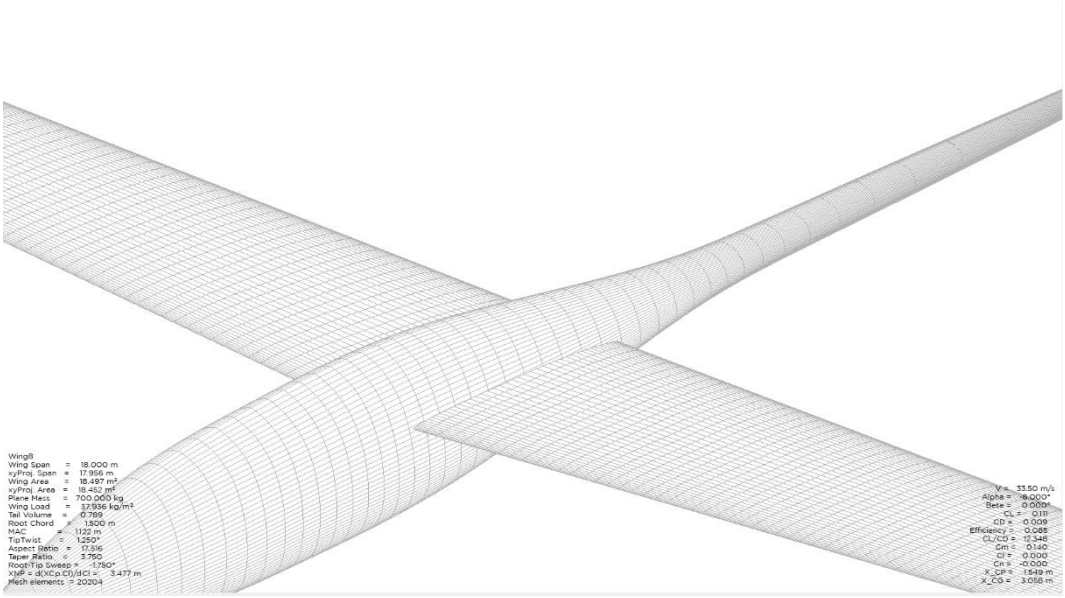

Figure 5.5 Final design mesh elements in close view

The numerical analyses were performed on XFLR5 program, which uses vortex lattice method for three dimensional analysis. The Type1 (fixed speed) analysis together with VLM2 method used for the final design analysis, which uses ring vortexes on each mesh elements.

The analysis was firstly performed at the airspeed 33.5 m/s (120 km/h) and angle of attacks changing between -10 to 10 degrees with the increment of 0.5. However the program is not able to perform analysis higher than the stall angle of attacks, since vortex lattice method is built on the theory of potential flow, which neglects all viscous effects and makes small angle of attack approximation. So, as Figure 5.6 shows the results for the lift coefficient changing with angle of attack for our final sailplane design, the angle of attack of the results is changing from -10 to 8.5 degrees. It can be seen from the figure, at zero angle of attack, our sailplane has the lift coefficient value of approximately 0.66, which ensures our steady flight requirements. In addition, it was found to be our design is able to reach maximum lift coefficient of approximately 1.4.

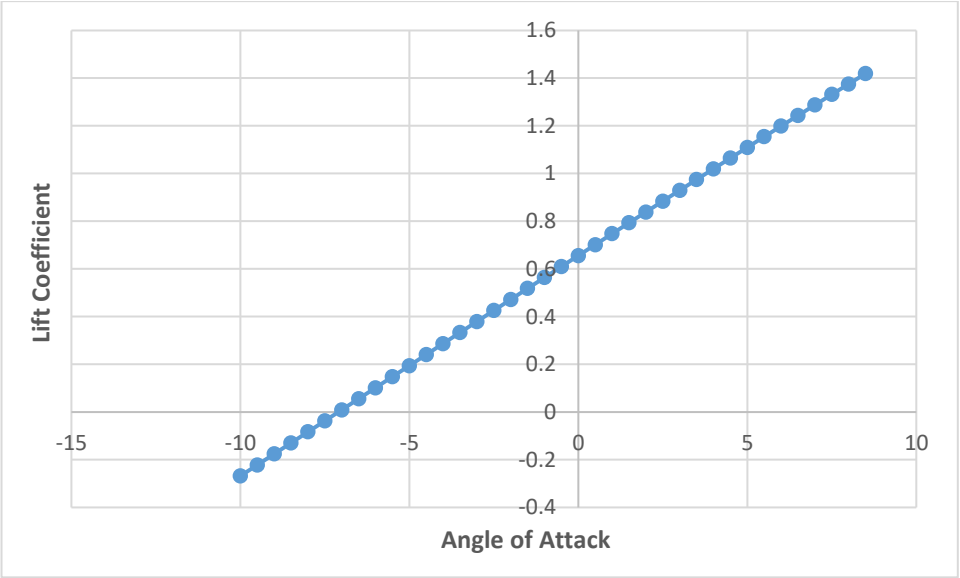

Figure 5.6 Final design lift coefficient versus angle of attack at 33.5 m/s airspeed

In Figure 5.7, the change of drag coefficient with angle of attack was given. The minimum drag coefficient was found to be 0.0058 at -7.5 degrees and the cruise drag coefficient (at 0^o angle of attack) was found to be 0.021.

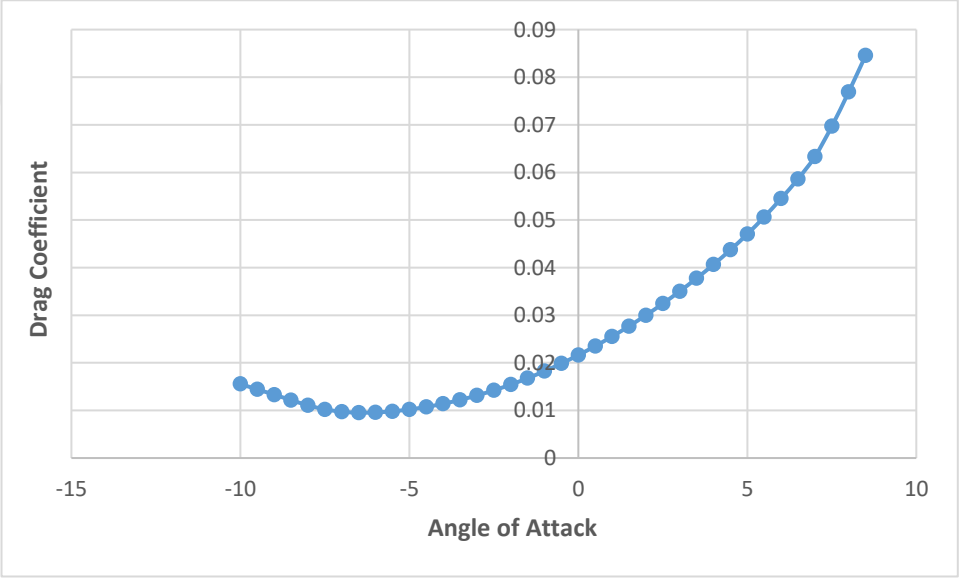

Figure 5.7 Final design drag coefficient versus angle of attack (33.5m/s airspeed)

The change in pitching moment coefficient, which is an important stability parameter, with angle of attack was given in Figure 5.8. As it was desired for aircrafts to have a negative pitching moment at cruise flight for the longitudinal static stability [6,21,51], it was clear from the figure that, the desired regime was obtained. The zero angle of attack pitching moment value was found to be -0.063.

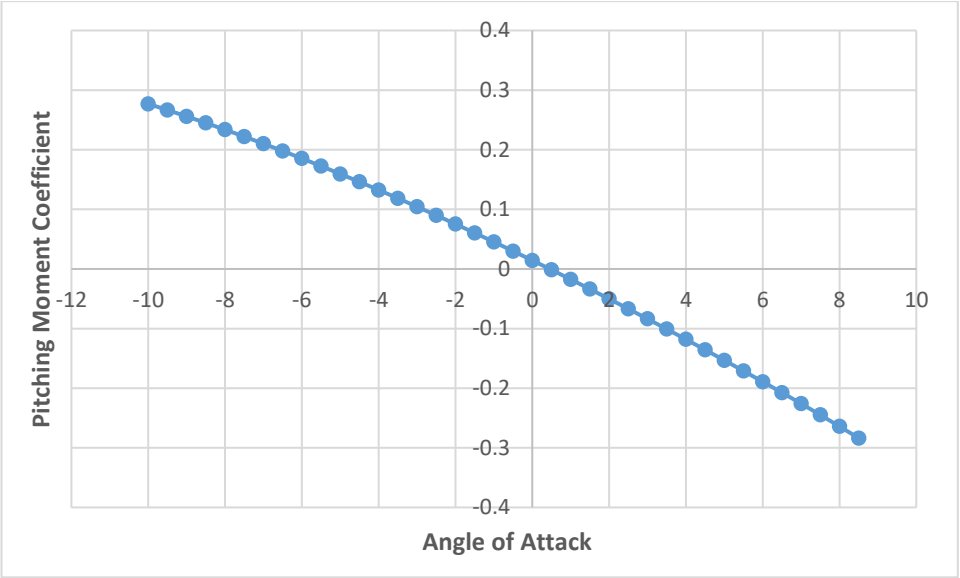

Figure 5.8 Final design pitching moment coefficient versus angle of attack (33.5m/s airspeed)

In Figure 5.9, another important parameter lift to drag ratio was given changing together with angle of attack. The figure shows that the maximum lift to drag ratio was 32.1 at -1.5 degrees angle of attack, which provides requirements of our design. In addition, the glide ratio was found to be 30.8 at zero angle of attack.

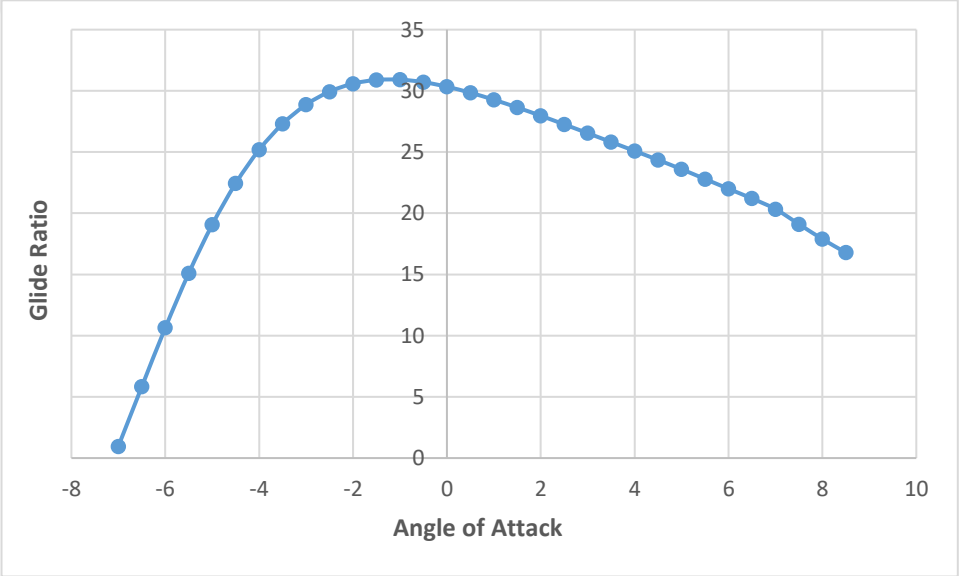

Figure 5.9 Final design glide ratio versus angle of attack (33.5m/s airspeed)

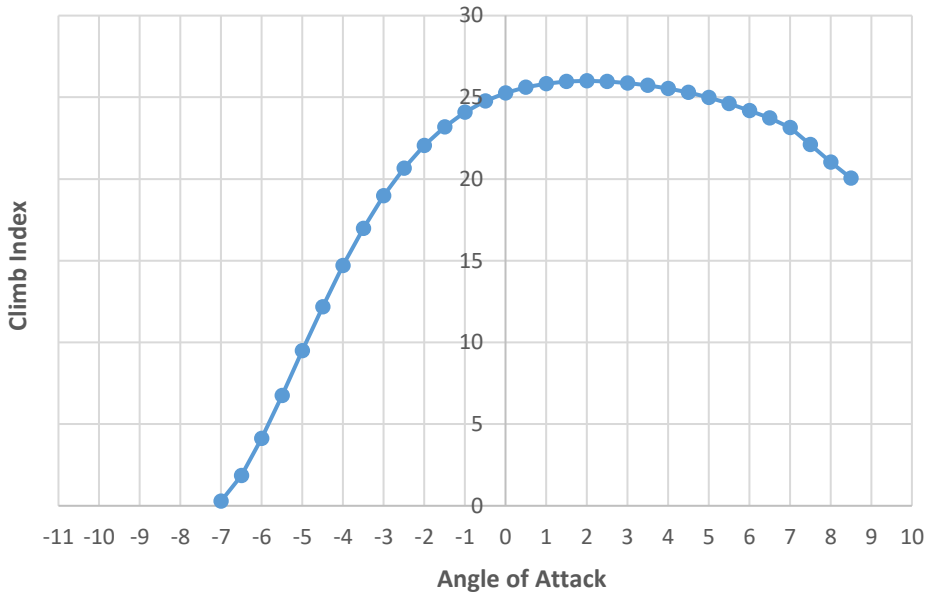

Figure 5.10 Final design climb index versus angle of attack

Figure 5.10 shows the change in climb index ($C_L^{3/2}/C_D$) with angle of attack. The maximum climbing index was found to be 26.3 at 2 degrees angle of attack.

After finding that our design satisfies the determined cruise flight conditions, second numerical analysis was performed on XFLR5 program to find the ideal performance values of our design. Type2 (fixed lift) analysis is able to give results depending on providing steady flight conditions. The air density and dynamic viscosity was used as their values at 1000 m altitude 1.112 kg/m^3 and 1.581x10^{-5} m^2/s, respectively. The range for the angle of attack was changed between -10 to 10 degrees.

Sink rate of a sailplane is an important performance parameter. The higher sink rate means the flight time to be higher. Figure 5.11 shows that, the minimum sink rate of our design is approximately 1 m/s at 99 km/h airspeed. The sink rate interval of our sailplane is found to be approximately 1 m/s to 1.21 m/s. This is an acceptable value, but need to be improved to have a high performance sailplane. There is existing high-performance sailplanes able to reach near 0.4-0.5 m/s sink rates [67].

Figure 5.11, speed polar, also shows that our sailplane have a stall speed of 80.71 km/h, which is a bit higher than our target value. It was also acceptable value for stall speed among the existing sailplanes, as stated in Table 3.1, but can be improved.

Best gliding speed of our design was also found to be approximately 105 km/h from Figure 5.11. This means the maximum range flight speed of our sailplane.

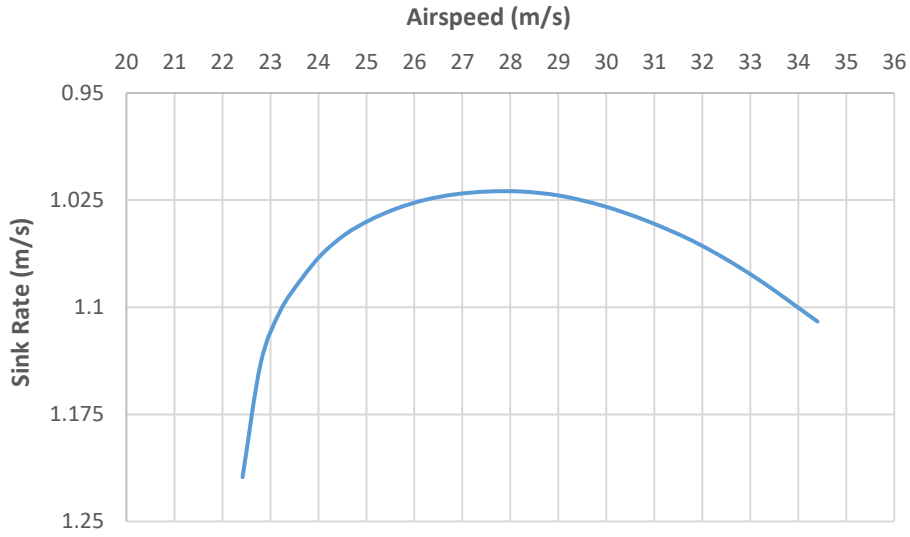

Figure 5.11 Final design speed polar

As Figure 5.13 shows that the zero angle of attack speed which provides steady flight conditions is 115 km/h (ideal cruise speed). This means that the speeds higher than this value can provide a steady cruise flight for our design. At the ideal cruise speed, it can be possible to maintain steady level-flight with minimum engine power.

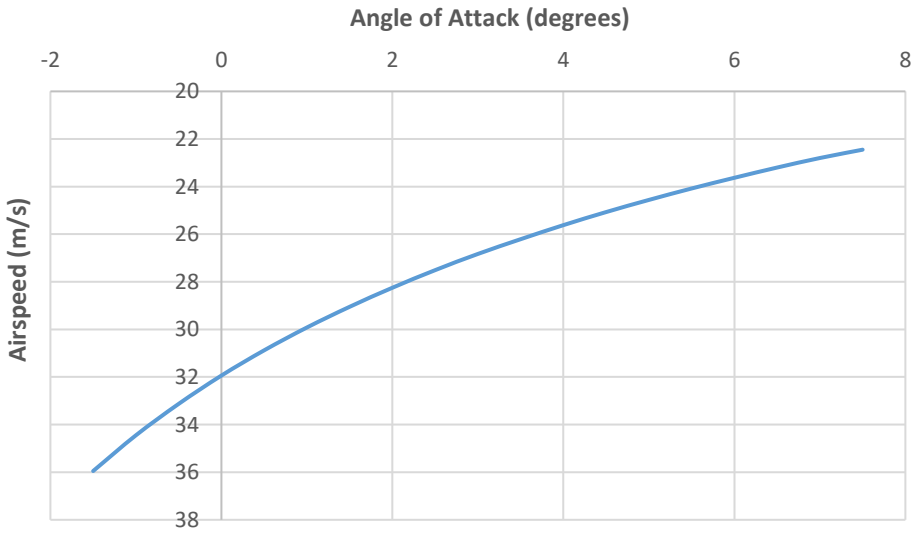

Figure 5.12 Final design airspeed versus angle of attack

The final design's three dimensional solid model was given in Figure 5.14. The two-dimensional and three-dimensional streamline views were given in Figures 5.15, 5.16 and 5.17, where the vortexes at the wing tips and wing-body interaction region were visually clearly seen.

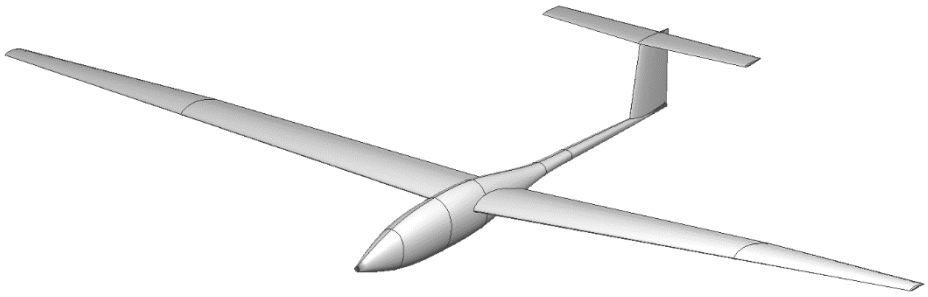

Figure 5.13 Final design in three dimensions

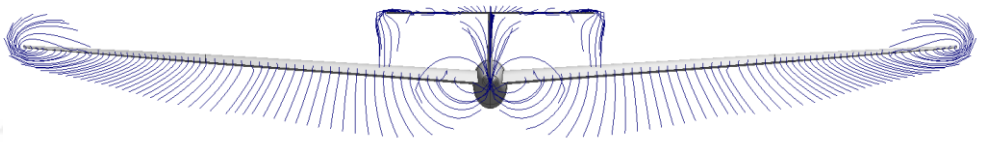

Figure 5.14 Front view of final design's streamlines front-view at zero angle of attack

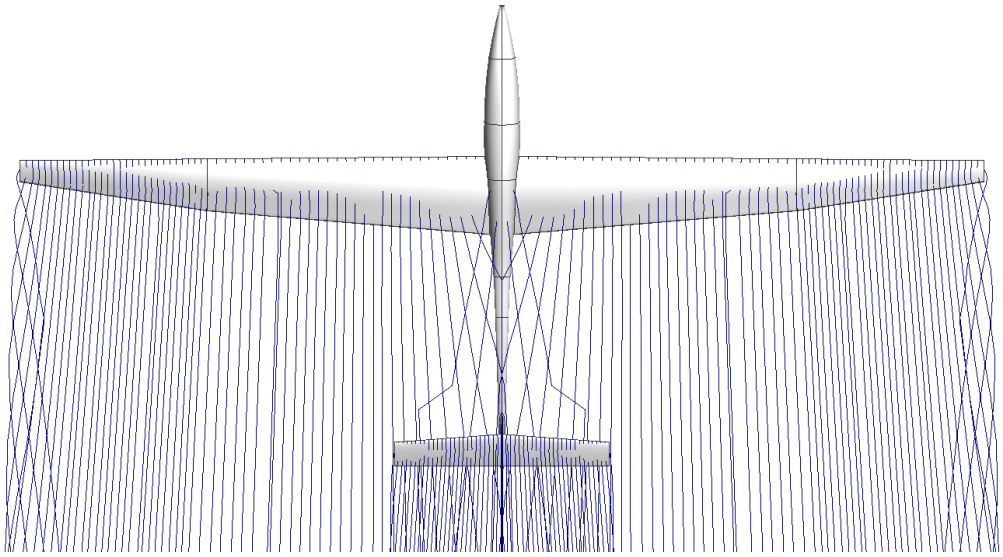

Figure 5.15 Top-view of final design's streamlines at zero angle of attack

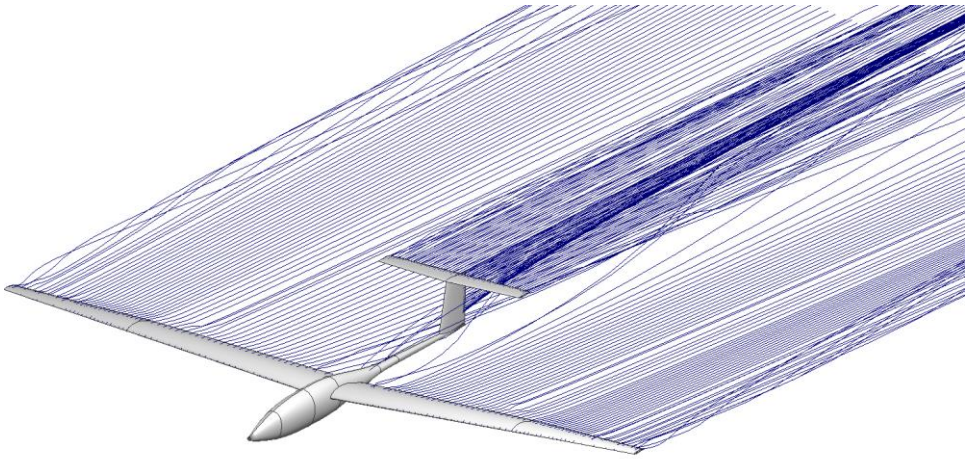

Figure 5.16 Three dimensional view of final design's streamlines at zero angle of attack

Figure 5.18 and 5.19 illustrates the streamlines of the sailplane at zero angle of attack and 8.5 degree angle of attacks. The figures clearly shows that, the streamlines leaving the main wing were not intersecting with the tail section at the interval of the operational angle of attacks.

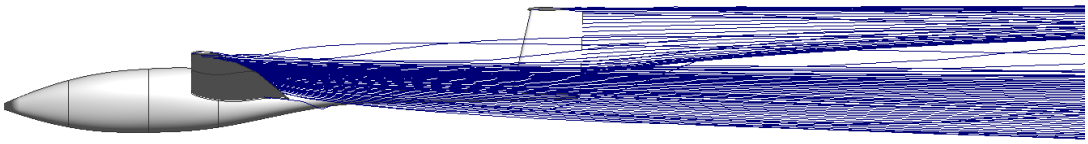

Figure 5.17 Final design streamlines at zero angle of attack

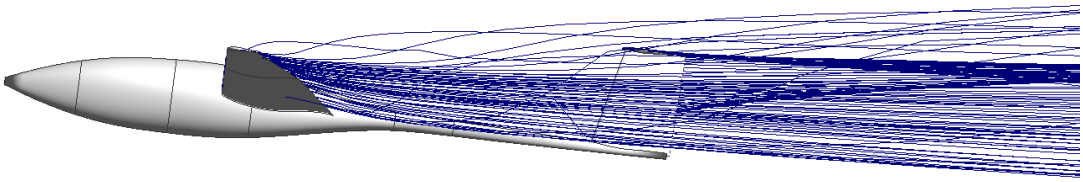

Figure 5.18 Final design streamlines at 8.5 degree angle of attack

The lift distributions of the final design at different angle of attacks were given in Figure 5.21. In conclusion, the final results of our design were gathered on Table 5.1.

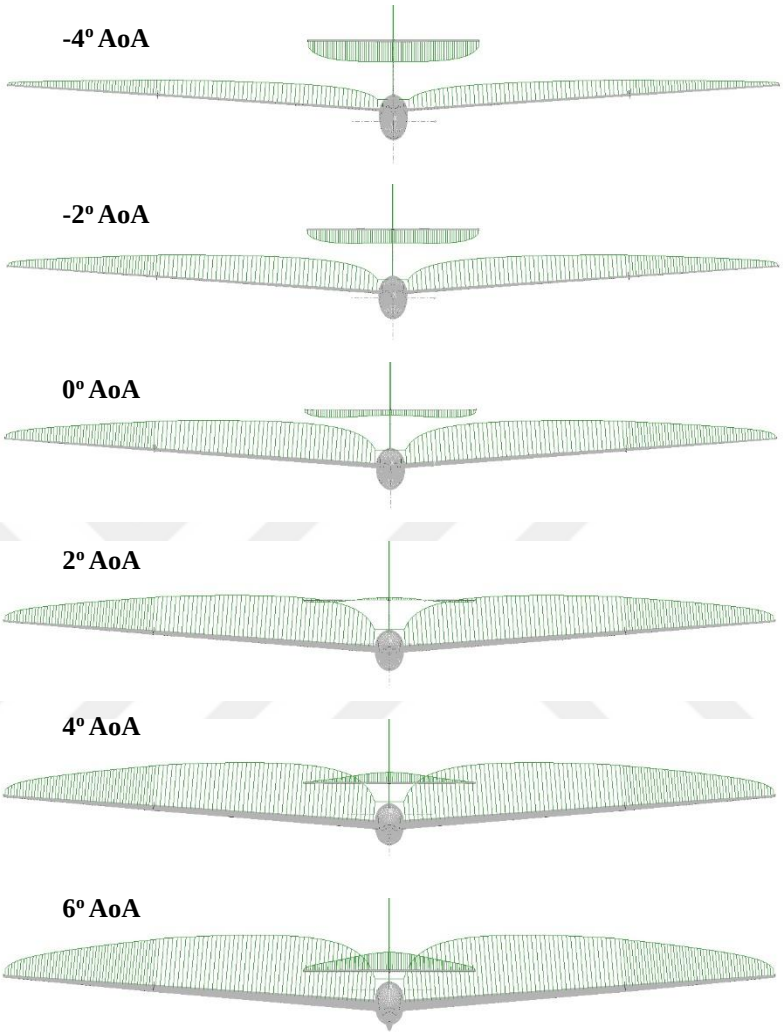

Figure 5.19 Final design lift distributions of wing and tail sections at different angle of attacks

Table 5.1 Specifications of the final design

Wing Area (m^2)	18.497
Horizontal Tail Area (m^2)	2.1
Vertical Tail Area (m^2)	1.17
Length(m)	8.6
Aspect Ratio	17.516
Mean Aerodynamic Chord (m)	1.122
Maximum Takeoff Weight (kg)	700
Maximum Wing Loading (kg/m^2)	37.93
Minimum Wing Loading (kg/m^2)	30.54
Stall Speed (km/h)	80.71
Ideal Cruise Speed (km/h)	115
Best Glide Speed (km/h)	128.1
Minimum Sink Speed (km/h)	99
Never Exceed Speed (km/h)	230
Maximum Glide Ratio	30.9
Minimum Sink Rate (m/s)	1.02
Zero lift drag coefficient (C_{D0})	0.0062
Propeller Diameter (m)	1
Number of Blades	5
Propeller Efficiency	0.6
Max. Static Thrust (kg)	115
Engine Power (kW)	25

CHAPTER 6

CONCLUSION

In this study, the aircraft design phases of requirements, conceptual design and preliminary design have been studied and applied for a two-seater electric-powered self-sustaining training sailplane design. The collected data about the existing sailplanes were taken into consideration as a starting point. The collected data of existing and historical sailplanes were made contribution at the initial estimations. In requirement defining phase, critical objective parameters were tried to be realistically estimated by means of this collected data. Conceptual design of the sailplane was determined with studying the pros and cons of the each part including wing, tail, landing gear and propulsion unit. In preliminary design phase, with the objective of designing aerodynamically efficient wing, tail and fuselage combination, each of the geometries were optimized to satisfy stability and especially level flight trim conditions by means of numerical analyzes. Center of gravity calculations were carried out, its location was optimized with trial and error and limitations were determined. In the end of the study, the aerodynamic performance parameters of the concluded design were obtained and revealed with numerical analyses. The aerodynamic performance results of the concluded design were found to be in good agreement with the previous studies.

6.1 Future Works

This study should be extended to next design steps of detail design and fabrication after the incomplete steps of the preliminary design, including stability and control issues, are continued and finished. Also performance parameters should be improved by using advanced optimization methods. Retractable propulsion unit need to be designed with a suitable electric motor and propeller so as to adapt to the main body. Structural tests, wind-tunnel tests and flight tests of the design should be performed at the detail design phase. In order to manufacture the final design, some molds should be designed for the main body, wing and tail sections at the fabrication phase.

REFERENCES

1. EASA. European Aviation Safety Agency. Annexes to the draft Commission Regulation on 'Air Operations - OPS'.
2. Federal Aviation Administration. 2007. Glider flying handbook. Skyhorse Publishing Inc.
3. Thomas F, Milgram J. 1999. Fundamentals of sailplane design. College Park, Maryland: College Park Press.
4. Frati S. 1946. The glider. Milan, Italy: Editore Ulrico Hoepli Milano.
5. Sadraey MH. 2012. Aircraft design: A systems engineering approach. John Wiley & Sons Ltd.
6. Gudmundsson S. 2013. General aviation aircraft design: applied methods and procedures. Butterworth-Heinemann.
7. White, L. (1961). Eilmer of malmesbury, an eleventh century aviator: a case study of technological innovation, its context and tradition. *Technology and Culture*. **2(2)**: 97-111.
8. John AD, Anderson J. 1989. Introduction to flight. McGraw-Hill.
9. Wilkins, J. 1802. The mathematical and philosophical works of the right rev. john wilkins. London, England: C. Whittingham.
10. Terzioğlu, A. (2007). The first attempts of flight, automatic machines, submarines and rocket technology in turkish history. *Foundation for Science Technology and Civilisation.* **634**.
11. Petrescu, R.V., Aversa R., Akash B., Bucinell R., Corchado J., Berto F., Mirsayar M., Apicella, A., Petrescu, F.I. (2017). History of aviation-a short review. *Journal of Aircraft and Spacecraft Technology*. **1(1)**: 30-49.
12. The glider designed by Jean-Marie Le Bris. Availabile at: https://en.wikipedia.org/wiki/Jean-Marie_Le_Bris#/media/File:LeBris1868.jpg Accessed 05.11.2018
13. A glider design from Jean-Marie Le Bris. Availabile at: https://en.wikipedia.org/wiki/Jean-Marie_Le_Bris#/media/File:LeBrisPatent1857.jpg Accessed 05.11.2018
14. The flight machine designed by Otto Lilienthal. Availabile at: https://i0.wp.com/todayinaviation.com/wp-content/uploads/2017/08/otto-lilienthal-german-engineer-1896.jpg?w=475 Accessed 05.11.2018
15. Otto Lilienthal flight machine design drawing. Availabile at: https://magazin.lufthansa.com/content/uploads/2016/08/FOTOFINDER-Art-and-History-2.13773019-HighRes-980x772.jpg Accessed 05.11.2018
16. Tang, D., Dowell E.H. (2001). Experimental and theoretical study on aeroelastic response of high-aspect-ratio wings. *AIAA journal*, **39(8)**: 1430-1441.
17. Guo, S. (2007). Aeroelastic optimization of an aerobatic aircraft wing structure. *Aerospace Science and Technology*. **11(5)**: 396-404.
18. Afonso, F., Vale, J., Oliviera, E., Lau, F., Suleman, A. (2017). et al., A review on non-linear aeroelasticity of high aspect-ratio wings. *Progress in Aerospace Sciences*. **89**: 40-57.

19. Hart, W. (1971). Glider fuselage design with the aid of computer graphics. *Computer-Aided Design*. **3(2)**: 3-8.
20. Kampf, K.-P., Crawley E.F., Hansman R.J. (1989). Experimental investigation of the crashworthiness of scaled composite sailplane fuselages. *Journal of Aircraft*. **26(7)**: 675-681.
21. Otani, I., Maughmer M. (2007). The conceptual design of a tailless sailplane having a stabilizing fuselage. *Technical Soaring*. **31(3)**: 79-89.
22. Boermans, L., Bennis F. (1992). Design and windtunnel tests of an airfoil for the horizontal tailplane of a standard class sailplane. *Technical Soaring*. **16(2)**: 35-40.
23. Murua, J., Martinez, P., Climent, H., Zyl, L., Palacios, R. (2014). T-tail flutter: potential-flow modelling, experimental validation and flight tests. *Progress in Aerospace Sciences*. **71**: 54-84.
24. Sanchez-Caramona, A., Cuerno-Rejado, C. (2018). Vee-tail conceptual design criteria for commercial transport aeroplanes. *Chinese Journal of Aeronautics.*
25. Drela, M. (1989). XFOIL: an analysis and design system for low reynolds number airfoils. *Low Reynolds Number Aerodynamics*. **54:**1-12.
26. Deperrois, A. (2009). XFLR5 analysis of foils and wings operating at low reynolds numbers. *Guidelines for XFLR5*.
27. Eppler, R., Somers D.M. (1980). A computer program for the design and analysis of low-speed airfoils. *NASA Technical Memorandum 80210*.
28. Craig, A.P., Hansman R.J. (1987). An experimental low reynolds number comparison of a wortmann FX67-K170 airfoil, a NACA 0012 airfoil and a NACA 64-210 airfoil in simulated heavy rain. *MIT Aeronautical Systems Laboratory Report. ASL 87-1*.
29. Smith, J., Graham H., Smith, J. (2008). The validation of an airfoil in the ground effect regime using 2-d CFD analysis. *26th AIAA Aerodynamic Measurement Technology and Ground Testing Conference*.
30. Lasauskas, E., Naujokaitis, L. (2009). Analysis of three wing sections. *Aviation*. **13(1)**: 3-10.
31. Wahidi, R., Bridges, D. (2009) Experimental investigation of the boundary layer and pressure measurements on airfoils with laminar separation bubbles. *39th AIAA Fluid Dynamics Conference*.
32. Xin, H.U.A., Rui, G.U., Jin, J.F., Liu, Y.R., Yi, M.A., Qian, C.O.N.G., Zheng, Y. (2010). Numerical simulation and aerodynamic performance comparison between seagull aerofoil and NACA 4412 aerofoil under low-reynolds. *Advances in Natural Science*. **3(2)**: 244-250.
33. Sudhakar, S. (2011). Experimental studies on SM4308 airfoil at low reynolds numbers. *Symposium on Applied Aerodynamics and Design of Aerospace Vehicle.*
34. Aslıhan V., Özdemir, U., Yükselen, A., İnalhan, G., (2014). Dikey iniş kalkış yapabilen bir insansız hava aracının (turaç*) aerodinamik analizi. *5. Ulusal Havacılık ve Uzay Konferansı.*
35. Hasan, M., El-Shahat, A., Rahman, M. (2017). Performance investigation of three combined airfoils bladed small scale horizontal axis wind turbine by BEM and CFD analysis. *Journal of Power and Energy Engineering*. **5(05)**: 14.
36. Castles W., (1938). Selection of the optimum aspect ratio for a cantilever sailplane. *Journal of the Aeronautical Sciences*. **5(10)**: 407-409.
37. Hicks, R.M., Henne, P.A. (1978). Wing design by numerical optimization. *Journal of Aircraft*. **15(7)**: 407-412.
38. Wakayama, S., Kroo, I. (1995). Subsonic wing planform design using multidisciplinary optimization. *Journal of Aircraft*. **32(4)**: 746-753.

39. Takahashi, T.T. (2011). Optimum aspect ratio for subsonic air vehicles. *Journal of Aircraft*. **48(6)**: 1984-1993.
40. Lei, S., Hua, Y., Yang, Z., Haoyu, Z., Jun, H. (2014). Dihedral influence on lateral–directional dynamic stability on large aspect ratio tailless flying wing aircraft. *Chinese Journal of Aeronautics*. **27(5)**: 1149-1155.
41. Hammerton, J.R., Su, W., Zhu, G., Swei, S.S. (2018). Optimum distributed wing shaping and control loads for highly flexible aircraft. *Aerospace Science and Technology*. **79**: 255-265
42. Della Vecchia, P., Malgieri, D., Nicolosi, F., Marco, A.D. (2018). Numerical analysis of propeller effects on wing aerodynamic: tip mounted and distributed propulsion. *Transportation Research Procedia*. **29**: 106-115.
43. Bravo-Mosquera, P.D., Cerón-Muñoz, H. D., Díaz-Vázquez, G., Catalano, F. M. (2018). Conceptual design and CFD analysis of a new prototype of agricultural aircraft. *Aerospace Science and Technology*. **80**: 156-176.
44. Qin, N., Vavalle, A., Moigne A.L. (2005). Spanwise lift distribution for blended wing body aircraft. *Journal of Aircraft*. **42(2)**: 356-365.
45. Lee, T., Gerontakos P. (2006). Effect of winglet dihedral on a tip vortex. *Journal of Aircraft*. **43(1)**: 117-124.
46. Lyons, A., Gross, A.V.D. 2007. Oxygen and nitrogen enriched atmospheres in aircraft. U.S. Patent No. 7,179,322. Washington, DC: U.S. Patent and Trademark Office.
47. EASA. European Aviation Safety Agency. 2008. Certification specifications for sailplanes and powered sailplanes.
48. FAI. Federation Aeronautique Internationale. 2017. Sporting code section 3 – gliding.
49. Lissaman, P. (2005). Wind energy extraction by birds and flight vehicles. *43rd AIAA Aerospace Sciences Meeting and Exhibit*.
50. Chatfield, C. (1928). Monoplane or biplane. *SAE Transactions*. 217-264.
51. Raymer, D.P. 2012. Aircraft design: a conceptual approach. Reston, Virginia: American Institute of Aeronautics and Astronautics, Inc.
52. DG 1001T Sailplane. Availabile at: https://www.dg-flugzeugbau.de/en/aircrafts/dg-1001/dg-1001t Accessed 05.11.2018
53. Tandem configuration sailplane. Availabile at: https://www.gliding.co.uk/buy-voucher Accessed 05.11.2018
54. Side-by-side configuration sailplane. Availabile at: https://steemkr.com/electric/@skypix/the-self-launching-all-electric-powered-pipistrel-taurus Accessed 05.11.2018
55. Pusher configuration sailplane. Availabile at: http://www.spr.aero/wcc-main-news/135-m-a-new-world-of-gliders.aspx Accessed 05.11.2018
56. Tractor configuration sailplane.
57. Forces on aircraft. Availabile at: http://aviationknowledge.wikidot.com/sop:elements-of-aircraft-performance Accessed 05.11.2018
58. Horstmann, K.-H. (1976). Neue Modellaufwindverteilungen und ihr einfluss auf die auslegung von segelflugzeugen. *OSTIV Publications*, **14**.
59. Forces on aircraft. Availabile at: https://m-selig.ae.illinois.edu/ads/coord_database.html Accessed 05.11.2018
60. McGhee, R.J., Walker, B.S., Millard B.F. (1988). Experimental results for the eppler 387 airfoil at low reynolds numbers in the langley low-turbulence pressure tunnel. *NASA Technical Memorandum 4062*.

61. Morgado, J., Vizinho, R., Silvestre, M. A. R., Páscoa, J. C. (2016). XFOIL vs CFD performance predictions for high lift low Reynolds number airfoils. *Aerospace Science and Technology*. **52**: 207-214.
62. NASA. National Aeronautics and Space Administration. 1976. Standard atmosphere. U.S. Government Printing Office, Washington, DC.
63. Holighaus, K. (1971). The influence of planform and airfoil on the design of high performance sailplane wings with very high aspect ratio (low re-numbers). *Soaring Symposia*.
64. Thang, N. T., Hai, D. N., Viet, T. K. (2017). Simulation of the steady flow around a flying wing by using inviscid and viscous incompressible flow models. *10th Vietnam National Congress on Mechanics.*
65. Axes of an aircraft. Availabile at: https://www.learntoflylv.com/three%20axis.gif Accessed 05.11.2018
66. Retracting propeller mechanism for sailplanes. Availabile at: https://d1k5w7mbrh6vq5.cloudfront.net/images/cache/7f/72/61/7f7261d34b61c37cf0785eff518f8916.gif Accessed 05.11.2018
67. Lundin, M.A. (2008). Optimal soaring: what is the best speed to fly? *Math Horizons*. **15(4)**: 12-15.